

THE EFFICIENCY OF GLOBULAR CLUSTER FORMATION

DEAN E. McLAUGHLIN¹

Department of Astronomy, 601 Campbell Hall
 University of California, Berkeley, CA 94720-3411
 dean@crabneb.berkeley.edu

Accepted for publication in The Astronomical Journal

ABSTRACT

The specific frequencies of globular cluster systems, $S_N \propto \mathcal{N}_{\text{tot}}/L_{V,\text{gal}} \propto M_{\text{gcs}}/M_{\text{stars}}$, are discussed in terms of their connection to the efficiency of globular cluster formation in galaxy halos, which is claimed to reflect a generic aspect of the star formation process as it operates even at the current epoch. It is demonstrated that the total *masses* of GCSs are little affected by the dynamical destruction of low-mass clusters at small galactocentric radii. This permits direct, empirical estimates of the cluster formation efficiency by mass, $\epsilon_{\text{cl}} \equiv M_{\text{gcs}}^{\text{init}}/M_{\text{gas}}^{\text{init}}$, even after 10^{10} years of GCS evolution. However, the standard practice of using only the stellar luminosities of galaxies as indicators of their initial total gas masses (and thus relating S_N to ϵ_{cl} in one step) leads to serious conceptual problems, that are reviewed here. The *first specific frequency problem*, which is the well known tendency for many brightest cluster galaxies to have higher than average S_N , is a global one; the *second specific frequency problem* is a local one, in which the more extended spatial distribution of GCSs relative to halo stars in some (not all) bright ellipticals leads to S_N values that increase with radius inside the galaxies. Extending similar suggestions in the recent literature, it is argued that these trends in S_N do not reflect any such behavior in the underlying ϵ_{cl} ; rather, *both* of these problems stem from neglecting the hot, X-ray emitting gas in and around many large ellipticals, and both may be alleviated by including this component in estimates of $M_{\text{gas}}^{\text{init}}$.

This claim is checked and confirmed in each of M87, M49, and NGC 1399, all of which have been thought to suffer from one or the other of these S_N problems. Existing data are combined to construct GCS surface density profiles that extend over nearly the whole extents of these three galaxies, and a non-parametric, geometrical deprojection algorithm is developed to afford a direct comparison between the *volume* density profiles of their GCSs, stars, and gas. It is found, in each case, that $\rho_{\text{cl}} \propto (\rho_{\text{gas}} + \rho_{\text{stars}})$ at radii beyond roughly a stellar effective radius, inside of which dynamical evolution may have depleted the initial GCSs. The constant of proportionality is the same in all three galaxies: $\epsilon_{\text{cl}} = 0.0026 \pm 0.0005$. Taken together, these results suggest that GCSs generally should be more spatially extended than stellar halos only in gas-rich galaxies that also have a high global specific frequency.

The implication that ϵ_{cl} might have had a universal value is supported by global GCS data for a sample of 97 giant ellipticals, brightest cluster galaxies, and faint dwarfs. The total globular cluster populations in all of these early-type systems are in excellent agreement with the predictions of a constant ϵ_{cl} at the level observed directly in M87, M49, and NGC 1399; all *systematic* variations in GCS specific frequency between galaxies are shown to result entirely from different relations, in different magnitude ranges, between $M_{\text{gas}}^{\text{init}}$ and the present-day $L_{V,\text{gal}}$. An identical ϵ_{cl} is also calculated for the Pop. II spheroid of the Milky Way, and is indicated (although less conclusively) for the ongoing formation of open clusters. The inferred universal cluster formation efficiency, of $\simeq 0.25\%$ by mass, should serve as a strong constraint on general theories of star and cluster formation. The associated inference of a non-universal formation efficiency for unclustered stars is considered, particularly in terms of the suggestion that this might result, both in dwarf galaxies and at large galactocentric radii in the brightest ellipticals, from feedback and galactic winds. Implications for a merger-formation model of early-type GCSs, and for the proposed existence of intergalactic globulars in clusters of galaxies, are briefly discussed.

Subject headings: galaxies: elliptical and lenticular, cD — galaxies: individual (M87, M49, NGC 1399)
 — galaxies: star clusters — globular clusters: general — stars: formation

1. INTRODUCTION

As the study of galaxy formation comes more and more to require a reliable description of star-gas interactions and feedback on relatively small spatial scales, it is forced towards questions that overlap with fundamental issues in star formation theory. Conversely, as evidence accumulates that most stars today—in environments ranging from the disk of the Milky Way to circumnuclear starbursts—are born not in isolation but in groups, the study of star formation in general seems increasingly to demand a focus on larger scales than might previously have been considered. Although these two disciplines have not yet converged—the smallest scales currently of importance for galaxy formation can still be one or two orders of magnitude greater than the “large” scales in star formation—they will necessarily continue to approach one

¹Hubble Fellow

another as further progress is made. It is therefore important to identify and understand those areas of truly common interest, on the largest stellar scales and the smallest galactic ones. In many ways, the systems of old globular clusters in galaxy halos are positioned just at this interface; they can potentially be exploited to constrain aspects of both local and global star-formation processes, in both protogalactic and present-day settings.

It has, indeed, long been recognized that the global properties of globular cluster systems (GCSs) might be used to good effect as probes of galaxy formation and evolution. (This is especially true of bright early-type galaxies, whose GCSs are more populous and better studied than those in typical spirals like the Milky Way.) For example, following the suggestion that large fractions of the GCSs in ellipticals may have formed in major merger events (e.g., Schweizer 1987; Ashman & Zepf 1992; Zepf & Ashman 1993), and the related discovery of young super star clusters in systems like the Antennae galaxies (Whitmore & Schweizer 1995), much recent discussion has centered on the interpretation of the distribution of metallicities (or broad-band colors) among E-galaxy globulars as clues to their hosts' dynamical histories (see Geisler, Lee, & Kim 1996; Forbes, Brodie & Grillmair 1997; Côté, Marzke, & West 1998; Kissler-Patig, Forbes, & Minniti 1998). A somewhat older approach has used just the total population of GCSs, as a function of parent galaxy luminosity, Hubble type, and local environment, to make arguments relating to issues such as biasing in a cold dark matter cosmology (West 1993); the merger history of ellipticals (Harris 1981; van den Bergh 1984; Ashman & Zepf 1992; Forbes et al. 1997); the formation of cD galaxies and their envelopes (McLaughlin, Harris, & Hanes 1993, 1994); star formation in galaxies at the centers of cluster cooling flows (Harris, Pritchet, & McClure 1995); the influence of early galactic winds on the evolution of giant ellipticals (Harris, Harris, & McLaughlin 1998); and even larger-scale aspects of galaxy clusters such as populations of intergalactic stars (e.g., West et al. 1995; Harris et al. 1998). Yet a third characteristic of GCSs—their radial distributions (the projected number density of globulars around a galaxy as a function of galactocentric radius)—has also served as the basis for discussions of elliptical galaxy formation (e.g., Harris 1986; Ashman & Zepf 1992; Kissler-Patig 1997; van den Bergh 1998).

Rather less developed, however, is a clear sense of the relevance of GCSs to *local* star formation on smaller scales: What relation, if any, do the fundamental properties of globular cluster systems bear to the way stars form now, in the dense clumps within Galactic giant molecular clouds? Can the study of one of these phenomena possibly shed light on the other? Larson (1988, 1993, 1996), has emphasized the possible parallels between the basic pattern of local star formation and the birth of globular clusters within large protogalactic clouds in a scenario for the collapse of galaxies from clumpy initial conditions (as in, e.g., the classic picture of Searle & Zinn 1978, and current models of hierarchical galaxy formation). A more quantitative discussion along these lines, including an exposition of links to several of the gross characteristics of GCSs, is given by Harris & Pudritz (1994). Most recently, McLaughlin & Pudritz (1996) and Elmegreen & Efremov (1997) have focussed in detail on the globular cluster luminosity function (the number of clusters per unit magnitude, from which may be derived the mass function dN/dm for the entire system of globulars in a given galaxy) in attempts to model this property of GCSs using our current understanding of present-day star formation in molecular clouds and their clumps.

The work presented in this paper further explores the connections between the formation of stars, globular clusters, and galaxies, by concentrating on two of the primary attributes of GCSs: their specific frequencies (or total populations) and radial distributions. The next Section discusses the significance of these GCS properties as they relate to general questions on the formation of stellar clusters. In §3 below, data are compiled from the literature, and a geometrical deprojection algorithm applied, to construct *volume* density profiles for the stars, the X-ray gas, and the globular clusters in three galaxies with well studied GCSs: M87 (the cD at the center of the Virgo Cluster), M49 (giant elliptical in Virgo), and NGC 1399 (cD galaxy in the Fornax Cluster). An intercomparison of the density profiles of the three halo components yields a point-by-point measure of the GCS contribution to the total luminous mass in each system, as a function of *three-dimensional* galactocentric radius, r_{gc} . These GCS mass ratios, which are constant throughout each galaxy (at large r_{gc}) and the same in all three, are interpreted as an indication of the formation efficiency of globular clusters. In §4, these results are supplemented with broader considerations of the GCSs in other early-type galaxies and in the Milky Way halo, and with a direct estimate for the relative formation rate of open clusters in the Galactic disk, to argue for the existence of a *universal efficiency, or probability, for the formation of a bound stellar cluster from a dense cloud of gas*. Section 5 discusses the implications of this for a few specific issues in galaxy and GCS formation and evolution, and §6 concludes with a summary.

2. THE EFFICIENCY OF CLUSTER FORMATION FROM GLOBULAR CLUSTER SYSTEMS

2.1. Cluster Formation Efficiencies

The possibility that globular cluster systems can be connected not only to galaxy formation, but to ongoing star formation as well, is suggested by the fact that this latter process operates largely in a *clustered mode*: by mass, most new stars in the Milky Way appear in groups within the largest clumps in molecular clouds, and only rarely in true isolation. This is, by now, an established empirical fact (e.g., Lada et al. 1991; Zinnecker et al. 1993), and it is easily seen (Patel & Pudritz 1994) to be a direct consequence of the different power-law slopes in the mass function of molecular clumps ($dN/dm \propto m^{-1.6}$, so that the largest clumps, which weigh in at 10^2 – $10^3 M_\odot$, contain most of the star-forming gas mass in any molecular cloud) and the stellar initial mass function ($dN/dm \propto m^{-2.35}$, putting most of the mass in young stars into $\lesssim 1 M_\odot$ objects). Similarly, young super star clusters, which tend to have sizes and masses that are generally comparable to the old globulars in the Milky Way, can account for as much as $\sim 20\%$ of the UV light in starburst galaxies (Meurer et al. 1995).

This is, however, *not* to say that all, or even most, stars are born into bona fide clusters that exist as coherent dynamical units for any length of time; on the contrary, it would appear that very few multiple-star systems actually form as gravitationally bound clusters. (A quantification of “very few” is one of the goals of this paper.) At some point during the collapse and fragmentation of a cluster-sized cloud of gas, the massive stars which it has formed will expel any remaining gas by the combined action of their stellar winds, photoionization, and supernova explosions. If the *cumulative* star formation efficiency of the cloud, $\text{SFE} = M_{\text{stars}}/(M_{\text{stars}} + M_{\text{gas}})$, is below a critical threshold when the gas is lost, then the blow-out carries away sufficient energy that the stellar group remaining is unbound, and disperses into the field. The precise value of this threshold SFE depends on details of the dynamics and magnetic field in the gas cloud before its self-destruction, and on the timescale over which the massive stars disperse the gas; but various estimates place it in the range $\text{SFE}_{\text{crit}} \sim 0.2\text{--}0.5$ (e.g., Hills 1980; Mathieu 1983; Elmegreen & Clemens 1985; Verschueren 1990; Lada, Margulis, & Dearborn 1984).

A complete theory of star formation must therefore be able to anticipate the final cumulative SFE in any single piece of gas with (say) a given mass and density, and thereby predict whether or not it will form a bound cluster. No such theory yet exists. More within reach are considerations of a statistical nature, in which a *distribution* of cumulative SFEs (and, thus, the fraction of clouds that achieve $\text{SFE} \geq \text{SFE}_{\text{crit}}$ before self-destruction) is calculated for an ensemble of star-forming clouds, in either a protogalactic or a present-day context (see, e.g., Elmegreen 1983; Elmegreen & Clemens 1985; Elmegreen & Efremov 1997). But even here, the systematic effects of a range in the initial masses of the gaseous clouds, or of changes in the assumed star formation law (which is probably the most outstanding “free” parameter here) have not been explored fully. It is therefore not clear that the dominant factor governing the formation of bound stellar clusters vs. unbound associations has been identified.

It is nonetheless possible to constrain any forthcoming theories of star and cluster formation with empirical evaluations of the probability that a cluster-sized cloud of gas is able to achieve a cumulative SFE of at least the critical 20%–50%. This probability—which can equally well be interpreted as that fraction of an ensemble of massive star-forming clouds which manages to produce bound stellar systems—is referred to here as the efficiency of cluster formation. As was indicated above, an estimate of this will be taken first from a detailed investigation of the old globular cluster populations in three giant elliptical galaxies; general arguments will then be used to show that the result also applies to globular cluster formation in other galaxies, and to the formation of disk clusters today.

A first (and very rough) assessment of the formation efficiency of globular clusters appeals to the most basic and most easily measured observable of a GCS: namely, its total population, \mathcal{N}_{tot} , summed over all cluster luminosities and galactocentric positions. This is usually compared to the integrated V -band luminosity of the parent galaxy’s halo (as a measure of its unclustered field star population) through the so-called specific frequency (Harris & van den Bergh 1981):

$$S_N \equiv \mathcal{N}_{\text{tot}} \times 10^{0.4(M_V^T + 15)} \propto \mathcal{N}_{\text{tot}}/L_{V,\text{gal}}. \quad (1)$$

Even though any observational derivation of S_N necessarily involves (possibly large) extrapolations of data that directly count only the brightest clusters in some spatially limited subset of a GCS, these estimates tend usually to be surprisingly robust. To date, specific frequencies have been obtained for of order 100 galaxies, some 80% of which are early-type systems (see the compilations of Harris 1991; Durrell et al. 1996; Kissler-Patig 1997; Blakeslee 1997; Blakeslee, Tonry, & Metzger 1997; Harris et al. 1998). Given this bias in the observational database, some of what follows will make use of results that are really specific to elliptical galaxies; spirals are brought more explicitly into the discussion in §4 below.

Specific frequency is easily related to the total masses of a galaxy’s GCS and of its unclustered halo stars, if both the mean mass of the individual globulars in the system and the mass-to-light ratio of the overall *stellar* component are known. As is discussed further in §3.1 below, the basic distribution of globular cluster masses is quite similar from galaxy to galaxy, so that the mean cluster mass in the Milky Way GCS— $\langle m \rangle_{\text{cl}} = 2.4 \times 10^5 M_{\odot}$ —serves as a reliable estimate for other systems as well. Meanwhile, the stellar mass-to-light ratios of large galaxies are essentially equal to the dynamical M/L in their *cores*, which are baryon-dominated. As is also discussed below (§4.1), observations show that the core M/L of hot galaxies increases with luminosity; but, even though this turns out to be rather an important consideration in detail, it will suffice for now to use a single value of $\Upsilon_V \equiv M/L_V = 7 M_{\odot} L_{\odot}^{-1}$ as a rough characterization of large ellipticals (van der Marel 1991; cf. Faber & Gallagher 1979; Binney & Tremaine 1987). The definition of S_N in equation (1) may then be rewritten as (cf. Zepf & Ashman 1993; Harris & Pudritz 1994; Harris et al. 1998)

$$S_N \simeq 2500 \left(\frac{\langle m \rangle_{\text{cl}}}{2.4 \times 10^5 M_{\odot}} \right)^{-1} \left(\frac{\Upsilon_V}{7 M_{\odot} L_{\odot}^{-1}} \right) \frac{M_{\text{gcs}}}{M_{\text{stars}}}. \quad (2)$$

To be clear, it is stressed again that the mass-to-light ratio applied here refers to measurements in the cores of ellipticals, and is not meant to include any dark matter other than stellar remnants. In any event, an inversion of this last expression yields

$$\frac{M_{\text{gcs}}}{M_{\text{stars}}} = 4.0 \times 10^{-4} S_N \left(\frac{\langle m \rangle_{\text{cl}}}{2.4 \times 10^5 M_{\odot}} \right) \left(\frac{\Upsilon_V}{7 M_{\odot} L_{\odot}^{-1}} \right)^{-1} \sim 2 \times 10^{-3} \left(\frac{S_N}{5} \right), \quad (3)$$

where $S_N \approx 5$ is suggested by the studies cited above as a representative value for early-type galaxies ranging in luminosity from $M_V^T \simeq -15$ to $M_V^T \simeq -22$. Of course, there is some uncertainty in this “mean” S_N , and some intrinsic scatter about

it. Moreover, the data suggest that S_N varies systematically with $L_{V,\text{gal}}$ —the simple scaling $\mathcal{N}_{\text{tot}} \propto L_{V,\text{gal}}$ that corresponds to a constant specific frequency is not strictly obeyed—particularly among dwarf ellipticals and between brightest cluster galaxies. These issues have been discussed in detail in the literature, and they are revisited here, in §2.2. With this caveat in mind, however, $M_{\text{gcs}}/M_{\text{stars}} \sim 2 \times 10^{-3}$ is useful as a crude, order-of-magnitude guide to a “typical” global GCS mass ratio in galaxy halos.

The advantage of working in terms of this *mass* ratio is that, whatever its precise value in any one system at the current epoch, it is expected to be a fairly well conserved quantity that has not changed drastically over the course of GCS and galaxy evolution in a Hubble time. *This is true even though the total population \mathcal{N}_{tot} of any GCS is bound to decrease over time*, as individual globulars are disrupted by the cumulative effects of external gravitational shocks and internal two-body relaxation (see, e.g., Aguilar, Hut, & Ostriker 1988; Ostriker, Binney, & Saha 1989; Capuzzo-Dolcetta 1993; Murali & Weinberg 1997a, 1997b, 1997c; Gnedin & Ostriker 1997; Vesperini & Heggie 1997; but cf. Portegies Zwart et al. 1998). These dynamical processes discriminate preferentially against low-mass and low-density globular clusters, and it turns out that even if large *numbers* of such objects are lost, no great change is effected in the total *mass* of the remaining GCS. This conclusion rests on the fact that the mass functions of GCSs—particularly those in early-type galaxies—are shallow enough that most of the total M_{gcs} is contained in the most massive members of the system; but these are the least susceptible to dynamical destruction. The implication is that the total mass of a GCS may not change much over its lifetime; thus, *if* the current stellar mass of a galaxy were a reliable indication of the total amount of gas that was initially available to form stars, then the presently observed ratio $M_{\text{gcs}}/M_{\text{stars}} \sim 2 \times 10^{-3}$ would serve as a rough, *global* estimate of the efficiency of globular cluster formation. Note that this reasoning also shows that galactic halos cannot be built up from disrupted globulars; see, e.g., Ashman & Zepf (1992) and Harris & Pudritz (1994). (One of the main conclusions of this paper will be that, in fact, M_{stars} is *not* always an adequate measure of an initial gas supply, and that $M_{\text{gcs}}/M_{\text{stars}}$ therefore cannot always be equated directly to a cluster formation efficiency. However, since most previous discussions of GCS specific frequencies do draw on this simple assumption at some level, it is of interest to develop some of its implications.)

A simple numerical example should emphasize the robustness of M_{gcs} . Thus, consider a newly formed system of globulars whose masses are distributed according to a power-law mass function between some lower and upper limits:

$$\left(\frac{d\mathcal{N}}{dm}\right)_{\text{init}} = K m^{-\gamma_2}, \quad m_\ell \leq m \leq m_u, \quad (4)$$

where $\gamma_2 > 0$ and reasonable choices for m_ℓ and m_u may be $500 M_\odot$ and $5 \times 10^6 M_\odot$. (The precise values are not critical here.) Now let this GCS be eroded over 10^{10} yr, keeping in mind that each cluster in the system has a definite, mass-dependent lifetime against the dynamical mechanisms mentioned above. In a rough approximation to a combination of complicated processes, there is then a mass scale (say m_*) above which few or no globulars will have disappeared by the current epoch. Thus, the GCS mass function at $m > m_*$ is effectively unchanged, even after a Hubble time, from the initial distribution. However, clusters with initial masses $m < m_*$ *can* have been removed from the system, and the GCS mass function below m_* may differ significantly from its initial form. If this low-mass end of the evolved $d\mathcal{N}/dm$ can also be described by a power-law, then the full, present-day GCS mass function is just

$$\left(\frac{d\mathcal{N}}{dm}\right)_{\text{obs}} = \begin{cases} K m_*^{\gamma_1 - \gamma_2} m^{-\gamma_1}, & m_\ell \leq m \leq m_* \\ K m^{-\gamma_2}, & m_* \leq m \leq m_u \end{cases}, \quad (5)$$

where $\gamma_1 < \gamma_2$ for consistency.

Observed GCSs do, in fact, have mass functions that conform to roughly this sort of double power law (Harris & Pudritz 1994; McLaughlin 1994; McLaughlin & Pudritz 1996)—although there is somewhat more structure than this at the highest cluster masses in $d\mathcal{N}/dm$, it can be safely ignored for the purposes of the present argument. Empirically, the mass scale m_* is *always* about $1.6 \times 10^5 M_\odot$; at this mass, the logarithmic slope of $d\mathcal{N}/dm$ changes rather abruptly from $\gamma_2 > 1$ to $\gamma_1 < 1$, with precise values that can vary slightly from galaxy to galaxy.² There are strong arguments to support the notion that observed GCS mass functions at $m > m_*$ are indeed accurate reflections of the formation distributions (namely, the high-mass sides of $d\mathcal{N}/dm$ in observed GCSs show no significant variation with galactocentric radius inside a single system, and are quite similar—though not identical—from galaxy to galaxy; see Harris & Pudritz 1994; McLaughlin & Pudritz 1996; Elmegreen & Efremov 1997). In addition, some theoretical studies (e.g., Surdin 1979; Okazaki & Tosa 1995; Vesperini 1997; Elmegreen & Efremov 1997) have suggested that the shallower slopes at lower masses might be caused entirely by dynamical evolution from an initial $d\mathcal{N}/dm \propto m^{-\gamma_2}$, roughly as described above. In reality, this view could very well be too extreme: empirically, the system of young super star clusters in the Antennae, which is not likely to have been severely affected by dynamical destruction, may have a mass function of the form (5) rather than (4) (Fritze-von Alvensleben 1999); and theoretically, such an initial shape to $d\mathcal{N}/dm$ may in fact be *preserved* during a Hubble time of dynamical evolution (Vesperini 1997). Thus, the intent here is not necessarily to argue for an

²It is this sharp change from an exponent of > 1 to one of < 1 at a well defined and nearly universal cluster mass that results in the characteristic peak of the globular cluster *luminosity* function in galaxies (the GCLF: the number of clusters per unit absolute magnitude, which is proportional to $d\mathcal{N}/d \ln m$; see McLaughlin 1994). This peak occurs at the luminosity corresponding to the mass m_* , i.e., at $M_V^0 \simeq -7.4$, for the $\Upsilon_V \simeq 2 M_\odot L_\odot^{-1}$ typical of globulars; its universality is what makes the GCLF attractive as a distance indicator (e.g., Jacoby et al. 1992; Whitmore 1997).

explanation of present-day GCS mass spectra in purely evolutionary terms, but to show that even if such is adopted as an extreme possibility, the implied time dependence of total GCS masses is quite weak.

Given equations (4) and (5), then, straightforward integrations allow for comparisons of the present GCS population to the initial one:

$$\frac{\mathcal{N}_{\text{tot}}^{\text{obs}}}{\mathcal{N}_{\text{tot}}^{\text{init}}} = \left(\frac{m_u}{m_*} \right)^{\gamma_2 - 1} \left\{ \frac{1 - (m_*/m_u)^{\gamma_2 - 1} + [(\gamma_2 - 1)/(1 - \gamma_1)][1 - (m_\ell/m_*)^{1 - \gamma_1}]}{(m_u/m_\ell)^{\gamma_2 - 1} - 1} \right\}, \quad (6)$$

and of the current total mass to its initial value:

$$\frac{M_{\text{gcs}}^{\text{obs}}}{M_{\text{gcs}}^{\text{init}}} = \left(\frac{m_*}{m_u} \right)^{2 - \gamma_2} \left\{ \frac{(m_u/m_*)^{2 - \gamma_2} - 1 + [(2 - \gamma_2)/(2 - \gamma_1)][1 - (m_\ell/m_*)^{2 - \gamma_1}]}{1 - (m_\ell/m_u)^{2 - \gamma_2}} \right\}. \quad (7)$$

Values of $\gamma_1 = 0.4$ and $\gamma_2 = 1.7$ may be taken as representative of the typical situation in elliptical galaxies (Harris & Pudritz 1994; McLaughlin 1994, 1995; McLaughlin & Pudritz 1996). With $m_\ell = 500 M_\odot$, $m_* = 1.6 \times 10^5 M_\odot$, and $m_u = 5 \times 10^6 M_\odot$, it is then easily seen that

$$\frac{\mathcal{N}_{\text{tot}}^{\text{obs}}}{\mathcal{N}_{\text{tot}}^{\text{init}}} = 0.036 \quad \text{and} \quad \frac{M_{\text{gcs}}^{\text{obs}}}{M_{\text{gcs}}^{\text{init}}} = 0.76 \quad (8)$$

in this simplistic scenario. Thus, *even though dynamical evolution reduces the total population of this hypothetical GCS by more than an order of magnitude, it diminishes the total mass by only $\sim 25\%$* . (The same line of argument also shows that the often appreciable uncertainties in the exact form of $d\mathcal{N}/dm$ at cluster masses $m < m_*$ —or even blind extrapolations from observations of only brighter clusters—do not seriously bias observational estimates of M_{gcs} in any galaxy.)

This result is best interpreted as an estimate for the possible depletion of a GCS *globally* (i.e., spatially averaged over the whole of a parent galaxy), because the values of γ_1 , γ_2 , and m_* used are taken from observations of $d\mathcal{N}/dm$ in projection, often over fairly large areas on the sky. Thus, the normalization K in equations (4) and (5) can be taken to include an implicit integration over galactocentric radius, and the exponents γ and mass scale m_* to be appropriate averages. The importance of these considerations is not actually clear, since radial dependences are not expected theoretically in current models for the initial GCS mass function (McLaughlin & Pudritz 1996; Elmegreen & Efremov 1997) and observational evidence for such trends at the current epoch is slight to non-existent (e.g., McLaughlin et al. 1994 and Harris et al. 1998; though see also Kavelaars & Hanes 1997 and Murali & Weinberg 1997b). Nevertheless, it should be noted that dynamical friction, gravitational shocks, and even evaporation couple to galactic tidal fields in such a way that if a GCS's present-day mass function *were* sculpted to any great extent by these processes, then the *local* ratios $\mathcal{N}_{\text{tot}}^{\text{obs}}/\mathcal{N}_{\text{tot}}^{\text{init}}$ and $M_{\text{gcs}}^{\text{obs}}/M_{\text{gcs}}^{\text{init}}$ would be expected to increase outwards from the center of the system, from values less than equation (8) at small galactocentric radii to near unity at large distances (e.g., beyond a stellar effective radius; see especially Murali & Weinberg 1997b).

Returning now to the main issue, the global efficiency of globular cluster formation in a galaxy may be defined as

$$\epsilon_{\text{cl}} \equiv M_{\text{gcs}}^{\text{init}}/M_{\text{gas}}^{\text{init}}, \quad (9)$$

where $M_{\text{gas}}^{\text{init}}$ refers to the total gas supply that was available to the protogalaxy, whether in a rapid monolithic collapse or, more likely, in a slower assembly (at high redshift) of many distinct, subgalactic clouds. From the preceding discussion, it is clear that if a newly formed GCS were able to evolve “passively”—that is, if its mass were potentially vulnerable only to reductions caused by forces internal to an isolated parent galaxy—then a present-day observation of M_{gcs} would suffice, to at least a $\sim 25\%$ level of accuracy globally, as a measure of $M_{\text{gcs}}^{\text{init}}$. Passive evolution also implies mass conservation for the galaxy as a whole, so that a reliable value for $M_{\text{gas}}^{\text{init}}$ could be obtained, at any epoch, from an inventory of the total mass in gas plus unclustered stars and stellar remnants. Thus, a good *observational estimate* of the global cluster formation efficiency in this simple situation is provided by

$$\hat{\epsilon}_{\text{cl}} \equiv \frac{M_{\text{gcs}}}{M_{\text{gas}} + M_{\text{stars}}}, \quad (10)$$

which is expected to be nearly a time-independent quantity.³

Realistically, of course, galaxies are not such pristine entities; interactions between systems may effect significant changes in both M_{gcs} and $(M_{\text{gas}} + M_{\text{stars}})$ over time, making it difficult to evaluate (or even clearly define) initial GCS and gas masses. For example, the formation history of an elliptical may include major mergers with gas-rich spiral systems, and it has been proposed that these might involve the formation of new globular clusters and substantial increases in M_{gcs} (e.g., Ashman & Zepf 1992; Kumai, Basu, & Fujimoto 1993a). Alternatively, additional globulars might be captured by a large galaxy that accretes small, gas-poor systems (e.g., Côté et al. 1998) or accumulates tidal debris from other members

³To be fully consistent, of course, the observational estimate of cluster formation efficiency should read $\hat{\epsilon}_{\text{cl}} = M_{\text{gcs}}/(M_{\text{gas}} + M_{\text{stars}} + M_{\text{gcs}})$; but, as §§3 and 4 below will show, M_{gcs} turns out *always* to be so small, relative to $(M_{\text{gas}} + M_{\text{stars}})$, that its contribution to the denominator of $\hat{\epsilon}_{\text{cl}}$ is utterly negligible.

in a cluster of galaxies (see Muzzio 1987). However, processes such as these also increase the total masses of gas and/or stars in the final system. In *large* galaxies (i.e., in those that do not suffer significant gas loss from strong galactic winds; cf. §4.2), any changes in the ratio $M_{\text{gcs}}/(M_{\text{gas}} + M_{\text{stars}})$ are bound to be smaller than changes in either of these quantities individually. The presently observed $\hat{\epsilon}_{\text{cl}}$ in any large galaxy with a complex dynamical history is then a mass-weighted average of the true ϵ_{cl} in some number of discrete star-formation events and individual accreted systems; and in the limit that the underlying efficiency of cluster formation is independent of environment and epoch (as the results of §§3 and 4 will suggest is nearly correct), it is still true that $\hat{\epsilon}_{\text{cl}} \simeq \epsilon_{\text{cl}}$ —just as in the case of passive evolution, and subject only to the small error associated there with the effects of GCS erosion by cluster evaporation and tidal disruption.

In gas-poor elliptical galaxies and the halos of spirals, equation (10) reduces to $\hat{\epsilon}_{\text{cl}} \simeq M_{\text{gcs}}/M_{\text{stars}}$, so that—as was mentioned above—the cluster formation efficiency can be obtained directly from observations of the global GCS specific frequency (cf. eq. [3]). More generally, however, ellipticals can contain large amounts of hot, X-ray emitting gas (e.g., Forman, Jones, & Tucker 1985), and when it happens that M_{gas} is non-negligible relative to M_{stars} , measurements of S_N are only low-order approximations to $\hat{\epsilon}_{\text{cl}}$ (which is itself only an estimate of the real efficiency ϵ_{cl}). Keeping this in mind, the observed systematics of both global *and* local GCS specific frequencies provide a useful starting point for an examination of the extent to which cluster formation efficiencies might vary from galaxy to galaxy, or from place to place within a single system.

2.2. The Specific Frequency “Problems”

As was intimated in the discussion around equation (3), not all galaxies have the same globular cluster specific frequency. There are several aspects to this: (1) Spiral galaxies tend to have lower S_N —at least when their GCS populations are normalized to their *total* (bulge plus disk) light—than do average ellipticals (Harris 1991). (2) Although a constant $S_N \approx 5$ is a fair *approximation* for many normal giant ellipticals, fits to the data suggest that, in fact, $S_N \propto L_{V,\text{gal}}^{0.2-0.3}$ (Kissler-Patig 1997; cf. Santiago & Djorgovski 1993). At the extremes of the early-type galaxy sequence, moreover, (3) the S_N values for centrally dominant or first-ranked members of galaxy clusters show a much steeper dependence on galaxy luminosity— $S_N \propto L_{V,\text{gal}}^{0.8}$ or so is implied by the correlations of Blakeslee (1997) and Harris et al. (1998)—and (4) specific frequencies actually appear to increase towards *lower* luminosities in dwarf ellipticals: $S_N \propto L_{V,\text{gal}}^{-0.4}$ (Miller et al. 1998; see also Durrell et al. 1996). Thus, some brightest cluster galaxies, and some of the faintest dwarfs, have global specific frequencies that exceed the “average” by factors of 3 or 4. All in all, observed S_N values span a range from ~ 1 to ~ 20 .⁴

As will be shown in §4 below, the first two of these points can be understood fairly easily. Here, it suffices to note that (1) when only the *halo* stars and globular clusters in the Milky Way are considered, and allowances made for the lower Pop. II mass-to-light ratio in our Galaxy vs. large ellipticals, $\hat{\epsilon}_{\text{cl}}$ here is no different from that in “normal” early-type systems. It is reasonable to expect that this result—which is contrary to the claim made by Zepf & Ashman (1993)—should hold in other spirals as well. Also, (2) the observed dependence of S_N on $L_{V,\text{gal}}$ among non-brightest cluster ellipticals is fully consistent with that expected from equation (2) for gas-poor systems with a uniform efficiency of cluster formation ($\hat{\epsilon}_{\text{cl}} \simeq M_{\text{gcs}}/M_{\text{stars}}$) and a mass-to-light ratio (Υ_V) that scales with luminosity in the way observed for galaxies in the fundamental plane. However, if taken at face value, items (3) and (4) just above appear to imply that GCS formation efficiencies can vary by as much as an order of magnitude from galaxy to galaxy, in a non-monotonic fashion and for reasons that have never been understood. These issues are not so readily dismissed. The high S_N “phenomenon” in many first-ranked cluster ellipticals, especially, has been discussed at length in the literature (e.g., McLaughlin et al. 1994; Harris et al. 1995; West et al. 1995; Forbes et al. 1997; Blakeslee 1997; Blakeslee et al. 1997; Harris et al. 1998), and is referred to here as the *first specific frequency problem*. Equally non-trivial, though only more recently recognized, is the *inverse* variation of S_N with $L_{V,\text{gal}}$ among dwarf ellipticals.

Local specific frequencies, which are obtained for a single GCS by comparing its projected radial distribution to its galaxy’s surface brightness profile (normalized as in eq. [1]), are also of interest here; they are related in the obvious way to the efficiency of cluster formation as a function of (projected) galactocentric radius, R_{gc} . Of particular importance is the fact that S_N is seen to be an *increasing* function of R_{gc} in many galaxies. This is equivalent to the well known fact that GCSs are often less centrally concentrated than the stellar halos of their parent galaxies. This statement has two contexts, which must be separated. First, it seems that the GCS of most any galaxy—spiral or elliptical, small or large—has an apparent core radius that is significantly larger than that of the unclustered field stars (e.g., Djorgovski & Meylan 1994; Lauer & Kormendy 1986; McLaughlin 1995; Forbes et al. 1996; Minniti, Meylan, & Kissler-Patig 1996; Côté et al. 1998); that is, the *central regions* of GCSs show projected radial distributions with slopes that are significantly shallower than those of the light profiles on kpc scales, so that the density ratio of the two halo components is an increasing function of radius. Second, the GCSs of some large galaxies are spatially more extended than the stellar halos on *larger scales*, $R_{\text{gc}} \sim 10$ –100 kpc (Harris & Racine 1979; Harris 1986). However, this is a less general result than that relating to the large core radii of globular cluster systems. It is true of many dominant cluster galaxies like M87 in Virgo (see the discussion in McLaughlin et al. 1995), and also of the M31 halo (Pritchett & van den Bergh 1994); but many elliptical systems (e.g., Durrell et al. 1996; Kissler-Patig et al. 1997), and the Milky Way itself (Harris 1976; Zinn 1985), show GCS and halo-star distributions that are in quite close agreement (and, thus, a constant local S_N) outside of any core regions. The physical factors that govern whether the GCS density falls off at the same rate as or more slowly than the

⁴It has also been claimed (Harris 1991; West 1993; Kumai, Hashi, & Fujimoto 1993b) that early-type galaxies in sparse groups have systematically lower S_N than those in high-density cluster environments. However, this correlation is uncertain, and apparently rather weak; if it does prove to be important, it will most likely be as a higher-order correction to the more basic trends discussed here.

unclustered halo density in a given system have not yet been identified. (No case has ever been found in which a GCS radial distribution is *steeper* than a galaxy's light profile.)

The first of these points is not easily related to the radial dependence of cluster formation efficiencies because, as was suggested in §2.1, the dynamical mechanisms that act to destroy globulars work most efficiently at small R_{gc} , where the stellar densities are highest. Although the cores of GCSs could quite plausibly have always been somewhat larger than those of halos or bulges generally (e.g., Harris & Pudritz 1994; Côté et al. 1998), it seems inevitable that any initial discrepancies must have been augmented by an inside-out erosion of the cluster system from tidal shocking, dynamical friction, and evaporation (Ostriker et al. 1989; Capuzzo-Dolcetta 1993; Murali & Weinberg 1997b). Detailed modelling is therefore required to disentangle the effects of formation and evolutionary processes in this instance. At galactocentric radii greater than a few kpc, however, the timescales on which the evolutionary mechanisms operate can exceed a Hubble time, and the studies cited here show that dynamics will not significantly affect GCS radial distributions beyond about one effective radius in the stellar halo (see also Aguilar et al. 1988). Thus, to the extent that the assumption $\bar{\epsilon}_{cl} \simeq M_{gcs}/M_{stars}$ is valid, the distension of GCSs relative to stellar halos and the concomitant systematic increase in local S_N in the outer parts of *some* galaxies would seem to say that bound clusters were sometimes (but not always, and for unknown reasons) *more* likely to form at larger R_{gc} , in gas that was presumably at lower ambient densities and pressures. This situation will be referred to as the *second specific frequency problem*.

It is clearly of interest, from the points of view of both galaxy and star formation, to verify whether these global and local S_N variations really do reflect differences in ϵ_{cl} —and, if so, to understand their origins. Accordingly, much attention has been paid to the first S_N problem in particular, usually in efforts to empirically correlate the S_N measurements for brightest cluster galaxies (BCGs) with global properties of the galaxies themselves or of the clusters they inhabit. One such correlation does appear to be of fundamental importance, as will be discussed momentarily, but it suggests that S_N varies in the face of *constant* ϵ_{cl} . Indeed, no proposed solution of the first specific frequency problem has identified a physical mechanism that could possibly lead to the superefficient production of bound star clusters in some galaxies (see the references given above). In fact, one suggestion—that high global specific frequencies (meaning $S_N \gtrsim 5$) in centrally located BCGs result from the acquisition of globulars and stars which are tidally stripped from the outer, high- S_N regions of other galaxies in a cluster—actually appears to rely on the existence of the *second* specific frequency problem (see Forbes et al. 1997; Côté et al. 1998); but this is itself essentially unexplained.⁵ Nor, to date, has any explanation (or prediction) been given for the high S_N that have now been observed in many faint dwarf galaxies.

The view is taken here that *the second specific frequency problem is inseparable from the first*, in the specific sense that both relate to the possible influence of environment on the probability of bound cluster formation. Any real insight into either one of these issues must therefore include a better understanding of the other. This view is in keeping with recent evidence (Forbes et al. 1997; Kissler-Patig 1997; van den Bergh 1998) for at least a rough correlation between global S_N values and GCS density-profile slopes in elliptical galaxies: those GCSs with the highest specific frequencies tend also to have the shallowest radial distributions. Such a correspondence hints strongly at (although it does not directly show) an intimate connection between an increasing local S_N and a high global S_N .

A significant development in this field has come with the recent recognition of a correlation between the global specific frequencies of BCGs and the X-ray luminosity of the hot gas in their parent clusters (West et al. 1995; Blakeslee 1997; Blakeslee et al. 1997). A relatively large and homogeneous sample of BCGs shows S_N values that increase from about 4, in clusters with X-ray luminosities (on 500-kpc scales) $L_X \sim 10^{42}$ erg s⁻¹ at 0.5–4.5 keV, to $S_N \simeq 12$ for $L_X \sim 10^{45}$ erg s⁻¹. Three different interpretations have already been attached to this result:

West et al. (1995) propose that it points to the existence of intergalactic globulars which collect naturally at the centers of galaxy clusters and are superimposed in projection on any galaxy there. This would certainly boost the apparent total population N_{tot} of a central BCG, so that globulars need not have formed in situ with abnormally high specific frequency; but they would still have had to do so elsewhere in the cluster (see also Côté et al. 1998; Harris et al. 1998).

In a different approach, Blakeslee (1997) and Blakeslee et al. (1997) consider L_X to be mainly a reflection of the temperature of intracluster gas, and thus a measure of a cluster's mass and the depth of its potential. They then claim that the observed S_N – L_X correlation is consistent with the globulars in BCGs having formed in numbers directly proportional to the *total* mass, including dark matter, of their *entire* galaxy clusters (see Kavelaars 1998 for a similar suggestion on the scale of individual galaxies). In this scenario, cluster formation would obey a universal efficiency of sorts—although one which is quite different from that discussed here—and the first S_N problem would result from some process that caused the BCGs in more massive clusters to be systematically underluminous (i.e., underefficient in the production of unclustered field stars). Here, however, the role that the dark matter content of a galaxy cluster might play in the formation of globular clusters is not clear. Moreover, any rule such as $M_{gcs}^{init}/(M_{gas}^{init} + M_{dark}) = \text{constant}$ clearly can apply over only a limited range of conditions.

⁵It should be noted that the second S_N problem, and local specific frequencies generally, are not typically discussed in terms of cluster formation efficiencies, even though it is well understood that global S_N are of interest in this regard. The reason for this may be that mismatches between GCS and stellar radial distributions in E galaxies are usually attributed either to the globulars having formed “slightly before” the bulk of the unclustered halo stars (in a dissipational collapse scenario; Harris 1986), or to the expectation that a cluster system will be “puffed up” relative to the final light profile of an elliptical that forms in one or more major mergers of gas-rich systems with pre-existing GCSs (Ashman & Zepf 1992; Zepf & Ashman 1993). In either case, no particular radial variation in ϵ_{cl} would necessarily be required. However, the first of these arguments has not been sufficiently well developed to account quantitatively for the observed magnitude of the second S_N problem; and the second is actually inconsistent with the observation that systems with higher global S_N have spatially more extended GCSs (see the discussion of Forbes et al. 1997). Nor is it apparent, from either these suggestions, why there are also many galaxies whose GCSs and stellar halos have the *same* density profiles.

Thus, Harris et al. (1998) instead pursue the hypothesis that GCSs formed with a constant ϵ_{cl} defined essentially as in equation (9) above. This is adopted as a working *assumption* by Harris et al., who construct plausibility arguments for a universal value of $\epsilon_{\text{cl}} \sim 10^{-3}$ (as could be expected) and suggest that the higher global S_N in more X-ray luminous BCGs might have resulted from stronger (partial) galactic winds which heated larger fractions of their initial gas supplies to keV temperatures after an early bout of star and globular cluster formation. Such hot gas would be largely removed from further star formation—but still confined to the vicinity of these central cluster galaxies—and the final BCGs would be optically underluminous as a result.

It is this basic idea that is closest to the discussion in this paper (although many aspects of the quantitative analysis here differ significantly from those in Harris et al. 1998). That is, the fundamental point of the global S_N – L_X correlation for BCGs is the associated implication that the first specific frequency problem may stem, not from intrinsic variations in the global ϵ_{cl} of these systems, but from the fact that they can contain large amounts of gas. High gas mass ratios invalidate the assumption that $\hat{\epsilon}_{\text{cl}} \simeq M_{\text{gcs}}/M_{\text{stars}}$, and therefore cause S_N to overestimate the true globular cluster formation efficiency. If it is correct to infer from this that the “excess” globulars in systems with high global S_N are associated with hot gas, then the fact that the distribution of gas is generally more extended than that of the stars in ellipticals (e.g., Trinchieri, Fabbiano, & Canizares 1986; Fabbiano 1989) suggests a possible explanation for the second specific frequency problem as well as the first. These two issues would then be closely related—possibly even just different aspects of a single phenomenon—as was suggested above; and both might be settled simply by measuring the full estimator $\hat{\epsilon}_{\text{cl}} = M_{\text{gcs}}/(M_{\text{gas}} + M_{\text{stars}})$ both locally and globally in individual systems.

In the next Section, this universal- ϵ_{cl} hypothesis is *tested*, for the first time, by evaluating the observable $\hat{\epsilon}_{\text{cl}}$ as a function of galactocentric radius in each of the galaxies M87, M49, and NGC 1399. It turns out that the inclusion of the X-ray gas in M87 is indeed key to the alleviation of both the first and the second S_N problems there: once this is done, $\hat{\epsilon}_{\text{cl}}$ is constant locally, and essentially the same globally, in all three of these systems. The discussion is expanded to include other giant ellipticals and BCGs, as well as dwarf ellipticals, in §4. It is shown directly that all available GCS data are consistent with a single efficiency of cluster formation. Notably, the increase of S_N towards low $L_{V,\text{gal}}$ in the dwarfs (Miller et al. 1998; Durrell et al. 1996) can be explained in terms of this universal ϵ_{cl} once allowances are made for the effects of the violent gas outflows (a more extreme version of the feedback envisioned by Harris et al. 1998 for BCGs) that were driven by early bursts of star formation in these low-mass systems.

3. CASE STUDIES OF THREE GALAXIES

M87, M49, and NGC 1399 are ideally suited to a closer examination of these issues, for three reasons: (1) They are relatively nearby, making it possible to observe internal trends within the systems in the first place. M87 and M49 both are assumed here to lie at a distance of $D = 15$ Mpc, appropriate for the core of the Virgo Cluster (Pierce et al. 1994; Freedman et al. 1994). A relative distance modulus of $\Delta(m - M)[\text{Fornax} - \text{Virgo}] = 0.2$ (e.g., McMillan, Ciardullo, & Jacoby 1993; Tonry et al. 1997) then puts NGC 1399 at $D \simeq 16.5$ Mpc. (2) Each is a giant elliptical (M87 and NGC 1399 are actually type cD), and is therefore accompanied by a large GCS: $N_{\text{tot}} \simeq 13\,500$ for M87; 6 900 for M49; and 4 700 in NGC 1399 (e.g., Harris 1991; see also §5 below). And, most importantly, (3) even this small sample of three galaxies suffices to bring out all aspects of the two specific frequency problems summarized in §2.2: M87, as is well known, suffers from both; M49 does not show the first, but has long been thought to exhibit the second; and NGC 1399 has been claimed as an example of the first problem, but not the second.

Because of their proximity, these systems have been well studied in all respects of importance here. *B*-band surface photometry extends in M87 to a projected galactocentric radius of about $22' \simeq 95$ kpc (de Vaucouleurs & Nieto 1978, 1979); in M49, to a similar distance (King 1978; Caon, Capaccioli, & D’Onofrio 1994); and in NGC 1399, to $R_{\text{gc}} \simeq 14.5 = 70$ kpc (Killeen & Bicknell 1988; Caon et al. 1994). These measurements are easily converted to projected stellar mass density profiles $\Sigma_{\text{stars}}(R_{\text{gc}})$, as mass-to-light ratios have been obtained from a spectroscopic analysis applied uniformly to all three systems (van der Marel 1991). X-ray observations, which have been made with several different satellites, yield gas densities over still larger areas around each galaxy. Here, use will be made of the *ROSAT* data for M87 (taken from Nulsen & Böhringer 1995); of *ROSAT* data for M49 (Irwin & Sarazin 1996); and of *Einstein* observations in NGC 1399 (Killeen & Bicknell 1988). These studies all give the *volume* electron density $n_e(r_{\text{gc}})$, as a function of *three-dimensional* galactocentric radius, derived either from fits of a parametric function to the projected X-ray brightness profile or from a direct deprojection of the same. Finally, integrated optical magnitudes have been measured for globular clusters in these galaxies at radii $R_{\text{gc}} \sim 1 - 100$ kpc—generally, over most of the areas covered by the surface photometry of unresolved halo stars. These are used to construct projected GCS number densities, $N_{\text{cl}}(R_{\text{gc}})$, which are trivially converted to mass profiles, Σ_{cl} , once a mean globular cluster mass is specified. For M87, relevant investigations are those of Harris & Smith (1976), Harris (1986), Grillmair, Pritchet, & van den Bergh (1986), Lauer & Kormendy (1986), Cohen (1988), McLaughlin et al. (1993, 1994), McLaughlin (1995), Whitmore et al. (1995), and Harris et al. (1998). Data on M49 can be found in Harris & Petrie (1978), Harris & van den Bergh (1981), Harris (1986), Harris et al. (1991), and Lee, Kim, & Geisler (1998). The GCS of NGC 1399 has been observed by Hanes & Harris (1986), Bridges, Hanes, & Harris (1991), Wagner et al. (1991), and Kissler-Patig et al. (1997).

While surface brightness profiles and X-ray gas densities often can be obtained for most of an entire galaxy with a single set of observations—as is the case in the studies cited above—this is generally *not* so for GCS radial distributions. Older, photographic surveys, which did have large ($R \sim 100$ kpc) fields of view, were hampered by rather bright limiting magnitudes that became systematically more so towards smaller galactocentric radii. Newer, CCD photometry achieves deeper limiting magnitudes, and digital data reduction techniques can quantify and correct for any spatial variations; but

until very recently, CCD fields of view were quite small, and best suited to analyses of the central regions ($R_{gc} \lesssim 10$ kpc) of GCSs. Thus, the first step in comparing the stellar, gaseous, and globular cluster contents of any large galaxy is to combine existing photographic and CCD GCS data into a single, composite radial distribution that gives the projected density $N_{cl}(R_{gc})$, to a uniform limiting magnitude, over as large a range of galactocentric radius as possible. This is done for each of M87, M49, and NGC 1399 in §3.1. But then, the surface densities of stars and GCSs are related to their volume densities by an integral of the form $\Sigma \propto \int \rho dz$, while the observed X-ray brightness along some line of sight is proportional to $\int \rho_{gas}^2 dz$. A direct intercomparison of the *raw* GCS, optical, and X-ray imaging data in a galaxy therefore makes little sense. Thus, to discuss these three components simultaneously in M87, M49, and NGC 1399, either (1) their GCS and stellar surface densities can be deprojected and compared to their derived gas volume densities, or (2) the gas surface densities, $\Sigma_{gas}(R_{gc}) \propto \int \rho_{gas}(r_{gc}) dz$, can be obtained from the published volume density profiles and compared to the directly observed $\Sigma_{stars}(R_{gc})$ and $\Sigma_{cl}(R_{gc})$. The results of these two separate exercises are presented in §§3.2 and 3.3.

3.1. GCS Surface Densities

When joining GCS radial distributions from two or more separate studies of the same galaxy, two important factors must be taken into account. First, the GCS of a distant galaxy (essentially, any with $D \gtrsim 5$ Mpc) is usually identified as a centrally concentrated excess of point-like sources, above a more uniform distribution of unresolved background galaxies and foreground stars. The surface density of this “background,” N_b , is subtracted from the total density of point sources at any R_{gc} to form the surface density profile N_{cl} of the GCS alone; but N_b is a function of seeing conditions, detector characteristics, and limiting magnitude. Background corrections must therefore be applied separately to each of the datasets to be combined. Second, differences in limiting magnitude (call this V_{lim}) are of further importance because a deep survey will clearly see more globulars, at a given R_{gc} , than one with a bright limit. Before they can be simply matched onto one another, then, distinct background-corrected profiles $N_{cl}(R_{gc})$ must be normalized to the same effective V_{lim} .

The published GCS observations that will be used here for M87, M49, and NGC 1399 are summarized in Table 1. These papers were selected from the more numerous references cited above, simply because they tabulate all of the relevant data in full. The third column of Table 1 gives the minimum and maximum R_{gc} contained in each study’s field of view (note that $1' = 4.363$ kpc for a distance of $D = 15$ Mpc to M87 and M49, while $D = 16.5$ Mpc for NGC 1399 implies $1' = 4.800$ kpc); Column 4 gives the background surface density to the limiting magnitude in Column 5; and Column 6 lists the scalings applied to each dataset to bring them all to a common V_{lim} .

Generally, the background levels N_b have been determined and applied by the original authors, either from observations of a blank field near the observed GCS, or from “on-frame” extrapolations of counts at the edges of the GCS field itself (see Harris 1986); these values are reproduced in Table 1 only for completeness. The single exception to this is the M49 study of Lee et al. (1998), for which N_b has been derived here, using the method of Harris (1986). (It is possible, particularly

TABLE 1
PUBLISHED GCS RADIAL DISTRIBUTIONS

Galaxy and GCLF Parameters	Source	Radial Coverage (arcmin)	Background Density (arcmin ⁻²)	V_{lim} (mag)	Scale Factor
M87 $V^0 = 23.70$ $\sigma_V = 1.39$	McLaughlin (1995) ¹	0.153 – 1.965	3.5 ± 0.8	23.9	1.000
	McLaughlin et al. (1993)	1.210 – 9.090	6.3 ± 0.4	24.0	0.954
	Harris (1986)	1.000 – 22.52	5.8 ± 0.3	23.4	1.35
M49 $V^0 = 23.75$ $\sigma_V = 1.30$	Harris & Petrie (1978) ²	2.000 – 19.69	4.3 ± 0.3	23.3	1.000
	Harris & van den Bergh (1981) ²	0.732 – 12.15	3.3 ± 0.5	...	0.86 ³
	Harris et al. (1991)	0.600 – 2.304	2.88 ± 0.45	23.8	0.707
	Lee et al. (1998)	0.900 – 7.167	2.95 ± 0.30	23.45	0.892
NGC 1399 $V^0 = 23.90$ $\sigma_V = 1.20$	Kissler-Patig et al. (1997)	0.761 – 9.463	6.1 ± 0.3	24.0	1.000
	Hanes & Harris (1986)	0.734 – 13.97	5.40 ± 0.45	23.4	1.575

¹See also Harris et al. (1998).

²As given by Harris (1986).

³See the discussion of Harris (1986).

with on-frame estimates, to overestimate N_b and produce spurious curvature at large radii in a subtracted N_{cl} profile. As is discussed below, however, this is not a major concern in the composite GCS radial distributions obtained here.) The limiting magnitudes V_{lim} in Table 1 are also those quoted in the original papers.⁶ These have been used to renormalize the individual N_{cl} profiles, by adopting—for computational convenience—a standard Gaussian approximation to the globular cluster luminosity function (GCLF, $dN/d \ln m$; cf. §2.1). That is, with the number of globulars at a given apparent magnitude given roughly by $dN/dV \propto \exp[-(V - V^0)^2/2\sigma_V^2]$ (see Harris 1991), then the density of clusters to some limiting magnitude, say $N_{cl}(V \leq V_{lim,2})$, is referred to the density up to some other limit, i.e., $N_{cl}(V \leq V_{lim,1})$, through

$$\frac{N_{cl}(V \leq V_{lim,1})}{N_{cl}(V \leq V_{lim,2})} = \frac{1 + \text{erf}[(V_{lim,1} - V^0)/\sqrt{2}\sigma_V]}{1 + \text{erf}[(V_{lim,2} - V^0)/\sqrt{2}\sigma_V]} . \quad (11)$$

The right-hand side of this expression is just the scaling factor given in Column 6 of Table 1, where $V_{lim,1}$ for each GCS has been taken as the observed limiting magnitude in the first of each set of references. Thus, the published radial distributions for M87 have all been normalized to an effective $V_{lim} = 23.9$; for M49, to $V_{lim} = 23.3$; and to $V_{lim} = 24.0$ in NGC 1399. The Gaussian peaks V^0 and dispersions σ_V used in equation (11) are given in the first column of Table 1. These parameters are taken from the fits of Whitmore et al. (1995) and Harris et al. (1998) to the M87 GCLF, from Lee et al. (1998) for M49, and from Kohle et al. (1996) for NGC 1399. Note that all of the scale factors derived here are rather modest, and thus do not introduce significant uncertainty into the final, combined N_{cl} profiles.

A few practical notes should be made regarding this scaling procedure. First, it is applied to the GCS densities at every observed galactocentric radius, and it therefore assumes that there is no intrinsic radial variation in the GCLF or the underlying GCS mass function. As was also mentioned in §2.1 above, this is a reasonable assumption that is directly supported by the observations themselves. Second, the limiting magnitudes for the photographic studies of Harris & Petrie (1978) and Harris (1986) are rather poorly determined; Harris quotes only approximate ranges for V_{lim} . The values adopted here, which are fully consistent with these ranges, have been chosen to give scaled $N_{cl}(R_{gc})$ that agree well with more recent CCD studies with accurately known V_{lim} . And third, the scaling applied to the M49 GCS counts of Harris & van den Bergh (1981) has not been calculated in this way at all; rather, the factor of 0.86 is derived, by Harris (1986), by requiring a good overall agreement with the N_{cl} profile of Harris & Petrie (1978).

The results of this exercise are illustrated in Fig. 1. Clearly, the different projected density profiles in each GCS

⁶Not all of the photometry in these studies is in the V band, however. A mean globular cluster color of $V - R = 0.5$ has been adopted to convert the R -band data of McLaughlin (1995) to V magnitudes; a mean $V - T_1 = 0.45$ brings the Washington photometry of Lee et al. (1998) onto the same system; and approximate transformations between photographic and V -band magnitudes are discussed in Harris' earlier papers on M87 and M49.

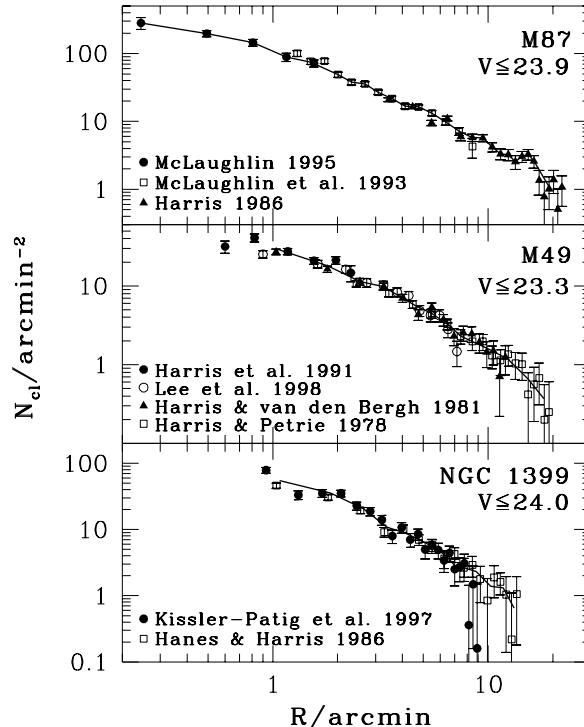


FIG. 1.— Published surface density profiles $N_{cl}(R_{gc})$ for the GCSs of M87, M49, and NGC 1399. Points refer to individual studies, normalized as in Table 1 to the effective limiting magnitudes indicated; bold lines describe the composite distributions given in Tables 2, 3, and 4.

corroborate each other. It remains only to extract a single N_{cl} at each R_{gc} , in each system, from the overlapping data that have been collected. It is not generally possible to simply average different densities at a given R_{gc} , since profiles such as these are constructed by counting clusters in a series of wide, circular annuli that need not coincide from study to study. Instead, Fig. 1 shows that a perfectly acceptable approach is to simply adopt one of the (scaled) profiles over some range in R_{gc} , and then switch to any other that might extend beyond that range. At this point, it must be kept in mind that ultimately the data will be deprojected to yield volume GCS densities, $n_{\text{cl}}(r_{\text{gc}})$. The method developed in the Appendix to do this requires that the inner and outer radii be known for the annuli used to define the composite N_{cl} . This further restricts the useful published datasets to those which contain this information on the radial bins as well (that is, *in addition* to just a density and a mean radius for each annulus).

In M87, then, a composite GCS profile is derived by using the data of McLaughlin (1995) from $R_{\text{gc}} = 0'.153$ to $R_{\text{gc}} = 1'.870$; those of McLaughlin et al. (1993) from $1'.870$ to $7'.870$; and those of Harris (1986) from $7'.870$ to $22'.52$. (In order to make annuli that do not overlap in the final N_{cl} , some interpolation is applied to the datasets around the matching points at $1'.870$ and $7'.870$.) For M49, the scaled profile of Harris & van den Bergh (1981) is used over $0'.732 \leq R_{\text{gc}} \leq 10'.96$, and that of Harris & Petrie (1978) for $10'.96 \leq R_{\text{gc}} \leq 19'.69$. And in NGC 1399, the densities of Kissler-Patig et al. (1997) are adopted for $0'.761 \leq R_{\text{gc}} \leq 7'.571$, with the data of Hanes and Harris (1986) continuing on out to $R_{\text{gc}} = 13'.97$. In all cases, CCD data have usually been chosen over photographic data in any regions of overlap. However, superseding this preference is a concern over possible errors in the background estimation N_b ; where this seems too high—for example, when the background-subtracted N_{cl} at the largest radii in a smaller-scale CCD study drop significantly below the densities indicated by a more extensive photographic survey (as in the outermost data points of Kissler-Patig et al. 1997 for NGC 1399)—the photographic profiles are given precedence. Enforcing consistency in this way between independent GCS datasets ensures that the question of potentially overestimated N_b values remains an issue only at the largest radii (beyond the regime of any overlap) in the widest-field observations of each galaxy.

The composite radial distributions thus obtained are listed in the third columns of Tables 2 through 4, as average surface densities in series of concentric circular annuli (with inner, outer, and average projected radii given in the first and second columns of the Tables). They are also drawn as the bold lines in the three panels of Fig. 1. There are two details of particular note. First, the densities for the innermost two annuli in M49 have been scaled up from the (already renormalized) GCS profile of Harris & van den Bergh (1981), by a further factor of 1.1, to put the composite N_{cl} at small radii into better agreement with the CCD data of Harris et al. (1991) and Lee et al. (1998). This ad hoc correction most likely just reflects some residual incompleteness in the photographic GCS counts at small R_{gc} , and in any event does not significantly affect the results which follow. Second, all of the N_{cl} profiles have been smoothed somewhat by rebinning, in order to allow for a more stable deprojection in §3.2 below: the outermost six annuli of Harris (1986) are combined into one for the M87 profile; the outermost 11 rings of Harris & Petrie (1978) are blended into 4 for M49; and the last 8 radial bins of Hanes & Harris (1986) become 4 in the NGC 1399 GCS. (As an added benefit of this smoothing, any possible errors in the subtracted N_b are expected to affect only the outermost *one or two points* in the final N_{cl} profiles.) Similarly, counts in the “Northeast” and “Northwest” sectors of NGC 1399 in the analysis of Kissler-Patig et al. (1997; see their Table 8) have been added together in every annulus they define; and these annuli have been combined in pairs to give the coarser profile in Table 4 here.

Given these radial distributions, it is a simple matter to derive the total *mass* surface density profiles of the GCSs. This requires, first, another multiplicative scaling of $N_{\text{cl}}(R_{\text{gc}})$ in each case, so that the number density of *all* globulars is properly reflected. (Note that the observations used here reach limiting magnitudes which are just at, or brighter than, the peak of the symmetric Gaussian that best fits the GCLF. This implies that most of the faint globulars are lost in the noise in these studies, and that half or fewer have been directly observed at any R_{gc} .) These final correction factors are obtained from equation (11) above, by setting $V_{\text{lim},1} = \infty$ and putting $V_{\text{lim},2}$ at the effective limit for each composite N_{cl} . In this way, it is found that the M87 distribution in Table 2 should be multiplied by 1.795; the M49 densities in Table 3, by 2.743; and the NGC 1399 numbers, by 1.875. Once this is done, the total number densities are multiplied by a mean globular cluster mass to obtain the mass densities $\Sigma_{\text{cl}}(R_{\text{gc}})$.

The mean cluster mass adopted here is $\langle m \rangle_{\text{cl}} = 2.4 \times 10^5 M_{\odot}$, which (as was mentioned in §2.1 above) is the value for the Milky Way GCS. In both its shape *and* its mass scale, the Galactic GCLF, or mass function, bears enough similarity to those of the cluster systems being discussed here (and, indeed, to most others: Harris 1991) that the same $\langle m \rangle_{\text{cl}}$ may safely be applied to them as well. The only issue is whether or not there is any systematic radial trend in mean globular cluster masses. It was also pointed out in §2.1 that there are no strong radial dependences observed in the GCLF of M87 (McLaughlin et al. 1994; Harris et al. 1998), suggesting that $\langle m \rangle_{\text{cl}}$ is constant with r_{gc} in this galaxy, and thus likely also in similar systems like M49 and NGC 1399. The question can be addressed in more detail only for the Milky Way, which—although clearly an imperfect substitute for these giant ellipticals—is the only galaxy where accurate luminosities and three-dimensional galactocentric distances both can be assigned to globulars on an individual basis.

Figure 2 shows that there is no dependence on radius in the observed $\langle m \rangle_{\text{cl}}$ of the Milky Way. The top panel plots the volume number density of globulars in the Galactic halo, derived from the database of Harris (1996); drawn as the solid line is a least-squares fit of a parametric density distribution in the family discussed by Dehnen (1993) and Tremaine et al. (1994). (Only metal-poor clusters have been counted, as these are the ones that display true halo kinematics: Zinn 1985; Minniti 1995.) In the bottom panel, the total *V*-band luminosities of the clusters (taken again from Harris 1996) have been summed separately in each radial bin, and converted to total cluster masses by applying a mass-to-light ratio of $\Upsilon_V = 2$ (Mandushev, Spassova, & Staneva 1991; Pryor & Meylan 1993). The mass densities ρ_{cl} that result are shown as the circular points. The solid line now corresponds to the same n_{cl} fit from the top panel, but multiplied by the average

TABLE 2
DENSITY PROFILE OF THE M87 GCS¹

Radius (arcmin)	R_{gc} (ave.)	N_{cl} (arcmin ⁻²)	r_{gc} (ave.)	n_{cl} (arcmin ⁻³)
0.153 – 0.328	0.244	282.6±55.8	0.245	243.7±155.6
0.328 – 0.655	0.494	197.2±19.9	0.505	89.34±34.01
0.655 – 0.983	0.808	145.3±16.5	0.827	68.58±20.55
0.983 – 1.310	1.157	89.10±12.40	1.152	18.16±12.94
1.310 – 1.870	1.500	74.46±8.78	1.602	19.33±5.23
1.870 – 2.160	2.010	48.92±4.25	2.018	11.36±3.56
2.160 – 2.490	2.320	37.81±3.26	2.328	4.015±2.391
2.490 – 2.880	2.680	35.75±2.80	2.689	6.404±1.722
2.880 – 3.320	3.090	26.93±2.05	3.104	3.423±1.183
3.320 – 3.830	3.570	21.74±1.65	3.580	2.875±0.818
3.830 – 4.430	4.120	16.78±1.34	4.135	0.926±0.587
4.430 – 5.110	4.760	16.38±1.23	4.776	1.447±0.469
5.110 – 5.900	5.490	13.26±1.13	5.512	1.202±0.360
5.900 – 6.820	6.350	9.79±0.93	6.368	0.768±0.271
6.820 – 7.870	7.330	7.16±0.96	7.354	0.442±0.219
7.870 – 8.973	8.403	5.82±0.73	8.431	0.184±0.166
8.973 – 9.962	9.454	5.68±0.69	9.474	0.346±0.154
9.962 – 10.95	10.44	4.20±0.65	10.46	0.222±0.135
10.95 – 11.93	11.43	3.32±0.61	11.45	0.079±0.124
11.93 – 12.92	12.42	3.23±0.61	12.43	0.156±0.120
12.92 – 13.90	13.40	2.55±0.58	13.41	0.008±0.113
13.90 – 14.87	14.38	3.05±0.57	14.39	0.067±0.104
14.87 – 15.84	15.35	3.27±0.57	15.36	0.143±0.103
15.84 – 16.81	16.32	2.59±0.55	16.33	0.212±0.093
16.81 – 22.52	19.46	1.01±0.43	19.77	0.024±0.010

¹Limiting magnitude $V_{\text{lim}} = 23.9$; divide by 0.5572 to obtain the density over all magnitudes.

TABLE 3
DENSITY PROFILE OF THE M49 GCS¹

Radius (arcmin)	R_{gc} (ave.)	N_{cl} (arcmin ⁻²)	r_{gc} (ave.)	n_{cl} (arcmin ⁻³)
0.732 – 1.464	1.035	29.83±2.53	1.129	8.041±1.684
1.464 – 2.196	1.793	18.00±1.61	1.848	3.818±0.874
2.196 – 2.928	2.536	11.40±1.11	2.575	1.163±0.543
2.928 – 3.660	3.274	9.82±1.06	3.304	1.307±0.426
3.660 – 4.392	4.009	7.02±0.80	4.034	0.759±0.292
4.392 – 4.996	4.684	5.48±0.63	4.699	0.464±0.279
4.996 – 5.992	5.471	4.51±0.59	5.505	0.384±0.169
5.992 – 6.988	6.471	3.29±0.52	6.500	0.276±0.138
6.988 – 7.981	7.467	2.30±0.48	7.493	0.120±0.120
7.981 – 8.973	8.462	1.97±0.45	8.484	0.092±0.097
8.973 – 10.95	9.912	1.62±0.31	9.985	0.070±0.044
10.95 – 13.90	12.33	1.18±0.23	12.47	0.054±0.026
13.90 – 16.81	15.28	0.66±0.22	15.39	0.028±0.023
16.81 – 19.69	18.19	0.37±0.21	18.28	0.010±0.005

¹Limiting magnitude $V_{\text{lim}} = 23.3$; divide by 0.3646 to obtain the density over all magnitudes.

mass calculated for all globulars with $2 \text{ kpc} \leq r_{\text{gc}} \leq 40 \text{ kpc}$. This shows that $\rho_{\text{cl}} = \langle m \rangle_{\text{cl}} n_{\text{cl}}$ to a good approximation at every r_{gc} , and therefore that the mean globular cluster mass is not a strong function of galactocentric radius. The other curves in the bottom panel of this Figure are discussed in §4.3. For now, the point is simply to lend some circumstantial support to the claim that $\langle m \rangle_{\text{cl}} \simeq 2.4 \times 10^5 M_{\odot}$ should not vary significantly with galactocentric radius in M87, M49, and NGC 1399.

The total projected mass densities for these three GCSs are shown as the filled circles in Fig. 3, where angular distances and areas have been converted to linear units using $D(\text{Virgo}) = 15 \text{ Mpc}$ and $D(\text{Fornax}) = 16.5 \text{ Mpc}$. The final Σ_{cl} have also been scaled upwards by additional factors of 300 – 400 for this Figure, to facilitate direct comparisons with the mass surface densities of the galaxies’ stars (drawn as lines). These latter distributions are derived from published B -band surface brightness profiles (M87: de Vaucouleurs & Nieto 1978, 1979; M49: King 1978, Caon et al. 1994; NGC 1399: Caon et al. 1994), according to the standard relation

$$\Sigma_{\text{stars}}/(M_{\odot} \text{ pc}^{-2}) = \Upsilon_B \times 10^{0.4(27.05 + A_B - \mu_B)} \quad (12)$$

for μ_B in units of mag arcsec^{-2} . (Extinctions of $A_B = 0.09 \text{ mag}$, 0, and 0 are adopted for M87, M49, and NGC 1399; see Burstein & Heiles 1984.) The stellar mass-to-light ratios Υ_B for all three galaxies come from van der Marel’s (1991) kinematic analysis of their cores; his values have been corrected for the distances D assumed here, and are taken to be independent of R_{gc} .

The comparisons of Σ_{cl} and Σ_{stars} in Fig. 3 illustrate the S_N “problems” in M87 and show that, contrary to previous claims, *they do not exist* in M49 and NGC 1399.

As was indicated above, the global specific frequency of M49 is quite normal; the most recent estimate places it at $S_N = 4.7 \pm 0.6$ (Lee et al. 1998). Given a stellar mass-to-light ratio of $\Upsilon_V = 7.5$ [which follows from $\Upsilon_B = 10.4$ and $(B - V) = 1.0$], equation (3) then implies that $M_{\text{gcs}}/M_{\text{stars}} = (1.7 \pm 0.2) \times 10^{-3}$ globally in this galaxy. In keeping with this, the middle panel of Fig. 3 shows directly that $\Sigma_{\text{cl}}/\Sigma_{\text{stars}} \simeq 2.3 \times 10^{-3}$ at essentially any $R_{\text{gc}} \gtrsim 15 \text{ kpc}$. This is slightly higher than the global GCS mass fraction because the globular cluster surface density profile is shallower than the stellar distribution at *small* galactocentric radii. As was discussed in §2.2, such a feature might result, at least in part, from the dynamical destruction of globulars in the densest regions of the galaxy. [Again, the theoretical work of Murali & Weinberg 1997b, or of Aguilar et al. 1988, suggests that the important spatial scale is generally of order a stellar effective radius, R_{eff} . These are marked by vertical lines for the galaxies in Fig. 3; note that $R_{\text{eff}}(\text{M49}) \simeq 16 \text{ kpc}$.] This aside, M49 has been put forward as an example of the second specific frequency problem (beginning with Harris 1986, and continuing on to Lee et al. 1998) on the basis of comparisons at *large* $R_{\text{gc}} \gtrsim R_{\text{eff}}$ between Σ_{cl} and the Σ_{stars} *derived from the surface photometry of King (1978)*. King’s data are shown as the dashed line in the middle of Fig. 3, and they clearly do suggest that the projected stellar density falls off more steeply with radius than the GCS density in M49. However, the solid line in this panel represents the more recent μ_B data of Caon et al. (1994), which include many more measurements at $R_{\text{gc}} \gtrsim 30 \text{ kpc}$ and do *not* show any GCS-halo discrepancy. The local specific frequency, which

TABLE 4
DENSITY PROFILE OF THE NGC 1399 GCS¹

Radius (arcmin)	R_{gc} (ave.)	N_{cl} (arcmin ⁻²)	r_{gc} (ave.)	n_{cl} (arcmin ⁻³)
0.761 – 1.518	1.075	54.88±4.60	1.171	13.74±0.31
1.518 – 2.274	1.858	35.30±3.10	1.915	7.719±0.163
2.274 – 3.031	2.625	20.64±2.11	2.666	4.288±0.949
3.031 – 3.788	3.388	10.81±1.48	3.420	1.141±0.607
3.788 – 4.544	4.149	8.77±1.27	4.175	0.957±0.472
4.544 – 5.301	4.908	6.72±1.10	4.930	0.618±0.393
5.301 – 6.058	5.667	5.31±0.97	5.686	0.496±0.314
6.058 – 6.814	6.425	3.93±0.86	6.442	0.402±0.267
6.814 – 7.571	7.183	2.61±0.79	7.197	0.108±0.261
7.571 – 8.104	7.833	2.60±0.99	7.840	0.093±0.332
8.104 – 9.573	8.808	2.32±0.71	8.854	0.175±0.134
9.573 – 11.04	10.21	1.39±0.68	10.32	0.045±0.111
11.04 – 12.50	11.75	1.32±0.55	11.78	0.095±0.097
12.50 – 13.97	13.21	0.65±0.62	13.24	0.024±0.023

¹Limiting magnitude $V_{\text{lim}} = 24.0$; divide by 0.5332 to obtain the density over all magnitudes.

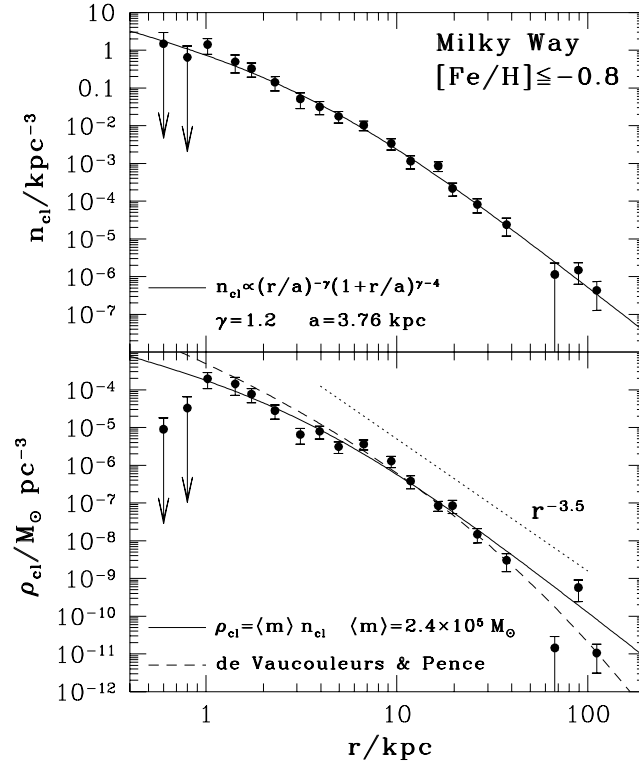


FIG. 2.— Volume number- and mass-density profiles of the metal-poor (halo) globular clusters in the Milky Way. Individual magnitudes, metallicities, and galactocentric radii for 112 clusters are taken from the compilation of Harris (1996). Solid curves represent a parametric fit to the n_{cl} distribution, which is multiplied by a mean cluster mass of $\langle m \rangle_{\text{cl}} = 2.4 \times 10^5 M_{\odot}$ to obtain the mass densities ρ_{cl} . The good fit to the data in both the top and bottom panels shows that $\langle m \rangle_{\text{cl}}$ is not a function of r_{gc} in the Milky Way. Broken curves in the bottom panel refer to the density profile $\rho_{\text{stars}}(r_{\text{gc}})$ of the Pop. II spheroid; see §4.3 of the text.

is proportional to $\Sigma_{\text{cl}}/\Sigma_{\text{stars}}$, then takes on a roughly constant value throughout the outer halo of M49, and the second S_N problem does not appear there.⁷ The differences between the light profiles of King (1978) and Caon et al. (1994) illustrate the difficulty of accurate sky subtraction at faint surface brightness levels, and make the point that background corrections are an important consideration in any discussion of galaxy (or GCS) structure on large spatial scales. The surface photometry of Caon et al. (1994) is adopted here for M49, and thus $\Sigma_{\text{cl}} \propto \Sigma_{\text{stars}}$ at large R_{gc} ; but this important caveat must be kept in mind.

In §3.2, it is shown that the gas in M49 adds up to a small fraction of its stellar mass, in which case the local cluster formation efficiency can be estimated by $\epsilon_{\text{cl}} = \rho_{\text{cl}}/(\rho_{\text{gas}} + \rho_{\text{stars}}) \simeq \rho_{\text{cl}}/\rho_{\text{stars}}$. The fact that $\Sigma_{\text{cl}} \propto \Sigma_{\text{stars}}$ therefore implies that ϵ_{cl} was essentially independent of galactocentric radius beyond about $R_{\text{eff}} \simeq 16$ kpc. An extrapolation of this result to smaller distances requires that the systematic decrease in $\Sigma_{\text{cl}}/\Sigma_{\text{stars}}$ there has resulted entirely from the gradual destruction of (initially bound) globulars over a Hubble time. As *possible* anecdotal support for this interpretation, recall that globally $M_{\text{gcs}}/M_{\text{stars}} \simeq 0.0017$ for M49, while locally $\Sigma_{\text{cl}}/\Sigma_{\text{stars}} \simeq 0.0023$ at large radii. If the latter number is assumed to have held all the way to the center of the galaxy initially, then a global $M_{\text{gcs}}^{\text{init}}/M_{\text{stars}}^{\text{init}} \simeq 0.0023$ is implied. In such a scenario, if M_{stars} were roughly conserved over a Hubble time while globulars were dynamically disrupted (their remains adding nothing significant to the total stellar mass), the global ratio of current to initial GCS masses would be $M_{\text{gcs}}/M_{\text{gcs}}^{\text{init}} \simeq 0.0017/0.0023 \sim 0.75$. This is surprisingly close to the result of the general GCS mass-function arguments in §2.1 (see eq. [8]). However, this could be just a coincidence; it remains possible that ϵ_{cl} really was lower at small galactocentric radii, i.e., that the GCS *formed* with a “core” which was somewhat larger than that of the unclustered stellar distribution, and which was only enhanced over time. The current data cannot settle the question either way.

The bottom panel of Fig. 3 shows that the second S_N problem does not exist beyond a stellar R_{eff} in NGC 1399, either. Every study of this GCS has appreciated this point, and it is not a new result (see the references cited above). (Note also that the surface brightness profile used here for NGC 1399, from Caon et al. 1994, is consistent with that of Killeen & Bicknell 1988 at large R_{gc} .) On the other hand, the global S_N in this galaxy—and therefore the local $\Sigma_{\text{cl}}/\Sigma_{\text{stars}}$ at

⁷Lee et al. (1998) have recently claimed evidence for a difference in the radial distributions Σ_{cl} of red (metal-rich) and blue (or metal-poor) globular clusters in M49. They argue that the former are more centrally concentrated, i.e., exhibit a steeper fall-off in density with R_{gc} , than the latter. They also suggest that the “red” component of the M49 GCS follows the galaxy’s stellar profile Σ_{stars} , while the “blue” component is spatially more extended (see also Forbes et al. 1997). However, since Lee et al. were unable to determine the background densities N_b separately in the blue and red subsets that they defined for the GCS, further observations are required to verify their claim (and comparisons then should perhaps be made with the surface brightness profile of Caon et al. 1994). Moreover, any real differences in the *volume* density profiles of red and blue globulars will be artificially amplified in projection. If Lee et al.’s result is confirmed, it will be important to understand in detail; but *all* of the GCSs discussed here are considered only in their entirety, without any attempt to distinguish between subpopulations.

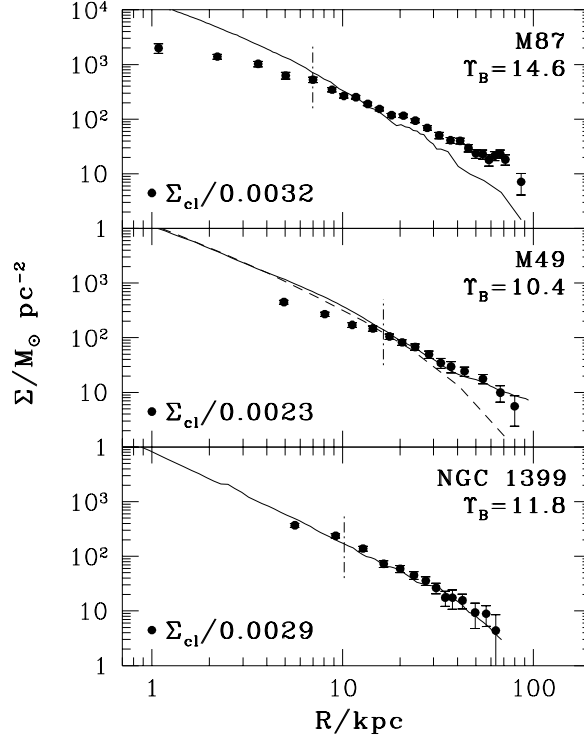


FIG. 3.— Comparison of the projected mass density profiles of globular clusters (points) with those of the unclustered halo stars (lines) in M87, M49, and NGC 1399. GCS densities have been corrected for photometric incompleteness (see text), and scaled up by the inverse of the cluster formation efficiencies derived in §3.2 below. Mass-to-light ratios for the stars are taken in each galaxy from van der Marel (1991). The broken vertical lines mark the effective radius of each galaxy: $R_{\text{eff}} = 7.0$ kpc for M87 (de Vaucouleurs & Nieto 1978), 16.4 kpc for M49 (Caon et al. 1994), and 10.2 kpc in NGC 1399 (Caon et al. 1994). The disparity between Σ_{cl} and Σ_{stars} in M87 (top panel) embodies the specific frequency “problems” there.

any single R_{gc} —has always been thought to be significantly higher than the normal, M49-like value of ~ 5 : the latest calculation claims $S_N = 12 \pm 3$ (Kissler-Patig et al. 1997).⁸ However, it is immediately apparent from Fig. 3 that this is *not* the case: the bulk scaling of $1/0.0029$ required to match the GCS radial distribution to the stellar mass profile in NGC 1399 is identical, within the observational uncertainties, to the $1/0.0023$ needed in M49. Since the gas mass is negligible compared to the stellar mass on < 70 -kpc scales in NGC 1399, as it is in M49, $\hat{\epsilon}_{\text{cl}} \simeq \Sigma_{\text{cl}}/\Sigma_{\text{stars}}$ holds for both systems, and their cluster formation efficiencies are inferred to have been essentially identical. The spuriously high global S_N values typically quoted for NGC 1399 can be traced back to the practice of assigning an absolute magnitude of $M_V \simeq -21.6$ to the galaxy (from the Third Reference Catalogue: de Vaucouleurs et al. 1991); but, in fact, $M_V \simeq -22.1$ is indicated by direct integration (to $R_{\text{gc}} = 70$ kpc, assuming $D = 16.5$ Mpc) of the surface brightness profiles of either Caon et al. (1994) or Killeen & Bicknell (1988). Given this brighter magnitude, and an estimated GCS population of $N_{\text{tot}} = 4700 \pm 400$ projected to within 70 kpc of NGC 1399 (see §5), equation (1) yields $S_N(\text{NGC 1399}) = 7.0 \pm 0.6$, much closer to the value for M49 (see also Ostrov et al. 1998). This is consistent with the alternate representation of the data in Fig. 3, and confirms that the *first* specific frequency problem is not an issue in NGC 1399.

It appears, therefore, that there are no S_N problems in either M49 or NGC 1399. There is no evidence for any fundamental variation in ϵ_{cl} from the total populations of these two GCSs, and the local $\hat{\epsilon}_{\text{cl}}$ in each is independent of galactocentric radius beyond $\simeq 1 R_{\text{eff}}$. These results lend some weight to the claim (§2.2) that the first and second specific frequency problems seem likely to appear, and should be solved, only together.

Both of these problems are genuine in M87, as the top panel of Fig. 3 attests. (The surface photometry of de Vaucouleurs & Nieto 1978, which is the standard, is well sampled and is supported by the independent studies of Oemler 1976 and King 1978; and the total M_V used to calculate the galaxy’s S_N is taken from integration of its μ_B profile.) The second specific frequency problem is evidenced by the shallower decline of Σ_{cl} compared to Σ_{stars} at $R_{\text{gc}} \gtrsim R_{\text{eff}} \simeq 7$ kpc. This also causes the first problem, since scaling the total GCS density upwards by the factors appropriate for M49 or NGC 1399 obviously puts Σ_{cl} well in excess of Σ_{stars} throughout most of the galaxy. Indeed, the most recent estimate for the global S_N of M87 is 14.1 ± 1.6 (Harris et al. 1998), which is fully a factor of three higher than that of M49. Here it is necessary to consider the distribution of hot gas—which is known to exist in great quantities around M87—in evaluating $\hat{\epsilon}_{\text{cl}}$ from equation (10).

⁸After this paper was submitted, a new study of NGC 1399 by Ostrov, Geisler, & Forte (1998) found that the specific frequency of its GCS is a much more modest $S_N = 5.6 \pm 1.0$. This result is consistent with that obtained here, and in fact is even closer to the value for M49; it supports the conclusion that NGC 1399 does not exhibit the first S_N problem.

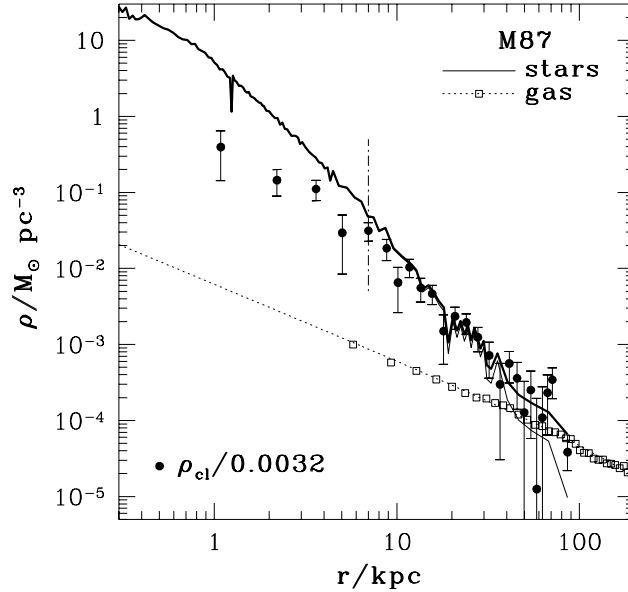


FIG. 4.— Comparison of the (mass) volume density profiles of the GCS (filled circles), halo stars (thin solid line), and X-ray gas (open squares and broken line) in M87. The volume densities of globular clusters and field stars follow from deprojections of the surface density profiles in Fig. 3. To deproject the galaxy surface photometry, it is assumed that $\rho_{\text{stars}} \propto r_{\text{gc}}^{-4}$ at large radii $r_{\text{gc}} \gtrsim 100$ kpc (see eqs. [A4], [A5], and [A8] of the Appendix). The vertical line segment is placed at the projected effective radius of the stellar light, as in Fig. 3. Thick black line is the sum of the stellar and gas densities. Note that ρ_{cl} is directly proportional to $(\rho_{\text{stars}} + \rho_{\text{gas}})$ beyond $r_{\text{gc}} \simeq R_{\text{eff}}$, giving a constant estimated cluster formation efficiency of $\hat{e}_{\text{cl}} = 0.0032 \pm 0.0005$ there. The sharp feature at $r_{\text{gc}} \simeq 20$ kpc marks the onset of the cD envelope in the stars and GCS of M87; it is visible as a smoother “hump” in projection (de Vaucouleurs & Nieto 1978; McLaughlin et al. 1993).

3.2. Volume Densities

The volume density profiles of circumgalactic and intracluster gas are routinely derived in the course of X-ray studies of elliptical galaxies. To include such a halo component in this discussion, it is first necessary either to deproject observed GCS and stellar surface densities, or to compute the gas surface density via a standard projection integral. In general, the first of these options potentially has the most insight to offer, since projected quantities always mix information from a wide range of physical radii.

An Appendix therefore develops a nonparametric deprojection algorithm which is explicitly designed to handle GCS data that have been binned in projected radius, R_{gc} (i.e., counted in circular annuli). This procedure returns a coarse volume density profile— n_{cl} vs. three-dimensional r_{gc} —expressed as a series of average densities in a number of concentric spherical shells. The algorithm is preferably applied to surface density profiles that extend to fairly large radii (so that corrections for cluster populations beyond the observed field of view can be estimated with confidence, and are as small as possible), and it makes most sense for N_{cl} distributions that are monotonically decreasing functions of R_{gc} (otherwise, the derived n_{cl} can be zero or negative in some shells). After re-binning to smooth some of the original data, as described above, the composite GCS radial distributions in Tables 2 through 4 satisfy each of these criteria. Equation (A5) of the Appendix has therefore been applied to each of these N_{cl} profiles, with $f(R_{i-1}, R_i)$ (a sort of “residual background” correction) calculated by assuming that $n_{\text{cl}} \propto r_{\text{gc}}^{-3}$ beyond the last observed radius of each GCS. (This reflects the fact that the projected N_{cl} shows roughly an R_{gc}^{-2} behavior at large R_{gc} in each case. In any event, only the outermost one or two points in each deprojected profile are affected—and then not greatly—by this choice.) The resulting n_{cl} are listed in the fifth columns of Tables 2, 3, and 4. The radii in the first columns, which delimit projected annuli in reference to the surface density data, are identified with the inner and outer three-dimensional radii of spherical shells in reference to the volume densities.

The deprojection algorithm is an iterative one: the volume density in a spherical shell with some mean radius is computed by first subtracting, from the projected density at that radius, the contribution of any globulars that actually lie at larger physical r_{gc} . Thus, the uncertainties of the derived n_{cl} at any two radii in one system are not independent. The (1- σ) errorbars quoted in Tables 2, 3, and 4 are the standard deviations of results from 1000 different deprojections in each case. Each trial deprojection in each GCS begins with a different N_{cl} profile, in which the surface density for any given annulus is drawn at random from a Gaussian distribution that is centered on the value given in Column 3 of the

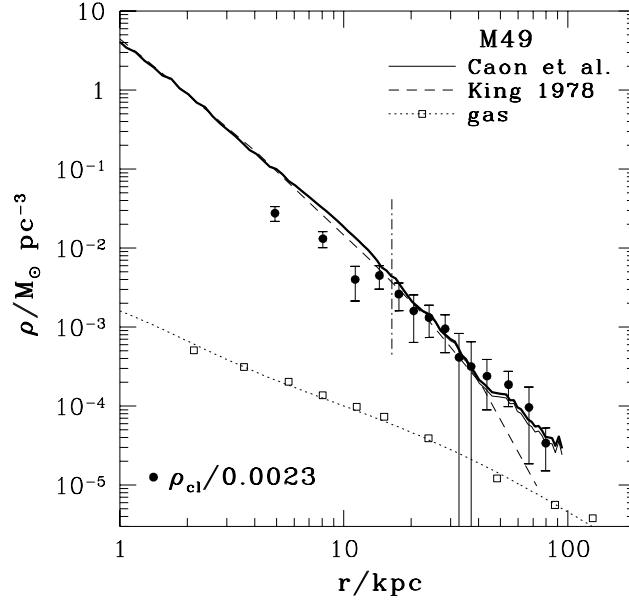


FIG. 5.— Same as Fig. 4, but for M49. Two separate stellar density profiles are shown in this case, derived by deprojecting the surface brightness profiles of King (1978; dashed line) and of Caon et al. (1994; thin solid line). The projected half-light radius of the latter is marked with a vertical line. For both deprojections, it is assumed that $\rho_{\text{stars}} \propto r_{\text{gc}}^{-2}$ at large radii. The bold line is the sum of ρ_{stars} (from the profile of Caon et al.) and ρ_{gas} (open squares and dotted line). At radii $r \gtrsim R_{\text{eff}}$, the ratio $\rho_{\text{cl}}/(\rho_{\text{stars}} + \rho_{\text{gas}})$ is again constant with radius, giving a best estimate of $\hat{\epsilon}_{\text{cl}} = 0.0023 \pm 0.0005$. This is within 30% of the value found in M87, and the two are identical within their errors.

appropriate Table, and that has a dispersion equal to the observational uncertainty there.

The tabulated number densities n_{cl} have the same limiting magnitudes as the corresponding surface densities, and are therefore multiplied by the same two factors (so effectively scaling to $V_{\text{lim}} = \infty$, and applying the mean globular cluster mass $\langle m \rangle_{\text{cl}} = 2.4 \times 10^5 M_{\odot}$) to find the total GCS mass densities $\rho_{\text{cl}}(r_{\text{gc}})$. These distributions are plotted as the filled circles in Figs. 4, 5, and 6, where the density in each spherical shell has been put at a radius \bar{r}_{gc} , given in Columns 4 of Tables 2–4, calculated according to equation (A10). As in Fig. 3, the ρ_{cl} profiles have been scaled up by factors of a few hundred in order to compare them directly with the stellar mass densities $\rho_{\text{stars}}(r_{\text{gc}})$ (thin solid lines in Figs. 4 to 6). These have been obtained by applying the algorithm of the Appendix to the projected profiles $\Sigma_{\text{stars}}(R_{\text{gc}})$ derived above from *B*-band surface photometry (see eq. [12]).⁹ It is immediately apparent that the good agreement seen in Fig. 3 between the GCS and stellar densities in NGC 1399 and M49 (for the data of Caon et al. 1994) persists after deprojection, as should be the case. More noteworthy is the fact that the discrepancy between ρ_{cl} and ρ_{stars} in M87, while certainly still present, is somewhat less pronounced than that between Σ_{cl} and Σ_{stars} . For example, the truly local picture given by Fig. 4 shows that the second S_N problem here is confined to galactocentric radii $r_{\text{gc}} \gtrsim 30$ –40 kpc, and does not extend inward to the ~ 15 kpc scales suggested by Fig. 3. This just reflects the fact that the projection of any two volume densities inevitably amplifies any small differences that may actually exist between them, and artificially associates disparities at large r_{gc} with smaller projected radii. A similar comment applies to the comparison of ρ_{cl} with ρ_{stars} in M49: it is now clear, from Fig. 5, that any argument for the second S_N problem in this galaxy could only be made for three-dimensional radii greater than about 50 kpc, and then (as in §3.1) only if King’s (1978) μ_B profile—which includes just a *single data point* at such large r_{gc} —were preferred over that of Caon et al. (1994).

The gas densities in these systems have been obtained from published *electron* number densities by way of the relation

$$\frac{\rho_{\text{gas}}}{M_{\odot} \text{pc}^{-3}} = 2.865 \times 10^{-5} \left(\frac{\mu}{0.60} \right) \left(\frac{n_e}{10^{-3} \text{cm}^{-3}} \right), \quad (13)$$

where a mean particle mass $\mu \simeq 0.6$ (in units of m_H) is equally appropriate for hot ($T \sim 10^7$ – 10^8 K) and highly ionized

⁹ All of the surface photometry used here has been averaged in circular annuli, as is required by the deprojection method in the Appendix. [Effective circular radii $R_{\text{gc}} = (ab)^{1/2}$ are assigned to elliptical isophotes with semi-major and -minor axes a and b .] Note that these data are generally published just as tables of μ_B vs. R_{gc} , with no information given on the inner and outer radii of any annuli used in the measurements. Thus, to apply equation (A5), annuli have been defined in an ad hoc manner, by setting boundaries at the geometric means $(R_1 R_2)^{1/2}$ of successive pairs of projected radii in the published data. Data points are generally spaced so closely as to make the difference between this and any other choice unimportant.

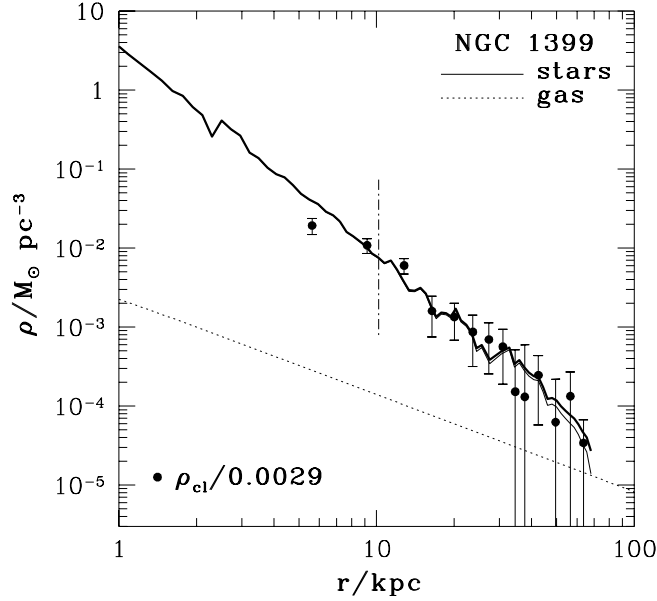


FIG. 6.— Same as Figs. 4 and 5, but for NGC 1399. Filled circles are again the GCS densities; thin solid line, the stellar densities (obtained by deprojection of B -band surface brightnesses, correcting for $\rho_{\text{stars}} \propto r_{\text{gc}}^{-2}$ beyond about 70 kpc); dotted line, the gas density; and bold solid line, the sum ($\rho_{\text{gas}} + \rho_{\text{stars}}$). As before, the vertical line is placed at the stellar R_{eff} . The estimated cluster formation efficiency is again independent of galactocentric radius: $\hat{\epsilon}_{\text{cl}} = 0.0029 \pm 0.0008$.

plasmas of any composition from primordial to solar.

The open squares for the M87 gas in Fig. 4 come from scaling the electron densities of Nulsen & Böhringer (1995) for the different Virgo distance assumed here (15 Mpc vs. their 20), according to $n_e \propto D^{-1/2}$. (These data were published as volume densities after Nulsen & Böhringer applied a deprojection algorithm, similar to that derived in the Appendix, to their *ROSAT* spectra.) The dotted line in Fig. 4 is a fit taken from McLaughlin (1999):

$$\rho_{\text{gas}}(\text{M87}) = 5.60 \times 10^{-6} M_{\odot} \text{pc}^{-3} \left(\frac{r_{\text{gc}}}{1070 \text{ kpc}} \right)^{-1} \left(1 + \frac{r_{\text{gc}}}{1070 \text{ kpc}} \right)^{-3}, \quad (14)$$

so that, essentially, $\rho_{\text{gas}} \propto r_{\text{gc}}^{-1}$ over the area of interest here. This fit has been used to compute the total $\rho_{\text{gas}} + \rho_{\text{stars}}$ at every radius with a measured stellar density; that sum is drawn as the bold solid line in the Figure.

Similarly, the open squares in Fig. 5 here use the n_e read from Irwin & Sarazin's (1996) Figure 6, after scaling to $D = 15$ Mpc from their assumed M49 distance of 25.8 Mpc. The dotted line in this Figure is a scaled fit (from Brighenti & Mathews 1998) to these data plus those of Trinchieri et al. (1986):

$$\rho_{\text{gas}}(\text{M49}) = \left[\frac{3.57 \times 10^{-3}}{1 + (r_{\text{gc}}/0.807 \text{ kpc})^2} + \frac{2.24 \times 10^{-4}}{1 + (r_{\text{gc}}/7.18 \text{ kpc})^{1.14}} - \frac{1.50 \times 10^{-5}}{1 + (r_{\text{gc}}/75.6 \text{ kpc})^{1.19}} \right] M_{\odot} \text{pc}^{-3}. \quad (15)$$

The heavy black line again represents the sum of $\rho_{\text{gas}} + \rho_{\text{stars}}$.

The broken line for ρ_{gas} in NGC 1399 (Fig. 6) comes from Tsai's (1993) fit to the X-ray observations of Killeen & Bicknell (1988), corrected for $D(\text{Fornax}) = 16.5$ Mpc:

$$\rho_{\text{gas}}(\text{NGC 1399}) = 1.03 \times 10^{-2} M_{\odot} \text{pc}^{-3} \left[1 + \left(\frac{r_{\text{gc}}}{0.304 \text{ kpc}} \right)^2 \right]^{-0.615}. \quad (16)$$

It is clear that stars outweigh the gas everywhere in M49 and NGC 1399: locally, $\rho_{\text{gas}}/\rho_{\text{stars}} \lesssim 0.3$ even at the largest radii in Figs. 5 and 6; globally, $M_{\text{gas}}/M_{\text{stars}} \sim 0.05$ within $r_{\text{gc}} = 100$ kpc and 70 kpc respectively. In both systems, then, $M_{\text{gcs}}/(M_{\text{gas}} + M_{\text{stars}}) \simeq M_{\text{gcs}}/M_{\text{stars}}$ and (albeit to slightly lower accuracy at very large r_{gc}) $\rho_{\text{cl}}/(\rho_{\text{gas}} + \rho_{\text{stars}}) \simeq \rho_{\text{cl}}/\rho_{\text{stars}}$. It is indeed valid to use standard specific frequencies as direct measures of globular cluster formation efficiencies in these two cases, as was done at the end of §3.1 above. To be complete, however, all of the stars, gas, and globular clusters can

now be used to estimate ϵ_{cl} more precisely, according to the basic equation (10). By summing the data at large r_{gc} in each of M49 and NGC 1399, then, average $\hat{\epsilon}_{\text{cl}}$ values are obtained:

$$\frac{M_{\text{gcs}}(r_{\text{gc}} > 12.5 \text{ kpc})}{M_{\text{gas}}(r_{\text{gc}} > 12.5 \text{ kpc}) + M_{\text{stars}}(r_{\text{gc}} > 12.5 \text{ kpc})} = 0.0023 \pm 0.0005 \quad (\text{M49}) \quad (17)$$

and

$$\frac{M_{\text{gcs}}(r_{\text{gc}} > 11 \text{ kpc})}{M_{\text{gas}}(r_{\text{gc}} > 11 \text{ kpc}) + M_{\text{stars}}(r_{\text{gc}} > 11 \text{ kpc})} = 0.0029 \pm 0.0008 \quad (\text{NGC 1399}) , \quad (18)$$

which account for the scalings applied to Σ_{cl} and ρ_{cl} in Figs. 3, 5, and 6. As has already been discussed, these are equally well interpreted as either local or global formation efficiencies, since the ratio $\rho_{\text{cl}}/(\rho_{\text{gas}} + \rho_{\text{stars}})$ shows no variations with r_{gc} beyond a stellar effective radius (or even inside this, in NGC 1399), i.e., outside those regions of the GCSs which could be significantly dynamically evolved. (As in Fig. 3, the stellar R_{eff} are marked with vertical broken lines in Figs. 4, 5, and 6.)

The situation is somewhat different for M87: referring to Fig. 4, $\rho_{\text{gas}}/\rho_{\text{stars}} > 1$ at all radii $r_{\text{gc}} \gtrsim 40$ kpc (which is where the second S_N problem begins in the deprojected data), and $M_{\text{gas}}/M_{\text{stars}} \simeq 0.35\text{--}0.40$ globally (i.e., integrated over scales $r_{\text{gc}} \leq 100$ kpc). The hot gas around M87 is therefore an important factor in calculating its cluster formation efficiency. As before, outside of the central regions of the galaxy it is found that

$$\frac{M_{\text{gcs}}(r_{\text{gc}} > 11 \text{ kpc})}{M_{\text{gas}}(r_{\text{gc}} > 11 \text{ kpc}) + M_{\text{stars}}(r_{\text{gc}} > 11 \text{ kpc})} = 0.0032 \pm 0.0005 \quad (\text{M87}) , \quad (19)$$

explaining the scaling factor applied to the M87 GCS densities in Figs. 3 and 4. Figure 4 shows that this average value is valid also as the local $\hat{\epsilon}_{\text{cl}} = \rho_{\text{cl}}/(\rho_{\text{gas}} + \rho_{\text{stars}})$ at any galactocentric position beyond about $R_{\text{eff}} = 7$ kpc; as in M49 and NGC 1399, the inferred globular cluster formation efficiency in M87 was independent of r_{gc} at large radii. In this case, however, if the gas were not included in the calculation, much larger—and radially varying—formation efficiencies would have been indicated: for example, $M_{\text{gcs}}(r_{\text{gc}} > 11 \text{ kpc})/M_{\text{stars}}(r_{\text{gc}} > 11 \text{ kpc}) = 0.0056 \pm 0.0008$, and $M_{\text{gcs}}(r_{\text{gc}} > 40 \text{ kpc})/M_{\text{stars}}(r_{\text{gc}} > 40 \text{ kpc}) = 0.0095 \pm 0.0023$. Note that the first of these ratios, $M_{\text{gcs}}/M_{\text{stars}} = 0.0056$ for $r_{\text{gc}} > 11$ kpc, is a factor of 2.4 higher than the corresponding quantity in M49. In combination with the different stellar mass-to-light ratios in these two galaxies ($\Upsilon_B = 14.6$ vs. 10.4; see van der Marel 1991, or Fig. 3 above), this just corresponds to the factor of 3 difference observed in their global S_N values. The high local and global specific frequencies in M87 are thus seen to result from the presence of a population of globular clusters that are intimately associated with the hot gas there.

3.3. Gas Surface Densities

As was mentioned earlier, an alternate comparison of a galaxy's gas distribution with its stars and globular clusters could make use of only surface densities— Σ_{stars} , Σ_{cl} , and a derived Σ_{gas} —as functions of projected R_{gc} . The advantage of such an approach is that Σ_{gas} is on an equal physical footing with Σ_{stars} and Σ_{cl} , and the latter are basically unmanipulated data with smaller relative uncertainties than the derived ρ_{stars} and ρ_{cl} profiles. The cost, aside from possible uncertainties in any extrapolations required to obtain Σ_{gas} from ρ_{gas} , is that differences between projected distributions are not easily related to local effects at some true, three-dimensional radius (e.g., recall the comparison between projected Σ_{cl} vs. Σ_{stars} and deprojected ρ_{cl} vs. ρ_{stars} in M87). More to the point, if the ratio $\Sigma_{\text{cl}}/(\Sigma_{\text{gas}} + \Sigma_{\text{stars}})$ varies as a function of R_{gc} in a galaxy, then variations in the physical quantity of real interest, the local $\hat{\epsilon}_{\text{cl}} = \rho_{\text{cl}}/(\rho_{\text{gas}} + \rho_{\text{stars}})$, are clearly indicated, but *cannot be properly quantified* without resorting to a deprojection of some sort. For this reason, the procedure of §3.2 must be favored as the best way, generally speaking, to measure local $\hat{\epsilon}_{\text{cl}}$.

That said, however, in the galaxies studied here, $\hat{\epsilon}_{\text{cl}}$ is found to be independent of radius at large r_{gc} , i.e., $\rho_{\text{cl}} \propto (\rho_{\text{gas}} + \rho_{\text{stars}})$. In this specific instance, it should then also happen that $\Sigma_{\text{cl}} \propto (\Sigma_{\text{gas}} + \Sigma_{\text{stars}})$ at large R_{gc} , with a constant of proportionality that is exactly $\hat{\epsilon}_{\text{cl}}$. It is therefore useful to compute Σ_{gas} and the projected analogue of $\hat{\epsilon}_{\text{cl}}$ in M87, M49, and NGC 1399, in order both to verify the results of §3.2 (which depend in good part on the behavior of ρ_{cl} at large r_{gc} , where the deprojected data are noisiest) and to obtain potentially higher-precision estimates of the cluster formation efficiencies in these systems.

First, then, the projected mass densities of gas are obtained from the volume density profiles in equations (14), (15), and (16), by way of the standard integral

$$\Sigma_{\text{gas}}(R_{\text{gc}}) = 2 \int_0^{\sqrt{r_{\text{max}}^2 - R_{\text{gc}}^2}} \rho_{\text{gas}}(r_{\text{gc}}) dz , \quad (20)$$

where the coordinate $z = (r_{\text{gc}}^2 - R_{\text{gc}}^2)^{1/2}$ measures distance along the line of sight, and r_{max} represents the total physical extent of the X-ray corona. For M87, this is taken to be the virial radius of the Virgo Cluster: $r_{\text{max}} \simeq 1.5$ Mpc (see McLaughlin 1999). For M49, which is not at the center of Virgo, $r_{\text{max}} = 500$ kpc is adopted. NGC 1399 lies at the center of the Fornax Cluster, which is somewhat less massive than Virgo (e.g., Jones et al. 1997), and r_{max} is set at 1 Mpc there.

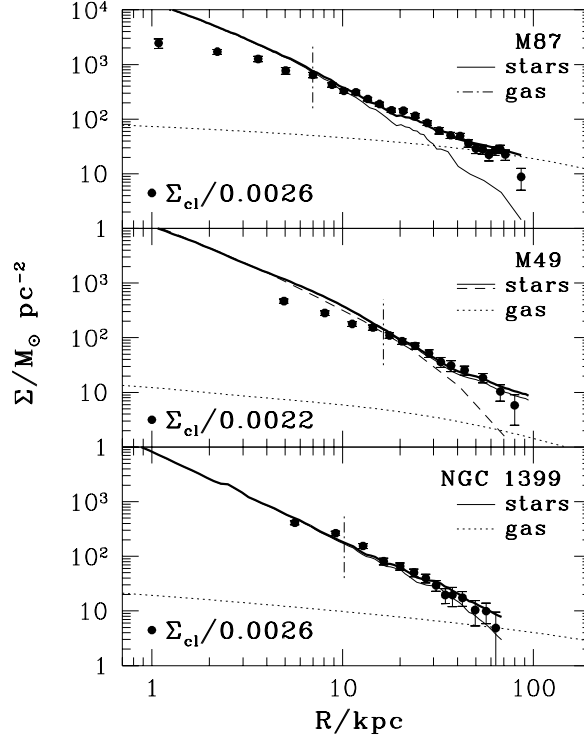


FIG. 7.— Comparison of GCS, stellar, and gas *surface* densities in M87, M49, and NGC 1399. The bold solid line in each panel traces the sum $\Sigma_{\text{gas}} + \Sigma_{\text{stars}}$, and the galaxies' effective radii are marked as in Fig. 3. Also as in Figs. 3 and 5, the solid and dashed lines for the stellar densities in M49 refer to the surface photometry of Caon et al. (1994) and King (1978), respectively. The implied values of $\hat{\epsilon}_{\text{cl}}$ are essentially the same as those derived from the volume density profiles in all three galaxies, although the $\simeq 20\%$ lower value in M87 may be significant. The cluster formation efficiency is again inferred to have been locally invariant in each of these systems (at least beyond $R_{\text{gc}} \simeq R_{\text{eff}}$), and not significantly different from one to the other.

There is a certain arbitrariness to each of these choices for r_{max} , but any of them can be changed by a factor of a few without affecting the conclusions which follow.

The resulting Σ_{gas} profiles are shown in Fig. 7, along with the same Σ_{stars} and Σ_{cl} profiles plotted in Fig. 3 above (although the Σ_{cl} have been scaled up by slightly different factors in the current Figure). It is easily seen that $\Sigma_{\text{cl}} \propto (\Sigma_{\text{gas}} + \Sigma_{\text{stars}})$ at large R_{gc} in each galaxy, just as expected following the analysis in §3.2. Moreover, the constants of proportionality are in reasonable agreement with the $\hat{\epsilon}_{\text{cl}}$ derived from the deprojected data: by taking the direct mean of the surface-density ratios beyond the galaxies' effective radii (so as once again to avoid a zone of potential GCS erosion), it is found that

$$\left\langle \frac{\Sigma_{\text{cl}}}{\Sigma_{\text{gas}} + \Sigma_{\text{stars}}} \right\rangle_{R_{\text{gc}} \gtrsim R_{\text{eff}}} = \begin{cases} 0.0026 \pm 0.0003, & \text{M87} \\ 0.0022 \pm 0.0004, & \text{M49} \\ 0.0026 \pm 0.0006, & \text{NGC 1399} . \end{cases} \quad (21)$$

The result for M49 is indistinguishable from that obtained in either §3.1 or §3.2, owing to the truly low gas densities in this galaxy. Similarly, the projected $\hat{\epsilon}_{\text{cl}}$ in NGC 1399 is identical, within the uncertainties, to the deprojected quantity $\rho_{\text{cl}}/(\rho_{\text{gas}} + \rho_{\text{stars}}) = 0.0029 \pm 0.0008$. The number in equation (21) is formally 10% smaller because of the apparently large projected gas densities at radii $R_{\text{gc}} \gtrsim 40\text{--}50$ kpc in NGC 1399. However, these values are almost certainly overestimates: in deriving Σ_{gas} , the shallow volume density profile of equation (15), which roughly has $\rho_{\text{gas}} \propto r_{\text{gc}}^{-1.2}$, has been assumed to hold even on Mpc spatial scales in Fornax—well beyond the range of actual X-ray observations—and this is likely unrealistic. On the other hand, the projected $\hat{\epsilon}_{\text{cl}} = 0.0026 \pm 0.0003$ indicated for M87 in Fig. 7 might genuinely be slightly smaller than the 0.0032 ± 0.0005 inferred from deprojected quantities. The 20% difference between these two numbers is significant at just the 1- σ level, however, and—although it is interesting that the former is actually closer to the values for M49 and NGC 1399—it is not obvious which is more reliable. The X-ray gas density around M87 (eq. [14]) has again been extrapolated to unobserved radii to compute Σ_{gas} , but in this case the basic profile actually follows the dark matter distribution in Virgo (McLaughlin 1999), and exhibits a realistic, steepening slope at large r_{gc} . Thus, although it is possible that Σ_{gas} is overestimated at large R_{gc} in M87, any argument for this is not as compelling as in NGC 1399.

The best measure of $\hat{\epsilon}_{\text{cl}}$ in M87 will therefore be taken as the error-weighted mean of the values (eqs. [19] and [21]) obtained by analyzing the deprojected and projected data there; in M49, the choice is of no consequence, but for definiteness the deprojected $\hat{\epsilon}_{\text{cl}}$ will be adopted; and the deprojected estimate will also be adopted for NGC 1399, to avoid any

concerns that its gas surface density might have been overestimated at large R_{gc} . Thus,

$$\hat{\epsilon}_{cl} = \begin{cases} 0.0028 \pm 0.0004, & \text{M87} \\ 0.0023 \pm 0.0005, & \text{M49} \\ 0.0029 \pm 0.0008, & \text{NGC 1399} \end{cases} \quad (22)$$

Once again, these can be seen as estimates of either local or global cluster formation efficiencies if the inner several kpc of M87 and M49 are excluded from the discussion.

4. A UNIVERSAL EFFICIENCY FOR CLUSTER FORMATION

The results of the previous Section clearly show that *working in terms of stellar masses rather than luminosities and including the gas in M87 removes both the first and second specific frequency problems there*: in all three of M87, M49, and NGC 1399, it is found that $\rho_{cl} \propto (\rho_{gas} + \rho_{stars})$, in identical proportions within the uncertainties, outside of the central, possibly dynamically depleted regions of the GCSs. (At the most, differences between the constants of proportionality in M87 and M49 might remain at the $\sim 20\%$ level; but again, this is easily taken up in the observational uncertainties, and in any case is a significant improvement over the 300% difference in their specific frequencies.) The interpretation put to this is that globular clusters formed with an essentially constant efficiency throughout all of these galaxies, at the level of

$$\epsilon_{cl}(\text{globular}) \equiv \frac{M_{gcs}^{\text{init}}}{M_{gas}^{\text{init}}} \simeq \frac{M_{gcs}}{M_{gas} + M_{stars}} = 0.0026 \pm 0.0005, \quad (23)$$

which is the error-weighted mean of equation (22).

It should be kept in mind that these are all large galaxies with complex evolutionary histories. Thus, as was discussed in §2.1, what has been measured here is necessarily a *mass-weighted average* of ϵ_{cl} , possibly over multiple distinct episodes of in situ cluster formation and/or of the accretion of globulars formed elsewhere. Nevertheless, the uniformity of the observational estimates $\hat{\epsilon}_{cl}$ in these systems—both as a function of r_{gc} within each and from one entire system to another—suggests that these concerns may not be too severe, and that equation (23) may still serve as a reliable guide to a single, possibly universal efficiency for cluster formation. This impression can now be checked quantitatively, albeit to rather lower precision than has proved possible with the excellent datasets for M87, M49, and NGC 1399, by appealing to observations of many other GCSs. All indications are that ϵ_{cl} is indeed similar, at least to first order, from galaxy to galaxy and from the protogalactic epoch to the present.

4.1. Other Ellipticals and BCGs

Given the definition for $\hat{\epsilon}_{cl}$ (eq. [10]), and denoting by G the global ratio M_{gas}/M_{stars} in a galaxy, the total population of any GCS may be written as

$$\mathcal{N}_{tot} = 2.92 \times 10^6 \hat{\epsilon}_{cl} (1 + G) \left(\frac{L_{V,gal}}{10^{11} L_{\odot}} \right) \left(\frac{\Upsilon_V}{7 M_{\odot} L_{\odot}^{-1}} \right) \left(\frac{\langle m \rangle_{cl}}{2.4 \times 10^5 M_{\odot}} \right)^{-1}. \quad (24)$$

This can, of course, also be derived from equation (2) above, which explicitly relates S_N to $\hat{\epsilon}_{cl}$ when $G = 0$.

Now, in the general discussion of §2, the stellar mass-to-light ratio was taken to be roughly similar from galaxy to galaxy. This is not exactly true, however: as was seen in §3, for example, the recovery of similar $\hat{\epsilon}_{cl}$ in M87 and M49 from their significantly different global and local S_N depends on the $\simeq 40\%$ larger Υ_B of M87 as well as on its greater gas mass. Thus, if other ellipticals are to be brought properly into this discussion, it is necessary first to account for the fact that Υ depends systematically on galaxy luminosity. This is a well known result of many fundamental-plane analyses of bright ellipticals, and it can be incorporated quantitatively in this analysis by referring to the study of van der Marel (1991; and references therein). Specifically, for a sample of 37 early-type systems, van der Marel obtains a mean R -band mass-to-light ratio of $\Upsilon_R = 3.32 h_{50} M_{\odot} L_{\odot}^{-1}$, corresponding to $\Upsilon_B = 5.93 h_{50}$, at a mean magnitude of $M_B \simeq -22.22 + 5 \log h_{50}$. For a galaxy color of $(B - V) = 1.0$ (typical of large ellipticals) and $H_0 = 70 \text{ km s}^{-1} \text{ Mpc}^{-1}$, this result corresponds to $\Upsilon_V = 6.0$ at an absolute magnitude of $M_V \simeq -22.5$, or $L_{V,gal} = 8.5 \times 10^{10} L_{\odot}$. In addition to this, van der Marel (1991) finds that Υ increases with L_{gal} as a power law with exponent 0.35 ± 0.05 . Since other studies of the fundamental plane have claimed a slightly shallower exponent of 0.25–0.30 (e.g., Faber et al. 1987; Pahre, Djorgovski, & de Carvalho 1995, and references therein), $\Upsilon_V \propto L_{V,gal}^{0.3}$ is adopted here. Thus,

$$\frac{\Upsilon_V}{M_{\odot} L_{\odot}^{-1}} = 6.3 \left(\frac{L_{V,gal}}{10^{11} L_{\odot}} \right)^{0.3}. \quad (25)$$

It should be noted again that these mass-to-light ratios refer to the stellar populations in the cores of the galaxies, and are not unduly influenced by any dark matter on larger scales. If equation (25) is used in (24), the dependence $\mathcal{N}_{tot} \propto L_{V,gal}^{1.3}$, or $S_N \propto L_{V,gal}^{0.3}$, emerges naturally for constant $\hat{\epsilon}_{cl}$ and G . This is essentially the scaling found empirically by Kissler-Patig (1997).

The other point of concern is, of course, the hot gas content of ellipticals in general. To get a rough handle on this, notice that the (soft) X-ray luminosities of early-type systems scale with their blue luminosities as $L_X \propto L_B^x$, with $x \simeq 2-3$ (and with significant scatter about the mean trend: e.g., Forman et al. 1985; Brown & Bregman 1998). This scaling can be related to the ratio $G = M_{\text{gas}}/M_{\text{stars}}$ by noting that $L_X \propto \int \rho_{\text{gas}}^2 T_{\text{gas}}^{1/2} dV \propto M_{\text{gas}}^2 T_{\text{gas}}^{1/2} R^{-3}$ for the bremsstrahlung emission that dominates L_X in this context. Also, the slope x of the L_X - L_B relation is the same if L_V is used instead, so the implication is that $G^2 \propto R^3 T_{\text{gas}}^{-1/2} \Upsilon_V^{-2} L_V^{x-2}$. To go further, T_{gas} bears some relation to the stellar velocity dispersion: $T_{\text{gas}} \propto \sigma^{2y}$, with $y \simeq 0.7-1.5$ (Davis & White 1996; Brown & Bregman 1998); the V -band fundamental plane gives for the stellar quantities, $\sigma \propto L_V^{0.64} R^{-0.48}$ and $R \propto L_V^{1.1}$ (e.g., de Carvalho & Djorgovski 1989, 1992; Pahre et al. 1995); and, from equation (25) just above, $\Upsilon_V \propto L_V^{0.3}$. Putting all of this together, $G^2 \propto L_V^{x+0.7-0.11y}$. Evidently, the uncertainties in x and y are not crippling to this analysis, as $G \propto L_V^{1.5 \pm 0.25}$ is fairly representative of the range of possibilities. The scaling can be normalized to apply specifically to brightest cluster galaxies (BCGs) by using the observations of M87, which lies at the spatial and dynamical center of the Virgo Cluster.¹⁰ As was mentioned in §3.2, the global ($r_{\text{gc}} \leq 100$ kpc) ratio of gas to stars in M87 is $\simeq 0.4$ by mass. Since the V -band luminosity of the galaxy is about $8 \times 10^{10} L_{\odot}$ (from de Vaucouleurs & Nieto 1978, for $D = 15$ Mpc), it is then reasonable to set

$$G \approx 0.55 \left(\frac{L_{V,\text{gal}}}{10^{11} L_{\odot}} \right)^{1.5}. \quad (26)$$

Putting this and equation (25) both into equation (24), and holding $\hat{\epsilon}_{\text{cl}}$ fixed, it can be seen that the mean trend expected for \mathcal{N}_{tot} between $L_{V,\text{gal}} = 3 \times 10^{10} L_{\odot}$ and $2 \times 10^{11} L_{\odot}$ (so between an implied G of $\simeq 0.1$ and 1.6) is roughly $\mathcal{N}_{\text{tot}} \propto L_{V,\text{gal}}^{1.75}$. Despite the crudeness of the estimate of G used here, the power 1.75 is just that inferred from observational scalings presented by Harris et al. (1998) for a large sample of BCGs.

The full relation between \mathcal{N}_{tot} and $L_{V,\text{gal}}$ is drawn as the heavy black line in Fig. 8, where the total GCS populations of 65 early-type galaxies are plotted against their V luminosities. These data are the same as those plotted in Figure 11 of Harris et al. (1998), and the original references are given in that paper. The open circles in Fig. 8 here denote BCGs in a large number of rich clusters and a few poor groups; the filled symbols refer to other ellipticals, some in clusters and some more isolated. The bold curve has $\hat{\epsilon}_{\text{cl}} = M_{\text{gcs}}/(M_{\text{gas}} + M_{\text{stars}}) = 0.0026$, constant in all galaxies. Also shown, as the dashed line, is the result of keeping this uniform $\hat{\epsilon}_{\text{cl}}$, but setting $G \equiv 0$ in equation (24) while still having Υ_V increase with luminosity as in equation (25). The three dotted straight lines are loci of constant specific frequency, $\mathcal{N}_{\text{tot}} \propto L_{V,\text{gal}}$, as given by equation (1) for (from top to bottom in the Figure) $S_N = 15, 5$, and 1.5.

It is immediately obvious why a roughly constant $S_N \simeq 5$ is often assumed for large ellipticals such as these. It is equally clear, however, that such a simple characterization tends to overpredict \mathcal{N}_{tot} at low $L_{V,\text{gal}}$, and systematically underestimates it at high luminosities. Accounting for $\Upsilon_V \propto L_{V,\text{gal}}^{0.3}$ goes some of the way towards explaining this while allowing for a universal formation efficiency ϵ_{cl} ; and referring the GCS populations in BCGs to the galaxies' total stellar *plus gas* masses seems indeed to remove the rest of the first specific frequency problem in general.

It is encouraging that these rather broad considerations lead to a significantly improved description of the observed \mathcal{N}_{tot} - $L_{V,\text{gal}}$ dependence, in which there are no obvious *systematic* deviations from a uniform $\hat{\epsilon}_{\text{cl}} \simeq 0.0026$ (see also §4.4). There remains a good deal of scatter about the mean line in Fig. 8, but this could well reflect departures of individual galaxies from the fundamental plane, the mean L_X - L_B (or G - $L_{V,\text{gal}}$) relation, or the assumed $(B - V) = 1.0$, rather than any large variations in the fundamental efficiency of cluster formation. Note, for example, that the observed mass-to-light ratio of M87 is $\Upsilon_V \simeq 10.5$, some 80% higher than that expected from equation (25). Correcting for this would bring the $\hat{\epsilon}_{\text{cl}} = 0.0026$ curve in Fig. 8 just up to the M87 data point there. To rather a lesser degree, some of the scatter could also arise from GCS-to-GCS differences in the relative magnitude of any dynamical reduction of $M_{\text{gcs}}^{\text{init}}$ over a Hubble time.

It should be noted that this explanation of the first S_N problem differs somewhat from those previously proposed (see §2.2). In particular, Blakeslee (1997) and Blakeslee et al. (1997) showed a correlation between the specific frequencies on 40-kpc scales in BCGs, and the X-ray luminosities over much larger volumes ($R_{\text{gc}} \leq 500$ kpc) in their host clusters. These authors, along with West et al. (1995) and Harris et al. (1998), therefore interpret the phenomenon of high specific frequency as one associated in some way with entire clusters of galaxies. The analysis presented here, however, has attempted to address the problem more locally, by referring to the gas and stellar masses on similar spatial scales (typically $r_{\text{gc}} \lesssim 100$ kpc) to estimate G (eq. [26]) in individual systems; nowhere has any appeal been made to more global properties of galaxy clusters. This general approach is motivated, of course, by the observed situation in M87 specifically (§3). The correlation that does exist between BCG S_N and cluster-wide L_X (and other such relations; see the references cited) may simply stem from the fact that the gas around BCGs in rich clusters blends smoothly into the intracluster medium as a whole. Note that a relation of some kind between “local” L_X and \mathcal{N}_{tot} is also implied by Santiago & Djorgovski (1993), although they attach no specific interpretation to it.

Interestingly, the bold line in Fig. 8 departs significantly from linearity (i.e., from a simple power-law scaling between \mathcal{N}_{tot} and $L_{V,\text{gal}}$) for $M_{\text{gas}}/M_{\text{stars}} \gtrsim 0.1-0.2$, corresponding to $L_V \gtrsim 3-5 \times 10^{10} L_{\odot}$ or $M_V \lesssim -21.5$. This magnitude is similar to that which appears to divide ellipticals into two broad classes in terms of their kinematics, isophote shapes, and light distributions. (Lower-luminosity ellipticals generally show rapid rotation, flattened and disk-like isophotes, and steep cusps in their central densities, while brighter systems are slowly rotating, with round and boxy isophotes and

¹⁰The term BCG is used loosely here, to refer to the centrally dominant galaxies in groups as well as in rich clusters, even when these are not strictly ranked first by luminosity.

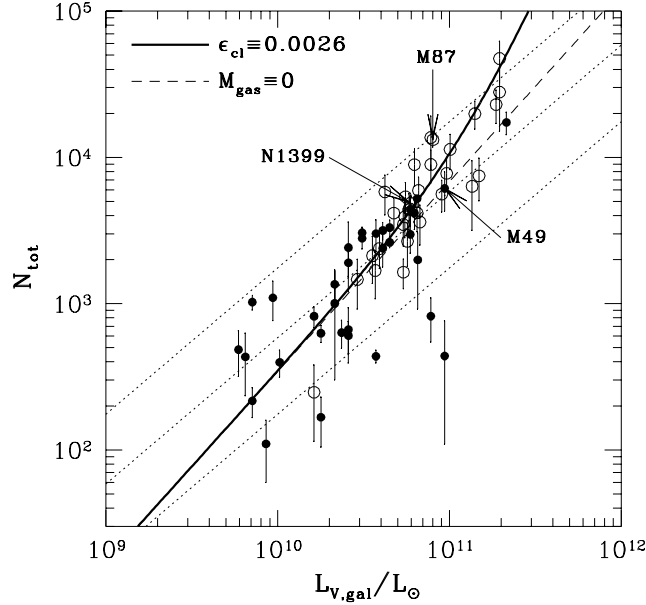


FIG. 8.— Observed total GCS populations, N_{tot} , vs. total galaxy luminosity, $L_{V,\text{gal}}$, for a sample of 65 giant ellipticals and BCGs (filled and open circles; from Harris et al. 1998, and references therein). Dotted lines have $N_{\text{tot}} \propto L_{V,\text{gal}}$, or constant $S_N = 15, 5$, and 1.5 . The systematic departure of BCGs from $S_N \approx 5$, at $L_{V,\text{gal}} \gtrsim 3 - 5 \times 10^{10} L_\odot$, is an illustration of the first specific frequency problem. The bold, solid curve is the prediction of an assumed universal cluster formation efficiency $\epsilon_{\text{cl}} = 0.0026$; the thin, dashed line is what that prediction would be if all ellipticals were completely devoid of gas. The two most extreme outliers are NGC 3557 and NGC 5018, each of which is relatively isolated and has $L_V \sim 10^{11} L_\odot$ ($M_V \simeq -22.5$) but $S_N < 1$.

shallower central density profiles; see, e.g., Davies et al. 1983; Bender et al. 1989; Nieto, Bender, & Surma 1991; Tremblay & Merritt 1996; Gebhardt et al. 1996; Faber et al. 1997.) This bears directly on the recent discussion of Kissler-Patig (1997; see also van den Bergh 1998), who used observed trends in GCS specific frequencies and radial distributions as further evidence for the empirical “dichotomy” of ellipticals. In particular, Kissler-Patig noted that the cluster systems in early-type galaxies with $M_V \gtrsim -21.5$ tend to have lower specific frequencies and steeper N_{cl} profiles than those in brighter galaxies. Although he went on to argue for a discontinuous change in the cluster formation efficiency for galaxies with L_V below and above $\approx 5 \times 10^{10} L_\odot$, Fig. 8 now shows that all of the data are well represented by a *continuously* increasing S_N that derives from a *constant* ϵ_{cl} and a *smoothly increasing* gas mass fraction, G ; the nonlinearity intrinsic to the resulting $N_{\text{tot}}-L_{V,\text{gal}}$ relation just happens to roughly mimic a break of sorts around $M_V \simeq -21.5$.

This interpretation can also account for another correlation suggested by Kissler-Patig (1997), namely, that S_N appears to be lower in (faint) ellipticals whose isophotes show disk-like deviations from pure ellipses, and higher in those (brighter) galaxies with more box-like shapes. These isophotal perturbations are themselves correlated with the X-ray luminosities of ellipticals (Bender et al. 1989), in the sense required qualitatively to explain this observation of GCSs again in terms of a constant ϵ_{cl} and a systematically increasing gas-to-stellar mass ratio. This raises the interesting question of which, of gas content or isophote shape, is the more fundamental property of elliptical galaxies; the present discussion, at least, would appear to favor the first alternative.

Finally, although the slopes of GCS radial distributions cannot be addressed directly by Fig. 8, it seems natural that, given a fixed ϵ_{cl} , ellipticals with large gas contents (and thus high global S_N) should generally have shallower GCS density distributions, relative to their stellar profiles, at large galactocentric radii (simply because $\rho_{\text{gas}}/\rho_{\text{stars}}$ usually increases with r_{gc} in early-type galaxies). As was suggested in §2.2, then, the first and second S_N problems should be closely related, with $G = M_{\text{gas}}/M_{\text{stars}}$ the controlling factor in both. Again, this is consistent with the observed trend (noted by Forbes et al. 1997; Kissler-Patig 1997; and van den Bergh 1998) towards weaker dependences of N_{cl} on R_{gc} in brighter and higher- S_N galaxies. This proposal should, of course, be checked on a case-by-case basis, as it was for M87 in §3.2 above, in as many systems as possible.

4.2. Dwarf Ellipticals

If the bold line in Fig. 8 is extrapolated into the regime of dwarf ellipticals, $L_{V,\text{gal}} \lesssim 2 \times 10^9 L_\odot$, it clearly implies that global $S_N < 2$ should be observed in these faint galaxies. This is completely at odds with the data of Durrell et al. (1996) and Miller et al. (1998), who find an average $S_N \approx 5$ for a large sample of dE’s in the Local Group, in other groups

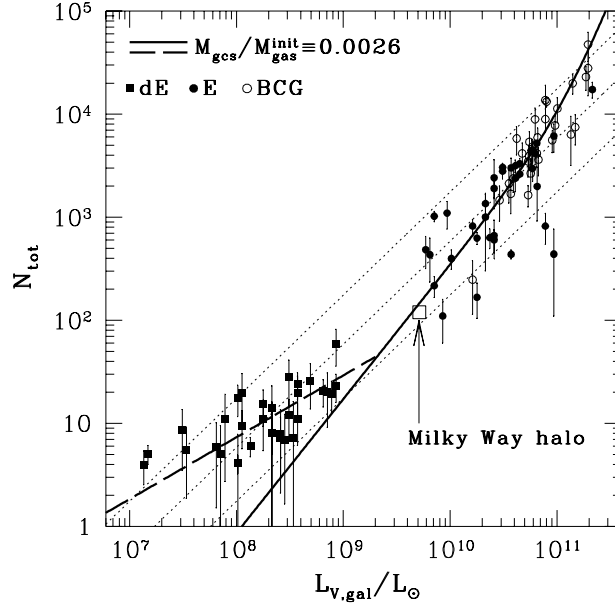


FIG. 9.— \mathcal{N}_{tot} vs. $L_{V,\text{gal}}$ for early-type systems, now including 32 dwarf ellipticals with $L_{V,\text{gal}} \lesssim 2 \times 10^9 L_{\odot}$ (solid squares; Durrell et al. 1996 and Miller et al. 1998). Filled and open circles represent the same giant ellipticals and BCGs plotted in Fig. 8. The dotted lines of constant $S_N = 15, 5$, and 1.5 , and the heavy solid curve with $\epsilon_{\text{cl}} \equiv 0.0026$ are also the same as those shown in Fig. 8. The bold, dashed line is the prediction for the same constant $\epsilon_{\text{cl}} = M_{\text{gcs}}^{\text{init}}/M_{\text{gas}}^{\text{init}} = 0.0026$, after correcting for significant gas loss in supernova-driven winds from dwarfs fainter than $M_V \simeq -18.5$. The large open square is plotted at the observed L_V and \mathcal{N}_{tot} of the Milky Way *spheroid*; see §4.3 of the text.

nearby, and in the Virgo and Fornax Clusters. In addition, Miller et al. claim evidence for an *increasing* S_N towards fainter $L_{V,\text{gal}}$.

This can be explained by first recalling that dwarf ellipticals do not fall on the fundamental plane of bright galaxies; thus, the scalings (25) and (26) do not apply to them. Also, these galaxies are bluer than their giant counterparts, so that the conversion to V -band mass-to-light ratios from measured Υ_R , as described above, is again inapplicable; and in any case, even the cores of dwarfs appear to be dominated by dark matter, so that their dynamical Υ_V are not necessarily representative of the stellar values. Most importantly—and likely at the heart of these other points—dE’s present sufficiently shallow potential wells that they should have suffered significant amounts of mass loss during supernova-driven winds in early bouts of star formation. Thus, even though these galaxies are gas-poor at the present, the appropriate observable $\hat{\epsilon}_{\text{cl}} = M_{\text{gcs}}/M_{\text{stars}}$ is *not an accurate estimator of the true cluster formation efficiency* $\epsilon_{\text{cl}} = M_{\text{gcs}}^{\text{init}}/M_{\text{gas}}^{\text{init}}$ (see Durrell et al. 1996 for the first suggestion that this is an important consideration in understanding dwarf GCSs). Even still assuming that the GCSs now have $M_{\text{gcs}} \simeq M_{\text{gcs}}^{\text{init}}$, allowance has to be made for an additional factor $M_{\text{stars}}/M_{\text{gas}}^{\text{init}} < 1$. The relation analogous to equation (24) in this case is therefore

$$\mathcal{N}_{\text{tot}} \simeq 1.7 \times 10^4 \frac{M_{\text{gcs}}}{M_{\text{gas}}^{\text{init}}} \left(\frac{M_{\text{gas}}^{\text{init}}}{M_{\text{stars}}} \right) \left(\frac{L_{V,\text{gal}}}{2 \times 10^9 L_{\odot}} \right) \left(\frac{\Upsilon_V}{2 M_{\odot} L_{\odot}^{-1}} \right) \left(\frac{\langle m \rangle_{\text{cl}}}{2.4 \times 10^5 M_{\odot}} \right)^{-1}, \quad (27)$$

where $\Upsilon_V \simeq 2$ should be a good representation of the stellar populations in systems fainter than about $2 \times 10^9 L_{\odot}$.

The specific model of Dekel & Silk (1986), which considers supernova-driven winds in dwarf galaxies that are dynamically dominated by dark matter halos, can be used to evaluate the ratio of initial gas to present stellar mass. That study finds that the winds from systems with velocity dispersions less than about 100 km s^{-1} , corresponding to $M_V \gtrsim -18.5$ at the current epoch, should have expelled whatever gas remained after a single burst of star formation. Moreover, as one moves towards shallower potential wells and fainter $L_{V,\text{gal}}$, the fractional mass lost, relative to the initial total, is naturally expected to increase. The predicted scaling, in the limit of very large mass loss and for a power spectrum similar to that in a standard cold dark matter cosmology, is roughly $M_{\text{gas}}^{\text{init}}/M_{\text{stars}} \propto L_{\text{gal}}^{-0.4}$. Taking the crude step of extrapolating this all the way to the critical velocity dispersion (i.e., to $L_{V,\text{gal}} \simeq 2 \times 10^9 L_{\odot}$), and assuming that any gas driven from brighter

and more massive galaxies was a negligible fraction of the total, the implication is that

$$\frac{M_{\text{gas}}^{\text{init}}}{M_{\text{stars}}} \simeq \left(\frac{L_{V,\text{gal}}}{2 \times 10^9 L_{\odot}} \right)^{-0.4}, \quad L_{V,\text{gal}} \leq 2 \times 10^9 L_{\odot}. \quad (28)$$

Substituting this in equation (27), and assuming a constant stellar $\Upsilon_V = 2$, yields $\mathcal{N}_{\text{tot}} \propto L_{V,\text{gal}}^{0.6}$ and $S_N \propto L_{V,\text{gal}}^{-0.4}$ for dwarf ellipticals. Although the picture of dE's as single-burst populations is now known to be incomplete (see, e.g., Mateo 1998), this result is nevertheless consistent with the observations of Miller et al. (1998).

Figure 9 uses the data from Durrell et al. (1996) and Miller et al. (1998) to place 32 nucleated and non-nucleated dwarf ellipticals into the $L_{V,\text{gal}} - \mathcal{N}_{\text{tot}}$ plane with the brighter galaxies from Fig. 8. (Of these, 16 are taken from Durrell et al., and 16 from Miller et al. Only GCSs detected at the $\geq 1\text{-}\sigma$ level are used.) The bold dashed line in the lower left of this plot comes from equations (27) and (28), assuming a constant $\epsilon_{\text{cl}} = M_{\text{gcs}}/M_{\text{gas}}^{\text{init}} = 0.0026$. The heavy solid line is the same as that in Fig. 8—i.e., it also has $\epsilon_{\text{cl}} = 0.0026$, but applies to fundamental-plane ellipticals—and the light, dotted lines correspond, as before, to constant $S_N = 15, 5$, and 1.5 . Once again, all the data appear consistent with a universal globular cluster formation efficiency. It will be important to properly confirm this with detailed models for the dE's in particular, and to flesh it out with observations of systems at $L_{V,\text{gal}} \sim (1 - 5) \times 10^9 L_{\odot}$ in general.

4.3. Globular Clusters in the Milky Way

One object that falls just inside this observational “gap” in luminosity is the stellar *spheroid*—disk excluded—of the Milky Way. The total V -band luminosity here has been estimated by de Vaucouleurs & Pence (1978) to be $L_V \simeq 5.1 \times 10^9 L_{\odot}$ [after applying a color of $(B - V) = 0.65$ to their $M_B = -18.8$]. At the same time, the total number of globular clusters that are genuine halo objects, rather than part of the (thick) disk, is $\mathcal{N}_{\text{tot}} \simeq 110\text{--}120$. (Halo globulars are identified on the basis of their metallicity, $[\text{Fe}/\text{H}] \leq -0.80$; refer back to Fig. 2 above.) This is the point plotted as the large open square in Fig. 9.

In fact, de Vaucouleurs & Pence (1978) model the Galactic spheroid with an $R^{1/4}$ density law with effective radius $R_{\text{eff}} = 2.67$ kpc. Thus, in addition to predicting the absolute magnitude that would be seen by an external observer, it is also possible to parametrize the density profile of the entire stellar halo. To do this in three dimensions, Young's (1976) deprojection of the $R^{1/4}$ law may be used:

$$\frac{\rho_{\text{stars}}(r_{\text{gc}})}{M_{\odot} \text{pc}^{-3}} = 52.195 \left(\frac{\Upsilon_B}{M_{\odot} L_{\odot}^{-1}} \right) \left(\frac{L_B^{\text{tot}}}{L_{\odot}} \right) \left(\frac{R_{\text{eff}}}{\text{pc}} \right)^{-3} \exp \left[-7.669 \left(\frac{r_{\text{gc}}}{R_{\text{eff}}} \right)^{1/4} \right] \left(\frac{r_{\text{gc}}}{R_{\text{eff}}} \right)^{-7/8}, \quad (29)$$

which is valid for $r_{\text{gc}} \gtrsim 0.2 R_{\text{eff}}$. Substitutions can be made for L_B^{tot} and R_{eff} directly from the work of de Vaucouleurs & Pence. One way to estimate the B -band mass-to-light ratio of the Galactic Population II is to adopt the same $\Upsilon\text{--}L_B$ scaling used in §4.1, but to normalize the relation by adopting solar colors rather than the redder ones that apply in ellipticals. van der Marel's (1991) mean $\Upsilon_R = 3.32 h_{50}$ then corresponds to $\Upsilon_B = 4.65 M_{\odot} L_{\odot}^{-1}$ at $M_B = -21.49$ (for $H_0 = 70 \text{ km s}^{-1} \text{ Mpc}^{-1}$ assumed), and $\Upsilon_B \propto L_B^{0.3}$. The implied $\Upsilon_B(\text{halo}) \simeq 2.2 M_{\odot} L_{\odot}^{-1}$ for $M_B = -18.8$ is consistent with the mean $\Upsilon_V = 2$ for globular clusters, and with the $\Upsilon_V = 1.75$ adopted for the spheroid by Bahcall & Soneira (1980) in their model of the Galaxy. Equation (29) is therefore evaluated here with $\Upsilon_B = 2 M_{\odot} L_{\odot}^{-1}$.

The dashed line in the bottom panel of Fig. 2 in §3.1 above shows this density profile, scaled down by a factor of

$$\langle \epsilon_{\text{cl}} \rangle_{\text{MW}} = 0.0027 \pm 0.0004. \quad (30)$$

This value is obtained as the mean of the ratio $\rho_{\text{cl}}/\rho_{\text{stars}}$ over all galactocentric radii $2 \leq r_{\text{gc}} \leq 40$ kpc, and it accounts for the position of the Milky Way halo in Fig. 9. Such a basic correspondence between our Galaxy and early Hubble types was previously suggested, although developed from a somewhat different argument, by de Vaucouleurs (1993).

It is also evident from Fig. 2 that there is no second S_N problem in the Milky Way: $\rho_{\text{cl}} \propto \rho_{\text{stars}}$ obtains throughout the entire halo at $r_{\text{gc}} \gtrsim 3$ kpc—so again, beyond roughly an effective radius, within which the original GCS might have suffered significant dynamical depletion. This point has long been appreciated, although it is usually discussed in the context of the fact that the same rough rule $\rho \propto r_{\text{gc}}^{-3.5}$ is inferred both for the spheroid, from counts of RR Lyrae and horizontal-branch stars (e.g., Preston, Schectman, & Beers 1991; Kinman, Suntzeff, & Kraft 1994), and for the GCS, from simple power-law fits to its density profile (Harris 1976; Zinn 1985; Djorgovski & Meylan 1994). This power law is shown as the dotted line in the bottom panel of Fig. 2.

4.4. Scatter in the $L_V\text{--}\mathcal{N}_{\text{tot}}$ Plane

As a final test of the general viability of a single globular cluster formation efficiency, Fig. 10 plots the ratio of observed to predicted GCS \mathcal{N}_{tot} as a function of host galaxy luminosity for all of the 98 systems discussed thus far. The predicted \mathcal{N}_{tot} for fundamental-plane ellipticals and the Milky Way spheroid (filled circles and open square in the Figure) are given by equation (24), with the gas mass fraction G set identically to zero; for BCGs (open circles), by the same relation but with G as in equation (26); and for dE's (filled squares), by equation (27). In all cases, it has been assumed that $\epsilon_{\text{cl}} = 0.0026$. The median of the resulting ratios $\mathcal{R} \equiv \mathcal{N}_{\text{tot}}^{\text{obs}}/\mathcal{N}_{\text{tot}}^{\text{pred}}$ is 1.04, and the geometric mean is 0.98. Close to 80% (77/98) of these galaxies have $\frac{1}{2} \leq \mathcal{R} \leq 2$.

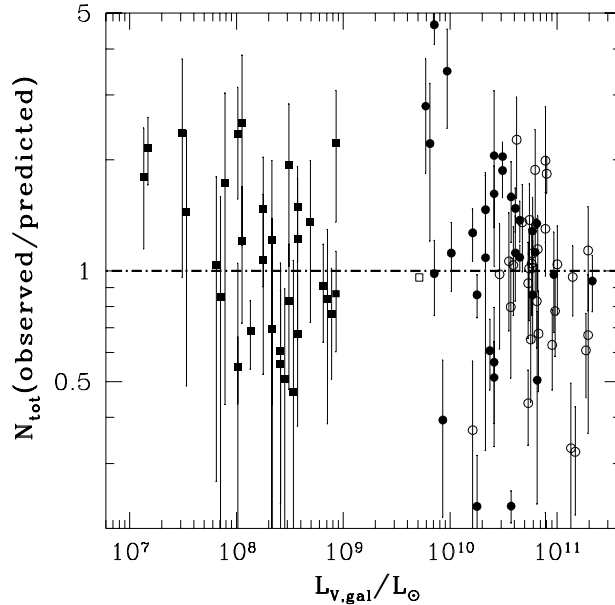


FIG. 10.— Ratio of observed \mathcal{N}_{tot} to the predicted values for all GCSs represented in Fig. 9, using $\hat{\epsilon}_{\text{cl}} = 0.0026$ in equation (24) or $M_{\text{gcs}}/M_{\text{gas}}^{\text{init}} = 0.0026$ in equation (27). Point types have the same meaning as in Fig. 9. The ratios for NGC 3557 and NGC 5018 are 0.07 and 0.17, and do not appear on the scale of this plot.

As was also mentioned in §4.1, but can perhaps be seen more clearly here than in Fig. 8 or Fig. 9, the deviations of observed \mathcal{N}_{tot} from the uniform- ϵ_{cl} prediction show no significant dependence on either galaxy luminosity or Hubble type. There are possibly two exceptions to this claim: (1) the GCS populations in the brightest BCGs, $L_{V,\text{gal}} \gtrsim 10^{11} L_{\odot}$, appear to fall below the values predicted with $\epsilon_{\text{cl}} = 0.0026$, by perhaps $\sim 50\%$ on average; and (2) the two faintest dwarfs, which happen to be the Local Group spheroidals Fornax and Sagittarius, both have \mathcal{N}_{tot} greater than predicted. These rough impressions may well not remain, in the mean, after future additions of GCS data from other very high- and low-luminosity galaxies; but even if they do, they need not imply the existence of fundamental variations in ϵ_{cl} . Rather, there is likely enough uncertainty in the adopted relation between gas mass fraction and $L_{V,\text{gal}}$ (eq. [26]) to account for the first item; and the second could reflect either a deficiency in the very simple correction (§4.2) for gas blow-out from very faint dwarfs, or the neglect of possibly extensive post-formation dynamical evolution in such low-mass galaxies (such as tidal stripping of their field stars; recall, for example, that Sagittarius is in the process of being accreted by the Milky Way).

Even if these issues are ignored completely, a least-squares fit to all of the data shown in Fig. 10 reveals an exceedingly weak dependence of $\mathcal{N}_{\text{tot}}^{\text{obs}}/\mathcal{N}_{\text{tot}}^{\text{pred}}$ on galaxy luminosity: $\mathcal{R} \propto L_{V,\text{gal}}^{-0.04 \pm 0.03}$. Fitting to only the fundamental-plane ellipticals and BCGs yields a steeper $\mathcal{R} \propto L_{V,\text{gal}}^{-0.2}$ or so, but this result appears to be driven by just three gE's with anomalously low or high GCS populations (cf. Fig. 8): NGC 3557, with $L_V = 9.4 \times 10^{10} L_{\odot}$ and $S_N = 0.4 \pm 0.3$; NGC 5018, which has $L_V = 7.8 \times 10^{10} L_{\odot}$ and $S_N = 0.9 \pm 0.3$; and NGC 4278, with $L_V = 7.1 \times 10^9 L_{\odot}$ but $S_N = 12.3 \pm 1.4$. If these systems are excluded, then $\mathcal{R}(\text{gE} + \text{BCG}) \propto L_{V,\text{gal}}^{0.02 \pm 0.04}$ is indicated instead. Similarly, the slopes of \mathcal{R} vs. $L_{V,\text{gal}}$ do not differ significantly from 0 for any of the individual Hubble-type samples represented in Fig. 10.

Thus, current observations of total GCS populations do show some scatter, and it will be important to understand—likely through detailed analyses, along the lines of §3, of more systems *individually*—whether or not this reflects an intrinsic scatter in the underlying globular cluster formation efficiency (see also §4.1). However, there is no clear evidence at present for any systematic departures from a mean global efficiency of $\epsilon_{\text{cl}} \approx 0.0026$.

4.5. Open Clusters

As was discussed in §2.1, the formation of stellar clusters continues to be an important element of star formation in general, and the existence of an apparently universal formation efficiency for globular clusters must reflect a generic piece of this process. However, the picture may still be incomplete: although the discussion to this point has included clusters that formed in a wide variety of environments—at galactocentric distances $r_{\text{gc}} \sim 10\text{--}100$ kpc, in galaxies spanning four orders of magnitude in total luminosity and inhabiting both poor groups and rich clusters—all of these formed at essentially a single epoch, and under physical conditions that were possibly much more extreme than those in, say, the disk

of the Milky Way today. It is important, therefore, to compare the protogalactic $\epsilon_{\text{cl}} \simeq 0.0026 \pm 0.0005$ to the frequency with which bound star clusters form in a typical quiescent galaxy at the current epoch. Disk clusters in the Milky Way present one opportunity to do this.

The rate of open cluster formation in the solar neighborhood has been estimated by Elmegreen & Clemens (1985) as $\mathcal{S}_{\text{cl}} \simeq (2.5 \pm 1) \times 10^{-7}$ clusters $\text{kpc}^{-2} \text{yr}^{-1}$. If the masses of the clusters range between $100 M_{\odot}$ and $5000 M_{\odot}$ according to $dN/dm \propto m^{-1.5}$ (from the luminosity spectrum dN/dL of van den Bergh & Lafontaine 1984), then a mean mass of $\simeq 700 M_{\odot}$ is indicated, and the formation rate becomes $\mathcal{S}_{\text{cl}} \simeq (1.8 \pm 0.7) \times 10^{-4} M_{\odot} \text{kpc}^{-2} \text{yr}^{-1}$. This is to be compared with the *total* star formation rate in the solar neighborhood, which includes those stars appearing in loose groups and unbound associations (or even in relative isolation) as well as in bound clusters. This rate is $\mathcal{S}_{\text{tot}} \simeq 4.5 \times 10^{-3} M_{\odot} \text{kpc}^{-2} \text{yr}^{-1}$ (e.g., McKee 1989).

Since the mean stellar mass is no different in clusters than in the field, the ratio of these two rates can be taken directly, to assess the local *number* fraction of stars born in clusters: $\mathcal{S}_{\text{cl}}/\mathcal{S}_{\text{tot}} \sim 0.04$. This is consistent with the classic estimate (e.g., Roberts 1957) of about 10%. However, the globular cluster ϵ_{cl} has been obtained here as a *mass* ratio, since this is the observable quantity that can be related directly to its formation value (see eq. [8]). To make a proper comparison with open cluster formation, it is therefore necessary to refer the mass going into newborn clusters (per unit area, per unit time) to the total mass of gas available for any kind of star formation. This latter figure can be derived from \mathcal{S}_{tot} using the mean star formation efficiency, $\langle \text{SFE} \rangle = \langle M_{\text{stars}}/M_{\text{gas}} \rangle$, averaged over many of the dense, star-forming (not necessarily cluster-forming) cores in giant molecular clouds. This number is only poorly known, but statistical arguments (e.g., Elmegreen 1983) suggest that it lies at the level of $\langle \text{SFE} \rangle \sim 5\% - 10\%$. Thus,

$$\epsilon_{\text{cl}}(\text{open}) \simeq \frac{\mathcal{S}_{\text{cl}}}{\mathcal{S}_{\text{tot}}/\langle \text{SFE} \rangle} \sim 0.002 - 0.004, \quad (31)$$

which is in reasonably good agreement with the result for globular cluster systems. The numerical value in equation (31) clearly should not be taken as definitive, given the very rough, order-of-magnitude nature of the argument that has produced it. That said, however, it is just the order-of-magnitude agreement between equations (31) and (23) which suggests that the basic mechanism of cluster formation may not have changed appreciably from protogalactic times to the present.

Another obvious place to check the current level of ϵ_{cl} is in starbursts and merging galaxies, which are forming massive young clusters in substantial numbers (e.g., Whitmore & Schweizer 1995; Meurer et al. 1995). Complete inventories of the star-forming gas mass in individual systems, and of the total mass in those of their young clusters that can be shown to be gravitationally bound (which to date has been done rigorously for only two objects: Ho & Filippenko 1996a, 1996b), would be of considerable interest. The results should be of particular relevance to the oft-made claim, which is now at the center of some debate (Sternberg 1998; Brodie et al. 1998), that these super star clusters are the modern-day equivalents of young globulars. If it turns out, for example, that strongly bound clusters in starbursts are forming in numbers very much in excess of those expected on the basis of $\epsilon_{\text{cl}} \simeq 0.25\%$ (as, e.g., the UV observations of Meurer et al. 1995 appear to suggest), then these spectacular events might *not* be representative of a ubiquitous phase in the formation of average elliptical galaxies.

5. DISCUSSION

The fact that the ϵ_{cl} values inferred here are everywhere so similar—over large ranges in radius inside M87, M49, and NGC 1399; from dwarf ellipticals to brightest cluster galaxies; and from massive, old globular clusters to smaller, much younger open clusters—should serve as a strong constraint on theories of star formation. The simplest interpretation is that the probability of attaining a cumulative star formation efficiency of $\text{SFE} \gtrsim 20\% - 50\%$ (see §2.1) in any dense clump of gas more massive than $\sim 10^2 - 10^3 M_{\odot}$ (so from open clusters on up) can depend only weakly, on average, on local environment (i.e., the density and pressure of ambient gas) or on factors such as global background density (meaning, e.g., in the protogalactic context, a $1\text{-}\sigma$ vs. a $3\text{-}\sigma$ density fluctuation; or a poor group of galaxies vs. a rich cluster). Moreover, implicit in plots like Figs. 8 and 9 is the fact that cluster formation efficiencies are also rather insensitive to metallicity: the mean abundances of the globulars in the galaxies represented there range over two orders of magnitude, from $[\text{Fe}/\text{H}] \simeq -2$ to $[\text{Fe}/\text{H}] \simeq 0$ (see Durrell et al. 1996; Forbes et al. 1997). Over a remarkably broad spectrum of physical conditions, therefore, it appears that similar fractions of star-forming gas—always about 0.25% by mass—are able to produce bound stellar clusters. The implicitly mass-averaged nature of the observational estimates of ϵ_{cl} has to be kept in mind, but would seem to be of little concern in most cases. It is therefore reasonable to place the efficiency of cluster formation alongside the globular cluster mass function dN/dm (McLaughlin & Pudritz 1996) and the mean globular cluster mass $\langle m \rangle_{\text{cl}}$ (e.g., Fig. 2 above) as robust and nearly universal physical quantities that must be derived from the most general aspects of the star formation process.

As a corollary to this, one implication of Figs. 8 and 9 above is that the efficiency of *unclustered* star formation could *not* have been universal. That is, in both dwarf elliptical and brightest cluster galaxies, where the data are consistent with $\epsilon_{\text{cl}} = M_{\text{gcs}}^{\text{init}}/M_{\text{gas}}^{\text{init}}$ having been constant in the mean, globular clusters apparently did form in precisely the numbers expected for the total amount of gas initially available to these systems. But then, the higher than average specific frequencies there are inferred to reflect larger ratios of $M_{\text{gas}}^{\text{init}}/M_{\text{stars}}$, so that lower than average amounts of this gas were converted into field stars. The data for dwarfs agree with a simple scenario in which most of the unused gas supply is driven entirely out of the galaxies by a strong wind following one major burst of star and cluster formation. If this is

basically correct, then the globulars in dE's quite possibly were able to form completely before the onset of such a wind, and they could conceivably have been instrumental in driving it; at the very least, if the protoclusters were still largely gaseous, they must have been already sufficiently dense and well defined that they could survive such a catastrophic event essentially intact. At the same time, field star formation must have been truncated by the wind, before reaching what would have been a “normal” efficiency of $M_{\text{stars}}/M_{\text{gas}}^{\text{init}} = 1 - \epsilon_{\text{cl}}$. Thus, *the massive and dense clumps of gas which ultimately formed bound star clusters had to have collapsed more rapidly than those which produced unbound groups and associations*. This conclusion may hold quite generally—one possible interpretation being that only those gas clouds in the highest-density tail of some distribution, in any setting, are able to achieve a high cumulative SFE—and it may be related to the fact that the globular clusters in dwarfs are generally somewhat bluer, and presumably more metal-poor, than the bulk of the field stars there (Durrell et al. 1996; Miller et al. 1998).

A similar feedback argument could also apply to BCGs, where it may be that especially strong early bursts of star and cluster formation led to the premature virialization of large amounts of protogalactic gas, and perhaps drove slow, *partial* galactic winds, most effectively in the low-density environs at large galactocentric radii (cf. Harris et al. 1998). The unused gas would have to remain hot to the present day, and more or less in the vicinity of the parent galaxy, in order to enter the observed L_X - L_B relation as inferred in §4.1. This requirement is consistent with the fact that BCGs are situated at or near the centers of their galaxy clusters, and thus at the bottoms of very deep potential wells. In this scenario, again, globulars would have had to form, in just the numbers expected of them, somewhat before field stars were able to do the same; and this truncation of unclustered star formation would have had to be more severe at large galactocentric radii (where the feedback is strongest). This could then account explicitly for the connection between the first and second specific frequency problems, i.e., between high global S_N and local $\Sigma_{\text{cl}}/\Sigma_{\text{stars}}$ ratios that increase with R_{gc} . It also gives a more specific context to the general claim (Harris 1986) that the shallowness of GCS radial distributions relative to the stellar light profiles in some ellipticals resulted from the globulars having formed slightly in advance of the stars there. The main demand on this picture for BCG formation is that it must be able to explain why $M_{\text{gas}}/M_{\text{stars}}$ increases with galaxy luminosity, i.e., why more massive BCGs apparently had larger fractions of their initial gas mass virialized early on. As Harris et al. (1998) discuss in some detail, this issue is likely related to the fact that brighter BCGs are generally found in more massive galaxy clusters, which may have presented higher-density and more turbulent environments that led to systematically higher star formation rates, and more violent feedback. Although speculative, these ideas are suggested directly by the GCS data, and are consistent with all those available. Since they are also obviously related to questions on the star-formation histories of dE's, on the origin of the L_X - L_B correlation in the brightest ellipticals, and on the nature of the intracluster medium, they should be addressed with considerably more rigor than has been applied here.

It is particularly striking that the cluster formation efficiency derived in §4.3 for the Milky Way halo is essentially indistinguishable from that which applied in M87, M49, and NGC 1399, and which appears to have held quite generally in ellipticals of most any description. This calls into serious question one of the primary motivations for the model of Ashman & Zepf (1992) and Zepf & Ashman (1993), who posit that ellipticals are formed primarily by the mergers of gas-rich spirals, and invoke preferential cluster formation during these events to account for what they claim is a typical factor of two difference in the observed ratios $M_{\text{gas}}/M_{\text{stars}}$ of late- and early-type systems. Although it is true that spirals have specific frequencies that are lower than those in bright E galaxies, by factors of perhaps 2–3 on average (as is exemplified by the Milky Way in Fig. 9 above; see also Harris 1991), it is now apparent that this is not necessarily a reflection of similar discrepancies in their more fundamental $\hat{\epsilon}_{\text{cl}}$. If the Milky Way is typical, it suggests that—even though stellar clusters certainly can form in merging galaxies—*mergers are not required to explain the relative GCS populations of spirals and ellipticals in general*. Conversely, whenever an elliptical does form by the major merger of two spirals, this is allowed to include cluster formation only at the standard efficiency of $\epsilon_{\text{cl}} \simeq 0.0025$.

Ashman & Zepf (1992) and Zepf & Ashman (1993) also attribute the second specific frequency problem to the formation of ellipticals by mergers of spirals with pre-existing GCSs. However, it is not clear that this is necessary either, if the extended spatial distribution of globulars in the brightest ellipticals is generally related to their association with hot gas at rather large galactocentric radii. In fact, a basic expectation of the original Ashman-Zepf scenario is that the second S_N problem should be *less* pronounced in galaxies with higher global S_N (which they hypothesize to have suffered greater numbers of major mergers). The sense of this predicted trend is *opposite* to the one implied here—with empirical support directly from the evidence in M87, and indirectly from the correlations of Forbes et al. (1997) and Kissler-Patig (1997)—in which a constant ϵ_{cl} combines with the larger $M_{\text{gas}}/M_{\text{stars}}$ in higher- S_N ellipticals, to produce greater contrasts in their projected Σ_{cl} and Σ_{stars} profiles. Although radial-profile and S_N data by themselves may not rule out the merger model for GCSs altogether, a revision to take account of the hot gas in large ellipticals is essential if it is to be at all viable. (See also Forbes et al. 1997 and Kissler-Patig et al. 1998 for critical discussions of this and other aspects of the basic idea.)

Finally, the GCS density profiles derived specifically for M87, M49, and NGC 1399 in §3 also are relevant to issues of the generic spatial structure of GCSs, and to the specific matter of the possible existence of intergalactic globulars in clusters of galaxies. To facilitate a discussion of these points, and for reference, Table 5 presents the results of least-squares fits of a few different parametric functions to the spatial distributions of the M87, M49, and NGC 1399 GCSs, as they are given in Tables 2, 3, and 4 above. The functions include (from left to right in Table 5) a power law with a constant-density core region; the cusped density profile suggested by Navarro, Frenk, & White (1996, 1997) as appropriate for cold dark matter halos; and the law popularized by Hernquist (1990) and applied widely to the light profiles of elliptical galaxies. In all cases, fits were performed by minimizing the residuals of the functions' *projected* density profiles relative to the N_{cl} data, which have smaller observational uncertainties than the volume densities do. The best-fit parameters thus obtained were then used to overlay the original, three-dimensional functions on the deprojected n_{cl} and verify that they provided

good descriptions of those as well. One consequence of this procedure is that no fit is given for the Hernquist (1990) profile, $n_{\text{cl}} \propto (r/a)^{-1}(1+r/a)^{-3}$, to the M87 GCS. Although it is possible to fit this function directly to the n_{cl} data, its projection affords a poor description of the full N_{cl} distribution. This almost certainly reflects the fact that the GCS profile in M87 appears about to become significantly shallower, at least temporarily, beyond the last radius ($r_{\text{gc}} \simeq 100$ kpc) for which cluster counts exist (because Fig. 4 suggests essentially that $\rho_{\text{cl}} \propto \rho_{\text{gas}}$ there). Such a change in slope is obviously not allowed by Hernquist’s density profile. Thus, the failure of this model in this case makes the point that *any* of the density fits in Table 5 should be taken at face value only over the ranges of r_{gc} that have been directly observed; extrapolations to much larger radii could potentially introduce appreciable systematic errors.

Table 5 has three interesting implications: (1) None of the available data *require* the existence of truly constant-density “cores” in GCSs. This was also mentioned by McLaughlin (1995) and it is, of course, plainly seen in Figs. 4 through 6. Evidence is emerging for a similar situation in elliptical galaxies generally (Crane et al. 1993; Gebhardt et al. 1996), and apparently also in galaxy clusters (Merritt & Tremblay 1994; Carlberg et al. 1997; McLaughlin 1999). (2) It has been suggested, particularly in the contexts of some dynamical analyses (e.g., Huchra & Brodie 1987; Weil, Bland-Hawthorn, & Malin 1997) that the M87 GCS directly reflects the distribution of dark matter in and around that galaxy. However, this is not true in any simple sense; neither of the n_{cl} fits given in Table 5 provides an adequate description of $\rho_{\text{dark}}(r_{\text{gc}})$ in M87. Instead, it is found there that $\rho_{\text{dark}} \propto \rho_{\text{gas}}$ (see McLaughlin 1999), in which case Fig. 4 shows that the GCS becomes a reliable tracer of the dark matter halo *alone* only on fairly large spatial scales (where the number densities become quite low). (3) The analytical fits to N_{cl} and n_{cl} offer a convenient way to extrapolate the observed densities to (slightly) smaller and larger radii than those observed, so as to compute the total GCS populations of these three galaxies. Thus, in M87, it is found that $N_{\text{tot}} = 13\,600 \pm 500$ clusters (over all magnitudes) are *projected* to distances $R_{\text{gc}} \leq 25' \simeq 110$ kpc from the galaxy’s center; in M49, there are $N_{\text{tot}} = 6\,850 \pm 550$ globulars within the same projected R_{gc} ; and in NGC 1399, $N_{\text{tot}} = 4\,700 \pm 400$ clusters have $R_{\text{gc}} \leq 14.5' \simeq 70$ kpc. These total “projected populations” are in good agreement with those estimated in many other studies (see the references cited in §3). However, it is now possible to determine the three-dimensional radius of the sphere which actually contains all of these clusters in each system. From either of the M87 fits in Table 5, it is found that 13 600 clusters are contained within $r_{\text{gc}} \simeq 150\text{--}160$ kpc; in M49, 6 850 globulars come from the sphere $r_{\text{gc}} \leq 140\text{--}150$ kpc; and the 4 700 globulars in NGC 1399 all have true galactocentric positions $r_{\text{gc}} \leq 90\text{--}95$ kpc. To put this another way, all three GCSs are sufficiently centrally concentrated that, in each case, some 85%–90% of the globular clusters projected onto the galaxy—so again, to within $R_{\text{gc}} \leq 110$ kpc for M87 and M49, and $R_{\text{gc}} \leq 70$ kpc for NGC 1399—really are located at those galactocentric distances in three dimensions.

This last point specifically can clarify and constrain the suggestion (White 1987; West et al. 1995; Côté et al. 1998) that the high specific frequencies in BCGs like M87 are due to the “contamination” of their GCSs, in projection, by a significant number of globular clusters that are associated with a galaxy cluster as a whole, rather than bound to the central galaxy itself. Harris et al. (1998) tried to test this idea in some detail for M87 in particular, working from the assumption (following White 1987) that any population of intergalactic globular clusters (IGCs) should generally be associated with the diffuse stellar light of the cD envelopes that surround many BCGs (i.e., these structures were considered to comprise primarily intracluster stars). This hypothesis leads to inconsistencies that prompted Harris et al. to reject IGCs as the main cause of the first specific frequency problem. While their arguments still stand within the framework that they constructed, it is now seen that the high S_N of M87 certainly, and likely those of other BCGs as well, can be traced to

TABLE 5
PARAMETRIC FITS TO GCS VOLUME DENSITY PROFILES¹

	$n_{\text{cl}} = n_0[1 + (r/a)^2]^{-\gamma/2}$			$n_{\text{cl}} = n_0(r/a)^{-1}(1 + r/a)^{-2}$		$n_{\text{cl}} = n_0(r/a)^{-1}(1 + r/a)^{-3}$	
	γ	a	$\log n_0$	a	$\log n_0$	a	$N_\infty = 2\pi a^3 n_0$
M87 ²	2.53±0.17	0.73±0.27	2.177 ^{+0.248} _{−0.193}	2.10±0.40	1.522 ^{+0.220} _{−0.180}
M49 ³	2.73±0.27	1.41±0.56	1.170 ^{+0.356} _{−0.187}	2.25±0.45	0.985 ^{+0.285} _{−0.219}	6.18±1.32	3260±475
N1399 ⁴	3.15±0.35	1.54±0.46	1.466 ^{+0.233} _{−0.124}	1.15±0.45	1.859 ^{+0.543} _{−0.351}	3.78±0.92	3630±460

¹For radii in arcminutes and densities in number per arcmin³.

²Normalizations n_0 apply to $V \leq 23.9$; divide by 0.5572 to obtain population over all magnitudes.

³Normalizations n_0 apply to $V \leq 23.3$; divide by 0.3646 to obtain population over all magnitudes.

⁴Normalizations n_0 apply to $V \leq 24.0$; divide by 0.5332 to obtain population over all magnitudes.

subsets of their GCSs that are associated with hot gas, and not necessarily with stars at all. This does appear to favor the basic notion of IGCs, since the gas around M87 extends to very large spatial scales, and traces out the potential well of the Virgo Cluster as a whole (McLaughlin 1999). If a constant $\hat{\epsilon}_{\text{cl}}$ holds all the way out, then, a cluster-wide population of globulars could be expected. However, since *all* of the 13 600 globular clusters which give M87 its high specific frequency in projection are physically associated with a volume of radius ~ 150 kpc around the galaxy, it is not obvious that any of them are truly “intergalactic” objects at the current epoch. Projection effects are *not* solely responsible for the high S_N of M87, and although intergalactic globular clusters may well exist, it is not clear that any have yet been observed.

Of course, since M87 is at the dynamical center of Virgo, it can be difficult to distinguish meaningfully between the galaxy and the cluster on 100-kpc scales. In the context of IGCs, the question evidently comes down to one of origin: did the globulars now seen right around M87 actually form there, or were many of them somehow brought in from much further than 150 kpc away? Any self-consistent answer to this must be able to account for the observed fact that $\rho_{\text{cl}} = 0.003(\rho_{\text{gas}} + \rho_{\text{stars}})$ at galactocentric radii $r_{\text{gc}} \sim 10$ –100 kpc in M87; that is, both the very existence and the normalization of this proportionality have to be explained. Although essentially any scenario which is able to do this would be allowed by the current data, none could be *preferred* over what remains the simplest option: that the bulk of the M87 GCS formed in situ, with a thoroughly standard and spatially constant ϵ_{cl} . Ultimately, only detailed evolutionary models, tailored specifically to the properties of M87 and Virgo and considering both stars *and* gas, can really decide what fraction of the galaxy’s GCS might have come originally from the cluster at large.

6. SUMMARY

Stars form mainly in groups, some of which emerge from their natal clouds of gas as gravitationally bound clusters. An understanding of cluster formation will therefore be integral to any full theory of star formation, and an important element of this is simply the frequency with which it occurs. That is, what is the likelihood that a star-forming cloud of gas—whether this be a dense clump in a Galactic giant molecular cloud, or a larger one in a protogalactic fragment—will achieve the high cumulative star formation efficiency (viz. SFE $\gtrsim 20\%$ –50%) that allows its stars to remain bound as a cluster after they have cleared away the gas? This paper has used observations of the globular cluster systems in galaxy halos to address this question, and to empirically evaluate the efficiency of cluster formation: by mass, $\epsilon_{\text{cl}} \simeq 0.25\%$. This is, by all appearances, nearly a universal number, and it should therefore serve as a strong constraint on theories of star and cluster formation in any context.

To arrive at this result, it was first shown (§2.1) that the total (global) *masses* of GCSs are quite robust, even over a Hubble time, against the dynamical processes that work to destroy low-mass globular clusters in the central regions of galaxies. With an observed M_{gcs} thus useful as a measure of the initial quantity, the specific frequencies of GCSs, $S_N \propto \mathcal{N}_{\text{tot}}/L_{V,\text{gal}} \propto M_{\text{gcs}}/M_{\text{stars}}$, serve as *crude* first estimates of the basic formation efficiency $\epsilon_{\text{cl}} \equiv M_{\text{gcs}}^{\text{init}}/M_{\text{gas}}^{\text{init}}$. To the *limited* extent that $S_N \approx 5$ is an adequate description of early-type galaxies, the implication is that $\epsilon_{\text{cl}} \sim 2 \times 10^{-3}$. The limiting factor in this simplest treatment of GCS data is the assumption that a galaxy’s current stellar mass always suffices as an estimate of its total initial gas mass; if taken too far, this quickly leads to some perplexing conclusions.

As was reviewed in §2.2, systematic variations in S_N exist along the entire sequence of early-type galaxies, from dwarf ellipticals (where $\mathcal{N}_{\text{tot}} \propto L_{V,\text{gal}}^{0.6}$ or so) through normal giants ($\mathcal{N}_{\text{tot}} \propto L_{V,\text{gal}}^{1.3}$) and on to the brightest ellipticals, including many of the central galaxies in groups and rich clusters ($\mathcal{N}_{\text{tot}} \propto L_{V,\text{gal}}^{1.8}$). If specific frequency were indeed a good estimator of ϵ_{cl} in general, the implication would seem to be that this also varied, for unknown reasons and in a non-monotonic fashion, as a function of galaxy luminosity. Closely related to this is the fact that the GCSs of some, but not all, large ellipticals are spatially more extended than their stellar halos. That is, local S_N values increase with projected R_{gc} in some systems, which naively would suggest that—again, for unknown reasons, and counter to any intuition—the efficiency of cluster formation *sometimes* increased with galactocentric radius.

An important clue to the true nature of both these “specific frequency problems”—which are most likely two aspects of a single phenomenon—lies in the observation that the global S_N in central cluster galaxies increases with the X-ray luminosity of their parent clusters. Some of the globulars in these systems ought then to be associated with the hot gas there; and $M_{\text{gas}}^{\text{init}}$ is approximated better by the present-day ($M_{\text{gas}} + M_{\text{stars}}$) than by M_{stars} alone. S_N then systematically overestimates the true cluster formation efficiency ϵ_{cl} , which instead is given empirically by $\hat{\epsilon}_{\text{cl}} = M_{\text{gcs}}/(M_{\text{gas}} + M_{\text{stars}})$. In addition, since a galaxy’s hot gas generally follows a shallower density profile than its stellar halo does, the “extra” clusters in very gas-rich (and high- S_N) ellipticals might well be expected to also show a radial distribution, ρ_{cl} or Σ_{cl} , that is distended relative to ρ_{stars} or Σ_{stars} .

These ideas, which extend similar suggestions in the recent literature, have been tested in detail for each of M87, M49, and NGC 1399. Data were collected from the literature on the GCSs, surface brightness profiles, and X-ray gas densities of these galaxies, covering spatial scales $r_{\text{gc}} \sim 1$ –100 kpc. In §3.1, new comparisons of the projected densities Σ_{cl} and Σ_{stars} in M49 and NGC 1399 (which are gas-poor) showed that, contrary to previous claims, neither galaxy suffers from either of the two specific frequency problems: The global S_N of M49 has a “standard” value of $\simeq 5$, and the local ratio $\Sigma_{\text{cl}}/\Sigma_{\text{stars}}$ is constant with radius (outside of a “core” region, $R_{\text{gc}} \lesssim R_{\text{eff}}$, that possibly has been dynamically depleted) if the recent surface-brightness profile of Caon et al. (1994) is used in the comparison rather than the older μ_B measurements of King (1978). The global specific frequency of NGC 1399 is similarly “average”, $S_N = 7.0 \pm 0.6$, if its GCS population is normalized to an absolute magnitude for the galaxy ($M_V \simeq -22.1$) that is significantly brighter than the value more commonly adopted. The ratio $\Sigma_{\text{cl}}/\Sigma_{\text{stars}}$ is also constant with radius in this galaxy, and has a value equal to that found in M49.

M87, at the center of the Virgo Cluster, is much richer in gas than either of M49 or NGC 1399, and both S_N problems are in evidence there. A discrete, geometrical deprojection algorithm was developed to enable a direct comparison between the volume densities ρ_{cl} , ρ_{stars} , and ρ_{gas} at all three-dimensional galactocentric radii in M87. It was found in §3.2 that $\rho_{\text{cl}} \propto (\rho_{\text{gas}} + \rho_{\text{stars}})$, beyond $r_{\text{gc}} \sim 8$ kpc, and that the constant of proportionality is the same as that in M49 and NGC 1399. *The cluster formation efficiency was constant with galactocentric radius inside each of these systems, and the same from one galaxy to another.* Specifically,

$$\epsilon_{\text{cl}} \simeq \frac{\rho_{\text{cl}}}{\rho_{\text{gas}} + \rho_{\text{stars}}} = \frac{M_{\text{gcs}}}{M_{\text{gas}} + M_{\text{stars}}} = 0.0026 \pm 0.0005 .$$

(Observed departures from this ratio in the central regions $r_{\text{gc}} \lesssim R_{\text{eff}}$ of M87 and M49 may have resulted, at least in part, from the dynamical destruction of globular clusters there.) Many globulars in M87 are indeed associated with its X-ray gas, and this is in fact responsible for the appearance of both specific frequency problems. This single case leads to the basic expectation—which should be tested in as many individual systems as possible—that real discrepancies between Σ_{cl} and Σ_{stars} should appear only in gas-rich ellipticals that also have high global specific frequencies.

The obvious generalization of these results is that most galaxies might have been subject to a single, common ϵ_{cl} . This possibility was explored, and borne out, in §4. Observations of global S_N (i.e., total GCS populations and galaxy luminosities) in 97 giant ellipticals, brightest cluster galaxies, and dwarf ellipticals *all* were shown to be consistent with the predictions of a universal ϵ_{cl} at the same level as that observed directly in M87, M49, and NGC 1399. The different scalings of S_N with $L_{V,\text{gal}}$ among normal giant ellipticals, central cluster galaxies, and dwarfs stem entirely from fundamentally different relations between $L_{V,\text{gal}}$ and $M_{\text{gas}}^{\text{init}}$ in these different physical regimes. These relations have been obtained from scaling arguments that employ the optical fundamental plane of bright ellipticals; the observed correlation between X-ray and optical luminosities in early-type systems; and the fractional gas loss expected in a specific model (Dekel & Silk 1986) for winds from a single burst of star formation in dark-matter dominated dwarf ellipticals. Observations of \mathcal{N}_{tot} vs. $L_{V,\text{gal}}$ still show some *scatter* about the mean prediction of constant ϵ_{cl} , and it will be important to clarify the significance and the origins of this. However, there are no *systematic* deviations from a universal cluster formation efficiency, in galaxies that span four orders of magnitude in total luminosity and GCS population.

Exactly the same ϵ_{cl} was shown, in §4, to have obtained for globular clusters in the spheroid, or stellar halo, of the Milky Way; and it was argued that it appears also to apply now, to the formation of *open* clusters locally in the Galactic disk. This remarkable robustness, in which a single cluster formation efficiency was and is realized in a great variety of local and global environments, demands a very general theoretical explanation. From a more empirical standpoint, it bears directly on current questions involving GCS and galaxy formation and evolution on large scales. Some of these were discussed in §5. Of considerable interest is the fact that, with ϵ_{cl} constant but $M_{\text{gcs}}/M_{\text{stars}}$ not, the efficiency of *unclustered* star formation could *not* have been universal; field star formation must have been suppressed, in a sense, in dwarf ellipticals and at large galactocentric radii in the brightest, most gas-rich ellipticals. The possibility that these points could be understood in terms of feedback processes seems promising (§5), and should be explored in quantitative models.

I am grateful to Bill Harris for providing the data plotted in Figures 8 and 9; to Ivan King and Chris McKee for helpful comments on an earlier draft of the paper; and to an anonymous referee for several valuable suggestions, including the addition of Figures 7 and 10. This work was supported by NASA through grant number HF-1097.01-97A awarded by the Space Telescope Science Institute, which is operated by the Association of Universities for Research in Astronomy, Inc., for NASA under contract NAS5-26555.

APPENDIX

DEPROJECTION ALGORITHM

The surface density data in Tables 2, 3, and 4 lend themselves well to a geometrical deprojection of the sort that is often applied to the X-ray emission from ellipticals and galaxy clusters (e.g., Fabian et al. 1981; Kriss, Cioffi, & Canizares 1983; Nulsen & Böhringer 1995). This technique makes only one assumption—that of circular symmetry—and is fully nonparametric. It also avoids the explicit differentiation of N_{cl} that is required in the standard Abel-transform approach to deprojection. Such a differentiation can be performed if an ad hoc parametrization is adopted for the global form of the density profile from the outset, but it is clearly desirable to minimize any such a priori restrictions. Although sophisticated, nonparametric algorithms that resort finally to an Abel integral have also been developed (e.g., Merritt & Tremblay 1994), they present a greater degree of complexity than is necessary here; and, in any case, they seem poorly suited to density profiles that are constructed from multiple observations with different fields of view and statistical corrections for different levels of background contamination and photometric incompleteness.

The assumption of spherical symmetry made here is not perfect (the isopleths of the M87 GCS, for one, are clearly non-circular in projection; see McLaughlin et al. 1994), but neither is it nonsensical: it takes azimuthally averaged surface densities and returns volume densities that are properly interpreted as angular averages at various galactocentric radii.

A simple example of the basic method, which should serve to define its geometrical set-up and mathematical notation, is illustrated in Fig. 11. The plane of the sky there is perpendicular to the plane of the page, and the two intersect in the line $z = 0$. Thus, the lines on the right, labelled by projected radius R_0 , R_1 , and R_2 , are lines of sight for an observer

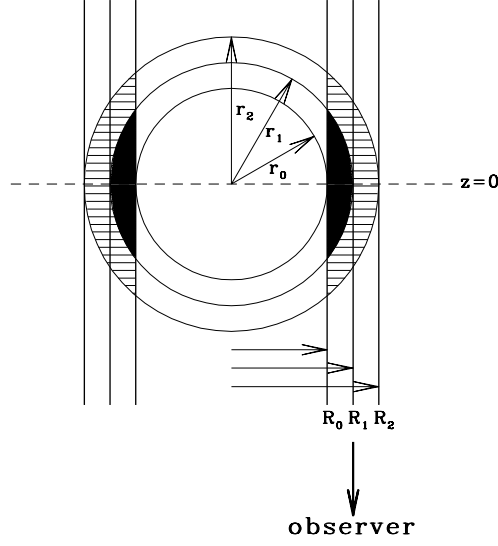


FIG. 11.— Illustration of a geometrical deprojection algorithm. The plane of the sky is perpendicular to the page. Radii r_0 , r_1 , and r_2 are three-dimensional quantities, and define spherical shells. Radii R_0 , R_1 , and R_2 are projected quantities referring to cylindrical shells aligned along the line of sight; these correspond to circular annuli on the plane of the sky.

situated off the bottom of the page. The bands $R_0 \leq R \leq R_1$ and $R_1 \leq R \leq R_2$, along with their mirror images on the left side of the Figure, are axial cross sections of cylinders that extend to $z = \pm\infty$; in the plane of the sky, of course, the corresponding cross sections are circular annuli. The circular annuli shown here are not those on the plane of the sky, however; rather, they are equatorial cross sections of spherical shells with three-dimensional radii $r_0 \leq r \leq r_1$ and $r_1 \leq r \leq r_2$. Evidently, these shells have been chosen such that $r_0 = R_0$, and so on. The origin $r = 0$ (through which passes the axis $R = 0$) represents the center of a spherical distribution of globular clusters, which are supposed to have been counted up in discrete cylinders $R_0 \leq R \leq R_1$ and $R_1 \leq R \leq R_2$ on the sky, to form the surface densities $N_{\text{cl}}(R_0, R_1)$ and $N_{\text{cl}}(R_1, R_2)$. From such data, it is possible to compute the fraction of clusters in each cylinder that actually reside in the spherical shells $r_0 \leq r \leq r_1$ and $r_1 \leq r \leq r_2$, and thus to form the average volume densities $n_{\text{cl}}(r_0, r_1)$ and $n_{\text{cl}}(r_1, r_2)$.

Suppose, for the moment (this will be relaxed just below), that $r_2 = R_2$ marks the outer edge of the GCS in question, i.e., $n_{\text{cl}}(r > r_2) \equiv 0$ and $N_{\text{cl}}(R > R_2) \equiv 0$. (It is assumed that the density N_b of any uniform distribution of background objects has already been subtracted to form N_{cl} from the raw data.) In this case, all of the objects seen in the outermost cylinder actually come from the outer spherical shell, i.e., from the hatched regions between R_1 and R_2 in Fig. 11. Since the number of globulars in this cylinder is just

$$\mathcal{N}_{\text{cl}}(R_1, R_2) = N_{\text{cl}}(R_1, R_2) \times \pi(R_2^2 - R_1^2) ,$$

all that is required is a calculation of the volume of the shell $r_1 \leq r \leq r_2$ which is intersected by the cylinder $R_1 \leq R \leq R_2$. Denoting this by $V_{\text{int}}(r_1, r_2; R_1, R_2)$, the volume density is obviously

$$n_{\text{cl}}(r_1, r_2) = \frac{\mathcal{N}_{\text{cl}}(R_1, R_2)}{V_{\text{int}}(r_1, r_2; R_1, R_2)} .$$

Moving inwards to the cylinder $R_0 \leq R \leq R_1$, the total number of clusters observed there includes a contribution from the spherical shell $r_1 \leq r \leq r_2$ (hatched regions between R_0 and R_1), as well as one from the shell of interest, $r_0 \leq r \leq r_1$ (solid region). The volume density in the outer shell has already been determined, and the volume of intersection between that shell and the inner cylinder can be calculated [call this $V_{\text{int}}(r_1, r_2; R_0, R_1)$], so the volume density in the inner shell is given by

$$n_{\text{cl}}(r_0, r_1) = \frac{\mathcal{N}_{\text{cl}}(R_0, R_1) - n_{\text{cl}}(r_1, r_2) V_{\text{int}}(r_1, r_2; R_0, R_1)}{V_{\text{int}}(r_0, r_1; R_0, R_1)} ,$$

where $\mathcal{N}_{\text{cl}}(R_0, R_1)$ and $V_{\text{int}}(r_0, r_1; R_0, R_1)$ have the same meanings as the corresponding quantities in the first cylinder, $R_1 \leq R \leq R_2$.

Clearly, this procedure can be extended and applied iteratively, from the outside in, to the projected number counts in any series of concentric, non-overlapping, circular annuli; it is only required that there be no gaps between any two consecutive annuli. Thus, let the annuli be defined on the plane of the sky by projected radii $R_0 < R_1 < R_2 < \dots < R_m$, i.e., set up m rings with $R_0 \leq R \leq R_1$; $R_1 \leq R \leq R_2$; and so on. Given average surface densities N_{cl} in each of these rings, the volume densities n_{cl} in the corresponding spherical shells $r_0 < r_1 < r_2 < \dots < r_m$ can be obtained once the volume of intersection between some generic shell $r_{j-1} \leq r \leq r_j$ and a cylinder $R_{i-1} \leq R \leq R_i$ is known. A sketch similar to Fig. 11 readily shows that this volume is, quite generally,

$$V_{\text{int}}(r_{j-1}, r_j; R_{i-1}, R_i) = \frac{4\pi}{3} \left[(r_j^2 - R_{i-1}^2)^{3/2} - (r_j^2 - R_i^2)^{3/2} + (r_{j-1}^2 - R_i^2)^{3/2} - (r_{j-1}^2 - R_{i-1}^2)^{3/2} \right], \quad (\text{A1})$$

for $i, j = 1, \dots, m$. This holds for any set of radii $\{r_{j-1}, r_j, R_{i-1}, R_i\}$, with the understanding that any term in parentheses which evaluates as negative is to be set to 0. An important application is to the case shown in Fig. 11, where, e.g., $r_1 = R_1$ and $r_2 = R_2$ and the volume common to the shell $R_1 \leq r \leq R_2$ and the cylinder $R_1 \leq R \leq R_2$ is $V_{\text{int}}(R_1, R_2; R_1, R_2) = (4\pi/3)(R_2^2 - R_1^2)^{3/2}$. It is most appropriate to define shells such that $r_i = R_i$ for all i , in which case the results given just above for $m = 2$ generalize to

$$\begin{aligned} n'_{\text{cl}}(R_{i-1}, R_i) &= \frac{N_{\text{cl}}(R_{i-1}, R_i) - \sum_{j=i+1}^m [n_{\text{cl}}(R_{j-1}, R_j) V_{\text{int}}(R_{j-1}, R_j; R_{i-1}, R_i)]}{V_{\text{int}}(R_{i-1}, R_i; R_{i-1}, R_i)} \\ &= \frac{3}{4(R_i^2 - R_{i-1}^2)^{1/2}} \left[N_{\text{cl}}(R_{i-1}, R_i) - \sum_{j=i+1}^m \frac{n_{\text{cl}}(R_{j-1}, R_j) V_{\text{int}}(R_{j-1}, R_j; R_{i-1}, R_i)}{\pi(R_i^2 - R_{i-1}^2)} \right]. \end{aligned} \quad (\text{A2})$$

Again, this assumes that any uniform background has already been subtracted to obtain the surface densities N_{cl} in every annulus $i = 1, \dots, m$.

This equation is not quite final, however, since its derivation has been facilitated by treating the outermost annulus seen in projection, $R_{m-1} \leq R \leq R_m$ (or the outermost spherical shell, $R_{m-1} \leq r \leq R_m$), as if it ended just at the “true edge” of some GCS. Of course, this will never actually be the case—if not because it makes little sense to associate sharp boundaries with such distributions in the first place, then because real observations and number counts can cover small fields of view within GCSs that are known to extend considerably further. This means that there is a second type of “background” contamination to be dealt with in any dataset, quite apart from that (already accounted for) due to a uniform distribution of unassociated galaxies and stars; corrections have to be made, in every annulus or shell, for the possible presence of bona fide globular clusters at radii $r > R_m$, beyond the last annulus for which a surface density can be directly measured. If the density distribution of such objects is denoted by $n_{\text{cl}}(r)$, their contribution to the projected number density in a cylinder $R_{i-1} \leq R \leq R_i$ is given by

$$N_{\text{cl}}^{\text{back}}(R_{i-1}, R_i) = \frac{4}{R_i^2 - R_{i-1}^2} \int_{R_{i-1}}^{R_i} R dR \int_{z_0(R)}^{\infty} n_{\text{cl}}(r) dz; \quad z_0(R) \equiv (R_m^2 - R^2)^{1/2}, \quad (\text{A3})$$

which is just an average of the projected densities along every line of sight contained in the cylinder. [As usual, the coordinate $z = (r^2 - R^2)^{1/2}$ here measures distance along these lines of sight; $z = 0$ defines the plane of the sky, as in Fig. 11.] It is most convenient to express this “background” surface density as a fraction of the observed N_{cl} in the outermost annulus $R_{m-1} \leq R \leq R_m$:

$$f(R_{i-1}, R_i) \equiv \frac{N_{\text{cl}}^{\text{back}}(R_{i-1}, R_i)}{N_{\text{cl}}(R_{m-1}, R_m)} = \frac{R_m^2 - R_{m-1}^2}{R_i^2 - R_{i-1}^2} \left[\frac{\int_{R_{i-1}}^{R_i} R dR \int_{z_0(R)}^{\infty} n_{\text{cl}}(r) dz}{\int_{R_{m-1}}^{R_m} R dR \int_0^{\infty} n_{\text{cl}}(r) dz} \right], \quad (\text{A4})$$

where $z_0(R)$ is defined as in equation (A3), and the second equality relies on the basic definition of average surface density in a circular annulus of finite width. The advantage of this formulation is that the form of $n_{\text{cl}}(r)$ cannot be directly measured for $r > R_m$, so the calculation of $N_{\text{cl}}^{\text{back}}$ necessarily depends on an extrapolation of some sort. Without any constraints on this extrapolation, it is conceivable that an artificial and unphysical situation such as $N_{\text{cl}}^{\text{back}}(R_{m-1}, R_m) > N_{\text{cl}}(R_{m-1}, R_m)$ could arise. This and similar difficulties are avoided, however, by only ever evaluating $N_{\text{cl}}^{\text{back}}$ in terms of f (which is guaranteed always to be < 1 when $i = m$) and the known N_{cl} at the largest projected radii observed.

Equation (A4) should therefore be used to subtract $N_{\text{cl}}^{\text{back}}$ from the total N_{cl} in every annulus before deprojecting the distribution according to equation (A2). The corrected volume densities in the spherical shells $i = 1, \dots, m$ may then be written as

$$n_{\text{cl}}(R_{i-1}, R_i) = n'_{\text{cl}}(R_{i-1}, R_i) - \frac{3}{4(R_i^2 - R_{i-1}^2)^{1/2}} f(R_{i-1}, R_i) N_{\text{cl}}(R_{m-1}, R_m). \quad (\text{A5})$$

Typically, when measured GCS surface densities extend to sufficiently large radius, an adequate estimate of f can be made by assuming a power-law distribution $n_{\text{cl}} \propto r^{-\alpha}$ in the outer reaches of the system, $r > R_m$; and in the case that α

is an integer, equation (A4) can be evaluated analytically. With $\alpha = 2$, for example,

$$f(R_{i-1}, R_i) = \frac{R_{m-1} + R_m}{R_{i-1} + R_i} \left[1 - \frac{2}{\pi} \frac{\left(\cos^{-1} \frac{R_i}{R_m} - \frac{R_{i-1}}{R_i} \cos^{-1} \frac{R_{i-1}}{R_m} \right) - \left(\sqrt{\frac{R_m^2}{R_i^2} - 1} - \sqrt{\frac{R_m^2}{R_i^2} - \frac{R_{i-1}^2}{R_i^2}} \right)}{1 - R_{i-1}/R_i} \right]. \quad (\text{A6})$$

For $\alpha = 3$,

$$f(R_{i-1}, R_i) = \frac{R_m^2 - R_{m-1}^2}{R_i^2 - R_{i-1}^2} \left[\frac{\sqrt{1 - \frac{R_{i-1}^2}{R_m^2}} - \sqrt{1 - \frac{R_i^2}{R_m^2}} - \ln \left(\frac{1 + \sqrt{1 - R_{i-1}^2/R_m^2}}{1 + \sqrt{1 - R_i^2/R_m^2}} \right)}{\ln(R_m/R_{m-1})} \right]. \quad (\text{A7})$$

And for $\alpha = 4$,

$$f(R_{i-1}, R_i) = \left[\frac{(R_{m-1} + R_m)R_m R_{m-1}}{(R_{i-1} + R_i)R_i R_{i-1}} \right] \times \left[1 - \frac{2}{\pi} \frac{\left(\frac{R_i}{R_{i-1}} \cos^{-1} \frac{R_{i-1}}{R_m} - \cos^{-1} \frac{R_i}{R_m} \right) - \frac{R_i}{R_m} \left(\sqrt{1 - \frac{R_{i-1}^2}{R_m^2}} - \sqrt{1 - \frac{R_i^2}{R_m^2}} \right)}{R_i/R_{i-1} - 1} \right]. \quad (\text{A8})$$

These three power-law exponents are expected to bracket the conditions that hold in real GCSs.

Finally, the volume densities derived in this way are a series of averages of a continuous $n_{\text{cl}}(r)$ in spherical shells of finite thickness. The question therefore arises as to how a single radius \bar{r}_i should be assigned to each shell so that the discrete distribution, $n_{\text{cl}}(R_{i-1}, R_i)$ vs. \bar{r}_i , represents the continuous one as faithfully as possible. (See Harris 1986 or King 1988 for a discussion of this issue in the two-dimensional context.) Clearly, the answer is to choose each $\bar{r}_i \in [R_{i-1}, R_i]$ such that

$$n_{\text{cl}}(R_{i-1}, R_i) = \frac{3}{R_i^3 - R_{i-1}^3} \int_{R_{i-1}}^{R_i} n_{\text{cl}}(r) r^2 dr = n_{\text{cl}}(\bar{r}_i). \quad (\text{A9})$$

If it is assumed that $n_{\text{cl}} \propto r^{-\alpha}$, the second equality is easily solved for \bar{r}_i in every shell. However, α will generally not be a constant from shell to shell; that is, a real GCS need not obey a single power-law density distribution over its entire extent (as is evident, for example, in Fig. 3 above). Moreover, α cannot be known a priori, and any attempts to derive it from the data must rely on fits to the average deprojected densities—fits which themselves depend on the values of \bar{r}_i . Fortunately, a complicated iterative procedure can be avoided by noting that observed radial distributions suggest that $0 \lesssim \alpha \lesssim 3$ anywhere in a typical GCS. This in turn suggests, and numerical experiments confirm, that simply using $\alpha = 3/2$ everywhere should lead to \bar{r}_i estimates that are acceptable substitutes for the exact solutions of equation (A9) in any realistic situation. Thus, the formula adopted here is

$$\bar{r}_i = \left[(R_{i-1}^{3/2} + R_i^{3/2})/2 \right]^{2/3}. \quad (\text{A10})$$

REFERENCES

- Aguilar, L., Hut, P., & Ostriker, J. P. 1988, *ApJ*, 335, 720
 Ashman, K. M., & Zepf, S. E. 1992, *ApJ*, 384, 50
 Bahcall, J. N., & Soneira, R. M. 1980, *ApJS*, 44, 73
 Bender, R., Surma, P., Döbereiner, S., Möllenhoff, C., & Madejsky, R. 1989, *A&A*, 217, 35
 Binney, J., & Tremaine, S. 1987, *Galactic Dynamics* (Princeton: Princeton Univ. Press)
 Blakeslee, J. P. 1997, *ApJ*, 481, L59
 Blakeslee, J. P., Tonry, J. L., & Metzger, M. R. 1997, *AJ*, 114, 482
 Bridges, T. J., Hanes, D. A., & Harris, W. E. 1991, *AJ*, 101, 469
 Brighenti, F., & Mathews, W. G. 1998, *ApJ*, 495, 239
 Brodie, J. P., Schroder, L. L., Huchra, J. P., Phillips, A. C., Kissler-Patig, M., & Forbes, D. A. 1998, *AJ*, 116, 691
 Brown, B. A., & Bregman, J. N. 1998, *ApJ*, 495, L75
 Burstein, D., & Heiles, C. 1984, *ApJS*, 54, 33
 Caon, N., Capaccioli, M., & D'Onofrio, M. 1994, *A&AS*, 106, 199
 Capuzzo-Dolcetta, R. 1993, *ApJ*, 415, 616
 Carlberg, R. G., et al. 1997, *ApJ*, 485, L13
 Cohen, J. G. 1988, *AJ*, 95, 682
 Côté, P., Marzke, R. O., & West, M. J. 1998, *ApJ*, 501, 554
 Crane, P., et al. 1993, *AJ*, 106, 1371
 Davies, R. L., Efstathiou, G., Fall, S. M., Illingworth, G., & Schechter, P. L. 1983, *ApJ*, 266, 41
 Davis, D. S., & White, R. E. 1996, *ApJ*, 470, L35
 de Carvalho, R. R., & Djorgovski, S. 1989, *ApJ*, 341, L37
 de Carvalho, R. R., & Djorgovski, S. 1992, *ApJ*, 389, L49
 de Vaucouleurs, G. 1993, *ApJ*, 415, 40
 de Vaucouleurs, G., & Nieto, J.-L. 1978, *ApJ*, 220, 449
 de Vaucouleurs, G., & Nieto, J.-L. 1979, *ApJ*, 230, 697
 de Vaucouleurs, G., & Pence, W. D. 1978, *AJ*, 83, 1163
 de Vaucouleurs, G., de Vaucouleurs, A., Corwin, Jr., H. G., Buta, R. J., Paturel, G., & Fouqué, P. 1991, *Third Reference Catalogue of Bright Galaxies* (New York: Springer)
 Dehnen, W. 1993, *MNRAS*, 265, 250
 Dekel, A., & Silk, J. 1986, *ApJ*, 303, 39
 Djorgovski, S., & Meylan, G. 1994, *AJ*, 108, 1292
 Durrell, P. R., Harris, W. E., Geisler, D., & Pudritz, R. E. 1996, *AJ*, 112, 972

- Elmegreen, B. G. 1983, *MNRAS*, 203, 1011
- Elmegreen, B. G., & Clemens, C. 1985, *ApJ*, 294, 523
- Elmegreen, B. G., & Efremov, Y. N. 1997, *ApJ*, 480, 235
- Fabbiano, G. 1989, *ARA&A*, 27, 87
- Faber, S. M., & Gallagher, J. 1979, *ARA&A*, 17, 135
- Faber, S. M., Dressler, A., Davies, R. L., Burstein, D., Lynden-Bell, D., Terlevich, R., & Wegner, G. 1987, in *Nearly Normal Galaxies*, ed. S. M. Faber (New York: Springer), 175
- Faber, S. M., et al. 1997, *AJ*, 114, 1771
- Fabian, A. C., Hu, E. M., Cowie, L. L., & Grindlay, J. 1981, *ApJ*, 248, 47
- Forbes, D. A., Brodie, J. P., & Grillmair, C. J. 1997, *AJ*, 113, 1652
- Forbes, D. A., Franx, M., Illingworth, G. D., & Carollo, C. M. 1996, *ApJ*, 467, 126
- Forman, W., Jones, C., & Tucker, W. 1985, *ApJ*, 293, 102
- Freedman, W., et al. 1994, *Nature*, 371, 757
- Fritze-von Alvensleben, U. 1999, *A&A*, in press (astro-ph/9812285)
- Gebhardt, K., et al. 1996, *AJ*, 112, 105
- Geisler, D., Lee, M. G., & Kim, E. 1996, *AJ*, 111, 1529
- Gnedin, O. Y., & Ostriker, J. P. 1997, *ApJ*, 474, 223
- Grillmair, C., Pritchet, C., & van den Bergh, S. 1986, *AJ*, 91, 1328
- Hanes, D. A., & Harris, W. E. 1986, *ApJ*, 309, 564
- Harris, W. E. 1976, *AJ*, 81, 1095
- Harris, W. E. 1981, *ApJ*, 251, 497
- Harris, W. E. 1986, *AJ*, 91, 822
- Harris, W. E. 1991, *ARA&A*, 29, 543
- Harris, W. E. 1996, *AJ*, 112, 1487
- Harris, W. E., & Petrie, P. L. 1978, *ApJ*, 223, 88
- Harris, W. E., & Pudritz, R. E. 1994, *ApJ*, 429, 177
- Harris, W. E., & Racine, R. 1979, *ARA&A*, 17, 241
- Harris, W. E., & Smith, M. G. 1976, *ApJ*, 207, 1036
- Harris, W. E., & van den Bergh, S. 1981, *AJ*, 86, 1627
- Harris, W. E., Harris, G. L. H., & McLaughlin, D. E. 1998, *AJ*, 115, 1801
- Harris, W. E., Pritchet, C. J., & McClure, R. D. 1995, *ApJ*, 441, 120
- Harris, W. E., Allwright, J. W. B., Pritchet, C. J., & van den Bergh, S. 1991, *ApJ*, 356, 359
- Hernquist, L. 1990, *ApJ*, 356, 359
- Hills, J. G. 1980, *ApJ*, 225, 986
- Ho, L. C., & Filippenko, A. V. 1996a, *ApJ*, 466, L83
- Ho, L. C., & Filippenko, A. V. 1996b, *ApJ*, 472, 600
- Huchra, J. P., & Brodie, J. P. 1987, *AJ*, 93, 779
- Irwin, J. A., & Sarazin, C. 1996, *ApJ*, 471, 683
- Jacoby, G. H., Branch, D., Ciardullo, R., Davies, R. L., Harris, W. E., Pierce, M. J., Pritchet, C. J., Tonry, J. L., & Welch, D. L. 1992, *PASP*, 104, 599
- Jones, C., Stern, C., Forman, W., Breen, J., David, L., Tucker, W., & Franx, M. 1997, *ApJ*, 482, 143
- Kavalaars, J. J., & Hanes, D. A. 1997, *MNRAS*, 285, L31
- Kavalaars, J. J. 1998, preprint (astro-ph/9806094)
- Killeen, N. E. B., & Bicknell, G. V. 1988, *ApJ*, 325, 165
- King, I. R. 1978, *ApJ*, 222, 1
- King, I. R. 1988, *PASP*, 100, 999
- Kinman, T. D., Suntzeff, N. B., & Kraft, R. P. 1994, *AJ*, 108, 1722
- Kissler-Patig, M. 1997, *A&A*, 319, 83
- Kissler-Patig, M., Forbes, D. A., & Minniti, D. 1998, *MNRAS*, 298, 1123
- Kissler-Patig, M., Kohle, S., Hilker, M., Richtler, T., Infante, L., & Quintana, H. 1997, *A&A*, 319, 470
- Kohle, S., Kissler-Patig, M., Hilker, M., Richtler, T., Infante, L., & Quintana, H. 1996, *A&A*, 309, L39
- Kriss, G. A., Cioffi, D. F., & Canizares, C. R. 1983, *ApJ*, 272, 439
- Kumai, Y., Basu, B., & Fujimoto, M. 1993a, *ApJ*, 404, 144
- Kumai, Y., Hashi, Y., & Fujimoto, M. 1993b, *ApJ*, 416, 576
- Lada, C. J., Margulis, M., & Dearborn, D. 1984, *ApJ*, 285, 141
- Lada, E. A., DePoy, D. L., Evans, N. J., & Gatley, I. 1991, *ApJ*, 371, 171
- Larson, R. B. 1988, in *IAU Symposium No. 126, Globular Cluster Systems in Galaxies*, ed. J. E. Grindlay and A. G. D. Philip (Dordrecht: Kluwer), 311
- Larson, R. B. 1993, in *ASP Conf. Ser. 48, The Globular Cluster-Galaxy Connection*, ed. G. H. Smith and J. P. Brodie (San Francisco: ASP), 675
- Larson, R. B. 1996, in *ASP Conf. Ser. 92, Formation of the Galactic Halo...Inside and Out*, ed. H. Morrison and A. Sarajedini (San Francisco: ASP), 241
- Lauer, T. R., & Kormendy, J. 1986, *ApJ*, 303, L1
- Lee, M. G., Kim, E., & Geisler, D. 1998, *AJ*, 115, 947
- Mandushev, G., Spassova, N., & Staneva, A. 1991, *A&A*, 252, 94
- Mathieu, R. D. 1983, *ApJ*, 267, L97
- Mateo, M. L. 1998, *ARA&A*, 36, 435
- McKee, C. F. 1989, *ApJ*, 345, 782
- McLaughlin, D. E. 1994, *PASP*, 106, 47
- McLaughlin, D. E. 1995, *AJ*, 109, 2034
- McLaughlin, D. E. 1999, *ApJ Letters*, 512, in press (astro-ph/9812242)
- McLaughlin, D. E., & Pudritz, R. E. 1996, *ApJ*, 457, 578
- McLaughlin, D. E., Harris, W. E., & Hanes, D. A. 1993, *ApJ*, 409, L45
- McLaughlin, D. E., Harris, W. E., & Hanes, D. A. 1994, *ApJ*, 422, 486
- McLaughlin, D. E., Secker, J., Harris, W. E., & Geisler, D. 1995, *AJ*, 109, 1033
- McMillan, R., Ciardullo, R., & Jacoby, G. 1993, *ApJ*, 416, 62
- Merritt, D., & Tremblay, B. 1994, *AJ*, 108, 514
- Meurer, G. R., Heckman, T. M., Leitherer, C., Kinney, A., Robert, C., & Garnett, D. R. 1995, *AJ*, 110, 2665
- Miller, B. W., Lotz, J. M., Ferguson, H. C., Stiavelli, M., & Whitmore, B. C. 1998, *ApJ*, 508, L133
- Minniti, D. 1995, *AJ*, 109, 1663
- Minniti, D., Meylan, G., & Kissler-Patig, M. 1996, *A&A*, 312, 49
- Murali, C., & Weinberg, M. D. 1997a, *MNRAS*, 288, 749
- Murali, C., & Weinberg, M. D. 1997b, *MNRAS*, 288, 767
- Murali, C., & Weinberg, M. D. 1997c, *MNRAS*, 291, 717
- Muzzio, J. C. 1987, *PASP*, 99, 245
- Navarro, J. F., Frenk, C. S., & White, S. D. M. 1996, *ApJ*, 462, 563
- Navarro, J. F., Frenk, C. S., & White, S. D. M. 1997, *ApJ*, 490, 493
- Nieto, J.-L., Bender, R., & Surma, P. 1991, *A&A*, 244, L37
- Nulsen, P. E. J., & Böhringer, H. 1995, *MNRAS*, 274, 1093
- Oemler, A. 1976, *ApJ*, 209, 693
- Okazaki, T., & Tosa, M. 1995, *MNRAS*, 274, 48
- Ostriker, J. P., Binney, J., & Saha, P. 1989, *MNRAS*, 241, 849
- Ostrov, P. G., Forte, J. C., & Geisler, D. 1998, *AJ*, 116, 2854
- Pahre, M. A., Djorgovski, S. G., & de Carvalho, R. R. 1995, *ApJ*, 453, L17
- Patel, K., & Pudritz, R. E. 1994, *ApJ*, 424, 688
- Pierce, M. J., Welch, D. L., McClure, R. D., van den Bergh, S., Racine, R., & Stetson, P. B. 1994, *Nature*, 371, 385
- Portegies Zwart, S. F., Hut, P., Makino, J., & McMillan, S. L. W. 1998, *A&A*, 337, 363
- Preston, G. W., Schectman, S. A., & Beers, T. C. 1991, *ApJ*, 375, 121
- Pritchet, C. J., & van den Bergh, S. 1994, *AJ*, 107, 1730
- Pryor, C., & Meylan, G. 1993, in *ASP Conf. Ser. 50, Structure and Dynamics of Globular Clusters*, ed. S. G. Djorgovski and G. Meylan (San Francisco: ASP), 357
- Roberts, M. S. 1957, *PASP*, 69, 59
- Santiago, B. X., & Djorgovski, S. 1993, *MNRAS*, 261, 753
- Schweizer, F. 1987, in *Nearly Normal Galaxies*, ed. S. M. Faber (New York: Springer), 18
- Searle, L., & Zinn, R. 1978, *ApJ*, 225, 357
- Sternberg, A. 1998, *ApJ*, 506, 721
- Surdin, V. G. 1979, *Sov. Astron.*, 23, 648
- Tonry, J. L., Blakeslee, J. P., Ajhar, E. A., & Dressler, A. 1997, *ApJ*, 475, 399
- Tremaine, S., Richstone, D. O., Byun, Y.-I., Dressler, A., Faber, S. M., Grillmair, C., Kormendy, J., & Lauer, T. R. 1994, *AJ*, 107, 634
- Tremblay, B., & Merritt, D. 1996, *AJ*, 111, 2243
- Trinchieri, G., Fabbiano, G., & Canizares, C. R. 1986, *ApJ*, 310, 637
- Tsai, J. C. 1993, *ApJ*, 413, L59
- van den Bergh, S. 1984, *PASP*, 96, 329
- van den Bergh, S. 1998, *ApJ*, 492, 41
- van den Bergh, S., & Lafontaine, A. 1984, *AJ*, 89, 1822
- van der Marel, R. P. 1991, *MNRAS*, 253, 710
- Verschueren, W. 1990, *A&A*, 234, 156
- Vesperini, E. 1997, *MNRAS*, 287, 915
- Vesperini, E., & Heggge, D. C. 1997, *MNRAS*, 289, 898
- Wagner, S., Richtler, T., & Hopp, U. 1991, *A&A*, 241, 399
- Weil, M. L., Bland-Hawthorn, J., & Malin, D. F. 1997, *ApJ*, 490, 664
- West, M. J. 1993, *MNRAS*, 265, 755
- West, M. J., Côté, P., Jones, C., Forman, W., & Marzke, R. O. 1995, *ApJ*, 453, L77
- White, R. E. 1987, *MNRAS*, 227, 185
- Whitmore, B. C. 1997, in *The Extragalactic Distance Scale*, ed. M. Livio, M. Donahue, and N. Panagia (Baltimore: STScI), 254
- Whitmore, B. C., & Schweizer, F. 1995, *AJ*, 109, 960
- Whitmore, B. C., Sparks, W. B., Lucas, R. A., Macchetto, F. D., & Biretta, J. A. 1995, *ApJ*, 454, L73
- Young, P. J. 1976, *AJ*, 81, 807
- Zepf, S. E., & Ashman, K. M. 1993, *MNRAS*, 264, 611
- Zinn, R. 1985, *ApJ*, 293, 424
- Zinnecker, H., McCaughrean, M. J., & Wilking, B. A. 1993, in *Protostars and Planets III*, ed. E. H. Levy and J. I. Lunine (Tucson: Univ. of Arizona Press), 429